nature structural & molecular biology

Formaldehyde catabolism is essential in cells deficient for the Fanconi anemia DNA-repair pathway

Ivan V Rosado[1], Frédéric Langevin[1], Gerry P Crossan[1], Minoru Takata[2] & Ketan J Patel[1,3]

Metabolism is predicted to generate formaldehyde, a toxic, simple, reactive aldehyde that can damage DNA. Here we report a synthetic lethal interaction in avian cells between *ADH5*, encoding the main formaldehyde-detoxifying enzyme, and the Fanconi anemia (FA) DNA-repair pathway. These results define a fundamental role for the combined action of formaldehyde catabolism and DNA cross-link repair in vertebrate cell survival.

Individuals afflicted with FA are prone to abnormal development and stem cell attrition and have a significant predisposition to cancer[1]. FA arises through germline inactivation of any one of 15 genes[2–4]. Most FA gene products operate together in an evolutionarily conserved pathway that eventually repairs DNA damage caused by certain chemotherapeutic agents that cross-link DNA[5–8]. However, such molecules cannot be the physiological source of DNA damage that precipitates the FA phenotype. Furthermore, chemotherapeutic cross-linkers cannot be the reason why the FA genes are conserved in all complex eukaryotes.

Recently we showed that acetaldehyde is a potential source of endogenous DNA damage necessitating repair by the FA-associated DNA-repair pathway[9]. However, acetaldehyde is not abundantly generated within cells, in contrast to formaldehyde (HCHO), the simplest reactive aldehyde[10]. Given that endogenous formaldehyde both is abundant and can attack DNA, we hypothesized that cells protect against this threat through the combined action of enzymatic detoxification and DNA repair. Here we examine the consequences of endogenous formaldehyde accumulation in DNA repair–deficient cell lines, revealing a fundamental role for the FA pathway in protecting cells against this reactive aldehyde.

Previous work has demonstrated that exogenous formaldehyde can be genotoxic. More specifically, chicken DNA repair–deficient cell lines deficient in the FA pathway downstream gene *FANCD2*, translesion synthesis (TLS) or homologous recombination (HR) show selective sensitivity to this aldehyde[11]. Formaldehyde-induced DNA damage has also been shown to be repaired by HR independently of the FA core complex[12]. We chose to extend these findings by testing formaldehyde genotoxicity in a human FA gene–deficient cell line (see **Supplementary Methods**). We used the human B cell line NALM-6 and its isogenic counterpart carrying an inactivation of the *FANCB* gene[13]. *FANCB*-deficient cells are very sensitive to formaldehyde (**Fig. 1a**),

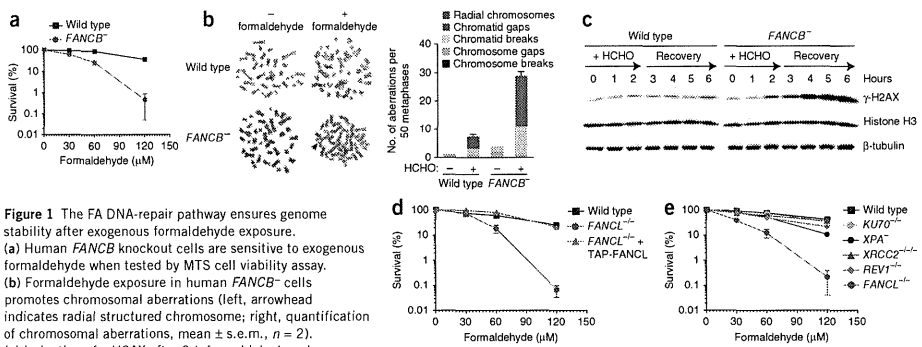

Figure 1 The FA DNA-repair pathway ensures genome stability after exogenous formaldehyde exposure. (**a**) Human *FANCB* knockout cells are sensitive to exogenous formaldehyde when tested by MTS cell viability assay. (**b**) Formaldehyde exposure in human *FANCB*$^{-}$ cells promotes chromosomal aberrations (left, arrowhead indicates radial structured chromosome; right, quantification of chromosomal aberrations, mean ± s.e.m., $n = 2$). (**c**) Induction of γ-H2AX after 2-h formaldehyde pulse treatment and release. (**d**) *FANCL* DT40 knockout cells are hypersensitive to formaldehyde; *FANCL*-complemented cell line is resistant to formaldehyde. (**e**) DT40 knockouts *XRCC2*, *KU70* and *REV1* are not hypersensitive to formaldehyde; *XPA*-deficient cells are mildly sensitive to formaldehyde.

[1]Medical Research Council Laboratory of Molecular Biology, Cambridge, UK. [2]Laboratory of DNA Damage Signaling, Department of Late Effect Studies, Radiation Biology Center, Kyoto University, Kyoto, Japan. [3]University of Cambridge, Department of Medicine, Addenbrooke's Hospital, Cambridge, UK. Correspondence should be addressed to K.J.P. (kjp@mrc-lmb.cam.ac.uk).

Received 29 June; accepted 16 September; published online 13 November 2011; doi:10.1038/nsmb.2173

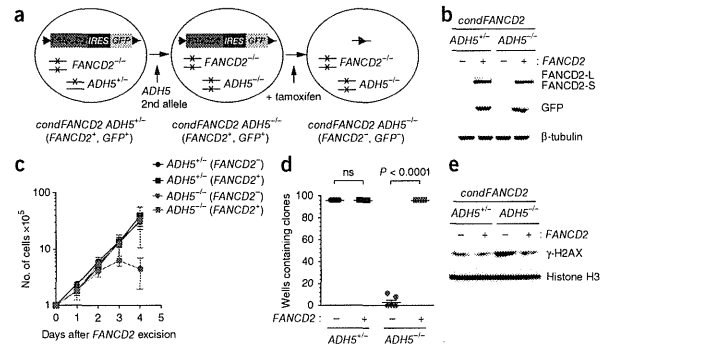

Figure 2 *FANCD2* and *ADH5* are synthetically lethal in DT40 cells. (**a**) Strategy outlining the conditional deletion of *FANCD2* in *ADH5*-null DT40 cells by addition of 4-OH tamoxifen. (**b**) Western blot of FACS GFP-positive (+) or -negative (–) sorted cells after 4-OH tamoxifen treatment for FANCD2 (top), GFP (middle) and β-tubulin (bottom). (**c**) Growth curve of FACS GFP^{+} and GFP^{-} sorted cells representing mean values of two independent experiments. Error bars define s.e.m. ($n = 2$). (**d**) Clonogenic survival assay of FACS GFP^{+} and GFP^{-} sorted cells plated at 50 cells per well into 96-well plates; mean values obtained from seven plates from two independent experiments. ($P < 0.0001$, Fisher's exact test. ns, nonsignificant.) (**e**) Induction of γ-*H2AX in FACS GFP*$^{-}$ *and GFP*$^{+}$ *sorted cells* lacking both *FANCD2* and *ADH5*.

and this sensitivity correlated with the accumulation of chromatid-type chromosome breakage and radial structure formation (**Fig. 1b**). These cells also showed enhanced induction of Ser139 phosphorylation of histone H2AX (γ-H2AX) (**Fig. 1c**), a marker of double strand breaks (DSBs).

We comprehensively tested formaldehyde sensitivity in both upstream and downstream components of the FA DNA-repair pathway using mutant chicken DT40 cell lines. Mutations in all the components of the FA pathway so far tested sensitized cells to formaldehyde (**Fig. 1d** and **Supplementary Fig. 1**). Cell lines deficient in the other major pathways of DNA repair were largely resistant to formaldehyde, with the exception of those deficient in nucleotide excision repair (specifically, mutant for the gene *XPA*), which showed mild sensitivity (**Fig. 1e**). In contrast to earlier results by others[11], we did not observe enhanced formaldehyde sensitivity in cells lines mutant for translesion synthesis (*REV1* and *REV3*) or homologous recombination (*XRCC2*, *XRCC3*, *RAD51C*, *RAD52* and *RAD54*) (**Supplementary Fig. 2**). This suggests that formaldehyde-induced DNA damage may not include interstrand cross-links.

Formaldehyde is generated endogenously within the nucleus as a byproduct of histone demethylation by the Jumonji demethylases and dealkylation of methylated DNA bases by AlkB orthologs (**Supplementary Fig. 3**)[10,14,15]. The cell prevents accumulation of endogenously generated formaldehyde through the action of alcohol dehydrogenase 5 (encoded by *ADH5*)[16]. To test whether the endogenous formaldehyde pool can be genotoxic, we generated an *ADH5*-knockout DT40 strain through gene disruption (**Supplementary Fig. 4a,b**). The *ADH5*$^{-/-}$ strain was readily obtained; this mutant's growth was not compromised, nor did it show increased sensitivity to exogenous formaldehyde under these conditions (**Supplementary Fig. 4c**). Next we attempted to inactivate the FA pathway in this strain by disruption of either the *FANCC* (one allele) or *FANCL* genes (two alleles). This proved unsuccessful (0/138 for *FANCC* and 0/781 for *FANCL*), suggesting that the combined inactivation of the FA pathway and *ADH5* could be synthetically lethal. We therefore constructed a DT40 *FANCD2*$^{-/-}$ strain that carries a conditional *FANCD2-IRES-GFP* expression cassette flanked by *lox*P sites (hitherto referred to as *condFANCD2*) (**Fig. 2a**). Owing to the presence of a 4-OH-tamoxifen–inducible Cre recombinase, 4-OH-tamoxifen treatment leads to excision of the *FANCD2-IRES-GFP* cassette, rendering the cells *FANCD2* deficient and *GFP* negative (*FANCD2*$^{-}$*GFP*$^{-}$). We then disrupted the *ADH5* gene in this strain to create the *condFANCD2 ADH5*$^{-/-}$ cell line, which lost FANCD2 and GFP expression upon treatment with 4-OH-tamoxifen, thereby generating *FANCD2*$^{-}$ *GFP*$^{-}$ cells. We purified this population by FACS (**Fig. 2b**) and followed the cells' fate in culture. The *FANCD2*$^{-}$ *GFP*$^{-}$ cells ceased growing after 3 d in culture (**Fig. 2c**), indicating that *FANCD2* has an essential role in cells lacking *ADH5*. Additionally, when *FANCD2*$^{-}$ *GFP*$^{-}$ cells were plated to isolate double-mutant clones, no viable *FANCD2*$^{-}$ *GFP*$^{-}$ cells were obtained in the *ADH5*$^{-/-}$ background (**Fig. 2d**). Finally, we observed a clear induction of γ-H2AX in the *FANCD2*$^{-}$ *GFP*$^{-}$ *ADH5*$^{-/-}$ cells but only a marginal increase in *FANCD2*$^{-}$ *GFP*$^{-}$ *ADH5*$^{+/-}$ cells (**Fig. 2e**).

In order to address whether the synthetically lethal interaction observed between *FANCD2* and *ADH5* was specific to the downstream component *FANCD2* or generalizable to core complex components, we generated a transcriptionally repressible *FANCL* knockout strain (**Fig. 3a**). The *ADH5*$^{+/-}$ cell was modified to express a *TAP-FANCL* transgene driven by a tetracycline-repressible promoter (*TetO*::*TAP-FANCL*). Both alleles of *FANCL* were knocked out in this strain, giving a *FANCL*$^{-/-}$*ADH5*$^{+/-}$ *TetO*::*TAP-FANCL* strain. We then proceeded to disrupt the second allele of *ADH5*, yielding the strain *FANCL*$^{-/-}$ *ADH5*$^{-/-}$ *TetO*::*TAP-FANCL*. Extinction of *TAP-FANCL* expression, and thus inactivation of the FA pathway, was observed upon addition of doxycycline to the culture medium. Within 2 d of doxycycline addition, TAP-FANCL expression was greatly diminished (**Fig. 3b**). This coincided with a cessation of proliferation and a marked decrease in viability only among cells deficient for *ADH5* (**Fig. 3c**). To quench endogenously produced formaldehyde, we exploited the chemistry between β-mercaptoethanol (β-ME) and aldehydes. Formaldehyde reacts readily with the thiol group of β-ME, giving a less reactive and more stable product, 2-((hydroxymethyl)thio) ethanol (**Supplementary Fig. 5**). Addition of 100 μM β-ME to the growth medium rescued the defect in cell proliferation and improved viability after repression of *TAP-FANCL* in *ADH5*$^{-/-}$ cells (**Fig. 3d**). Finally, using γ-H2AX as a marker of DSBs, we noted that cells lacking *ADH5* greatly induced γ-H2AX upon *FANCL* repression (**Fig. 3e**), in comparison to the *ADH5*-proficient cells. As predicted, addition of 100 μM β-ME suppressed this accumulation.

To summarize, we have shown by two independent approaches that inactivation of formaldehyde catabolism by disruption of *ADH5* results in synthetic lethality with upstream (*FANCL*) or downstream (*FANCD2*) components of the FA pathway. Our observation that FA-deficient chicken DT40 cells have an essential requirement for *ADH5* (and hence formaldehyde catabolism) contrasts with the requirement for *ALDH2* (encoding the enzyme that catabolizes acetaldehyde),

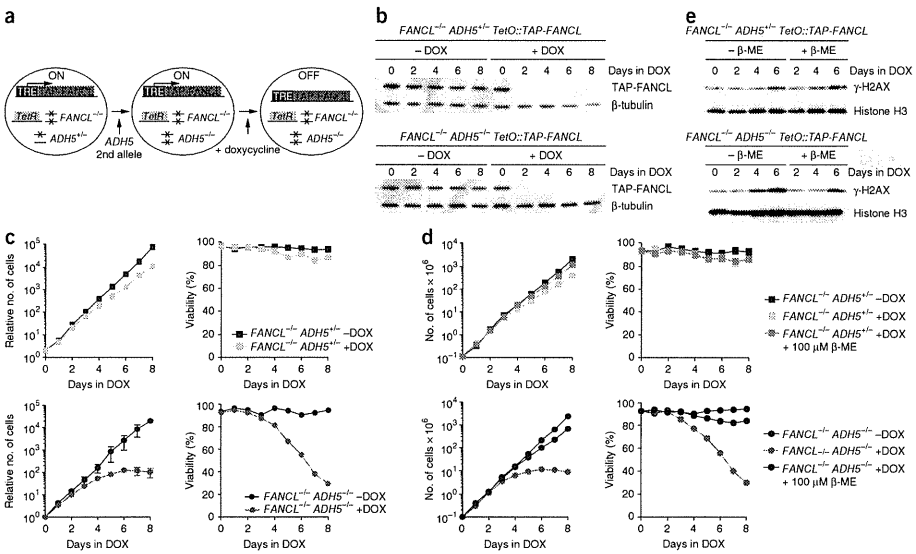

Figure 3 The FA core complex gene *FANCL* and *ADH5* are synthetically lethal in DT40 cells. (**a**) Strategy for conditional *FANCL* repression in *ADH5*-null DT40 cells by addition of doxycycline. (**b**) Conditional depletion of TAP-FANCL protein in doxycycline (DOX)-treated *FANCL*$^{-/-}$ *ADH5*$^{+/-}$ *TetO::TAP-FANCL* or *FANCL*$^{-/-}$ *ADH5*$^{-/-}$ *TetO::TAP-FANCL* cells. Whole cell extracts were western blotted with anti-tubulin IgG antibody (Sigma-Aldrich), which cross-reacts with TAP-FANCL. (**c**) Growth curves and viability plots of *FANCL* conditionally repressed cells in *ADH5*$^{+/-}$ and *ADH5*$^{-/-}$; each point represents mean values of two independent experiments. Error bars, s.e.m. (**d**) Growth curves of viable cells and viability plots of conditionally repressed *FANCL*$^{-/-}$ *ADH5*$^{+/-}$ or *ADH5*$^{-/-}$ *TetO::TAP-FANCL* cells in the presence of 2-mercaptoethanol (β-ME); each point represents mean values of two independent experiments. Error bars, s.e.m. (**e**) Induction of γ-H2AX following *FANCL* repression in *ADH5*$^{-/-}$ DT40 cells and its suppression following addition of β-ME.

whose absence is not synthetically lethal[9]. Thus, endogenous formaldehyde appears to be either more abundant and/or more potently genotoxic than acetaldehyde. It is striking that the full complement of FA genes is only found in higher eukaryotes; perhaps the expansion of FA genes coevolved with multicellularity and the emergence of stem cell pools[17,18]. Because we know that formaldehyde is produced as a byproduct of histone demethylation, our results lead us to predict that certain cell lineages with a propensity for extensive histone modifications might be particularly reliant on FA pathway repair. Endogenous formaldehyde genotoxicity might therefore explain the progressive attrition of germ and blood stem cells in FA.

Note: Supplementary information is available on the Nature Structural & Molecular Biology website.

ACKNOWLEDGMENTS

We thank N. Adachi and H. Koyama (Kihara Institute for Biological Research, Japan) for kindly providing NALM-6 human cell lines. We are grateful to J. Sutherland and K. Lang (MRC Laboratory of Molecular Biology) for chemical insight and to M. Daly and F. Zhang (MRC Laboratory of Molecular Biology) for invaluable help with flow cytometry. I.V.R. and F.L. are funded by the Fanconi Anaemia Research Fund and Children's Leukaemia Trust, respectively.

AUTHOR CONTRIBUTIONS

I.V.R. and K.J.P. designed the study and the experiments, and wrote the paper. I.V.R. performed the majority of the experiments presented. F.L. contributed to DT40 clonogenic assays and assisted in the generation of *ADH5*-deficient cell lines. G.P.C. helped with analysis of chromosome breaks. M.T. generated and provided the FANCD2 inducible cell line.

COMPETING FINANCIAL INTERESTS

The authors declare no competing financial interests.

Published online at http://www.nature.com/nsmb/.
Reprints and permissions information is available online at http://www.nature.com/reprints/index.html.

1. Muller, L.U. & Williams, D.A. *Mutat. Res.* **668**, 141–149 (2009).
2. Crossan, G.P. *et al. Nat. Genet.* **43**, 147–152 (2011).
3. Stoepker, C. *et al. Nat. Genet.* **43**, 138–141 (2011).
4. Kim, Y. *et al. Nat. Genet.* **43**, 142–146 (2011).
5. Joenje, H. & Patel, K.J. *Nat. Rev. Genet.* **2**, 446–457 (2001).
6. Patel, K.J. & Joenje, H. *DNA Repair (Amst.)* **6**, 885–890 (2007).
7. de Winter, J.P. & Joenje, H. *Mutat. Res.* **668**, 11–19 (2009).
8. Rosado, I.V., Niedzwiedz, W., Alpi, A.F. & Patel, K.J. *Nucleic Acids Res.* **37**, 4360–4370 (2009).
9. Langevin, F., Crossan, G.P., Rosado, I.V., Arends, M.J. & Patel, K.J. *Nature* **475**, 53–58 (2011).
10. Mosammaparast, N. & Shi, Y. *Annu. Rev. Biochem.* **79**, 155–179 (2010).
11. Ridpath, J.R. *et al. Cancer Res.* **67**, 11117–11122 (2007).
12. Noda, T. *et al. Biochem. Biophys. Res. Commun.* **404**, 206–210 (2011).
13. Nomura, Y., Adachi, N. & Koyama, H. *Genes Cells* **12**, 1111–1122 (2007).
14. Trewick, S.C., Henshaw, T.F., Hausinger, R.P., Lindahl, T. & Sedgwick, B. *Nature* **419**, 174–178 (2002).
15. Falnes, P.O., Johansen, R.F. & Seeberg, E. *Nature* **419**, 178–182 (2002).
16. Iborra, F.J. *et al. J. Histochem. Cytochem.* **40**, 1865–1878 (1992).
17. Mosedale, G. *et al. Nat. Struct. Mol. Biol.* **12**, 763–771 (2005).
18. Zhang, X.Y. *et al. PLoS Genet.* **5**, e1000645 (2009).

Brief report

Somatic mosaicism for oncogenic *NRAS* mutations in juvenile myelomonocytic leukemia

Sayoko Doisaki,[1] Hideki Muramatsu,[1] Akira Shimada,[1] Yoshiyuki Takahashi,[1] Makiko Mori-Ezaki,[2] Masanori Sato,[3] Hiroyuki Kawaguchi,[4] Akitoshi Kinoshita,[5] Manabu Sotomatsu,[6] Yasuhide Hayashi,[6] Yoko Furukawa-Hibi,[7] Kiyofumi Yamada,[7] Hideaki Hoshino,[8] Hitoshi Kiyoi,[8] Nao Yoshida,[9] Hirotoshi Sakaguchi,[1] Atsushi Narita,[1] Xinan Wang,[1] Olfat Ismael,[1] Yinyan Xu,[1] Nobuhiro Nishio,[1] Makito Tanaka,[1] Asahito Hama,[1] Kenichi Koike,[10] and Seiji Kojima[1]

[1]Department of Pediatrics, Nagoya University Graduate School of Medicine, Nagoya, Japan; [2]Department of Hematology Oncology, Saitama Children's Medical Center, Saitama, Japan; [3]Department of Pediatrics, Tokyo Dental College Ichikawa General Hospital, Ichikawa, Japan; [4]Department of Pediatrics, National Defense Medical College, Tokorozawa, Japan; [5]Department of Pediatrics, St Marianna University School of Medicine, Kawasaki, Japan; [6]Department of Hematology/Oncology, Gunma Children's Medical Center, Shibukawa, Japan; [7]Department of Neuropsychopharmacology and Hospital Pharmacy, Nagoya University Graduate School of Medicine, Nagoya, Japan; [8]Department of Hematology and Oncology, Nagoya University Graduate School of Medicine, Nagoya, Japan; [9]Department of Pediatrics, Japanese Red Cross Nagoya First Hospital, Nagoya, Japan; and [10]Department of Pediatrics, Shinshu University School of Medicine, Matsumoto, Japan

Juvenile myelomonocytic leukemia (JMML) is a rare pediatric myeloid neoplasm characterized by excessive proliferation of myelomonocytic cells. Somatic mutations in genes involved in GM-CSF signal transduction, such as *NRAS*, *KRAS*, *PTPN11*, *NF1*, and *CBL*, have been identified in more than 70% of children with JMML. The present study, we report 2 patients with somatic mosaicism for oncogenic *NRAS* mutations (G12D and G12S) associated with the development of JMML. The mutated allele frequencies quantified by pyrosequencing were various and ranged from 3%-50% in BM and other somatic cells (ie, buccal smear cells, hair bulbs, or nails). Both patients experienced spontaneous improvement of clinical symptoms and leukocytosis due to JMML without hematopoietic stem cell transplantation. These patients are the first reported to have somatic mosaicism for oncogenic *NRAS* mutations. The clinical course of these patients suggests that *NRAS* mosaicism may be associated with a mild disease phenotype in JMML. (*Blood.* 2012;120(7):1485-1488)

Introduction

Juvenile myelomonocytic leukemia (JMML) is a rare myeloid neoplasm characterized by excessive proliferation of myelomonocytic cells. Somatic mutations in genes involved in GM-CSF signal transduction, such as *NRAS*, *KRAS*, *PTPN11*, *NF1*, and *CBL*, have been identified in more than 70% of children with JMML.[1-3] The term "somatic mosaicism" is defined as the presence of multiple populations of cells with distinct genotypes in one person whose developmental lineages trace back to a single fertilized egg.[4] Somatic mosaicism of various genes, including some oncogenes, has been implicated in many diseases. For example, somatic mosaicism for *HRAS* mutations is found in patients with Costello syndrome.[5-7] Whereas germline mutations in causative genes (ie, *PTPN11*, *NRAS*, *NF1*, and *CBL*) are found in JMML patients,[3,8-11] the presence of somatic mosaicism for these genes has never been reported. In the present study, we describe 2 cases of JMML in which the patients display somatic mosaicism for oncogenic *NRAS* mutations (G12D and G12S).

Study design

Written informed consent for sample collection was obtained from the patients' parents in accordance with the Declaration of Helsinki, and molecular analysis of the mutational status was approved by the ethics committee of the Nagoya University Graduate School of Medicine (Nagoya, Japan).

Patient 1. A 10-month-old boy had hepatosplenomegaly and leukocytosis (72.1 × 10^9/L) with monocytosis (13.3 × 10^9/L; Table 1). The patient's BM contained 7% blasts with myeloid hyperplasia. Cytogenetic analysis revealed a normal karyotype and colony assay of BM mononuclear cells (BM-MNCs) showed spontaneous colony formation but GM-CSF hypersensitivity assay was not tested. The diagnostic criteria for JMML, as developed by the European Working Group on Myelodysplastic Syndrome in Childhood, was fulfilled,[12] and the patient was treated with IFN-α and 6-mercaptopurine. His clinical and laboratory findings gradually resolved without hematopoietic stem cell transplantation. However, 11 years after the diagnosis of JMML, the patient developed thrombocytopenia (7.6 × 10^9/L) and BM findings showed trilineage dysplasia with low blast count compatible with refractory anemia. The patient did not have any physiologic abnormalities, such as facial deformity, and there was no family history of malignancy or congenital abnormalities.

Patient 2. A 10-month-old boy had anemia, hepatosplenomegaly, and leukocytosis (31.8 × 10^9/L) with monocytosis (6.4 × 10^9/L; Table 1). The patient's BM exhibited myeloid hyperplasia and granulocytic dysplasia with 5% blasts. Cytogenetic analysis revealed a normal karyotype. Colony assay of BM-MNCs showed spontaneous colony formation and GM-CSF hypersensitivity. Although the diagnostic criteria for JMML were fulfilled,[12] the patient's clinical symptoms and leukocytosis improved spontaneously within a few months without cytotoxic therapy or hematopoietic stem cell transplantation. The patient has remained healthy and has experienced no hematologic or physiologic abnormalities. The most recent follow-up examination was conducted when the patient was 8 years of age.

Detailed methods for experiments are described in supplemental Methods (available on the *Blood* Web site; see the Supplemental Materials link at the top of the online article).

Submitted February 3, 2012; accepted June 11, 2012. Prepublished online as *Blood* First Edition paper, July 2, 2012; DOI 10.1182/blood-2012-02-406090.

The online version of this article contains a data supplement.

The publication costs of this article were defrayed in part by page charge payment. Therefore, and solely to indicate this fact, this article is hereby marked "advertisement" in accordance with 18 USC section 1734.

From bloodjournal.hematologylibrary.org at MEDICAL LIBRARY OF NAGOYA UNIV on January 10, 2013. For personal use only.

Table 1. Patient characteristics

	Patient 1	Patient 2
Age, mo	10	10
Sex	Male	Male
Liver, cm	12	5
Spleen, cm	8	10
WBCs, × 10^9/L	72.1	31.8
Monocytes, %	18.5	20
Blasts, %	4	2
Hb, g/dL	8.9	5.4
Platelets, × 10^9/L	59	100
HbF, %	2.1	1.7
BM blasts, %	7	5
Karyotype	46,XY [20/20]	46,XY [20/20]
Monosomy 7 (FISH)	Negative	Negative
Spontaneous colony formation	Positive	Positive
Gene mutation	*NRAS*, G12D 35G > A	*NRAS*, G12S 34G > A
Treatment	IFN-α-2b, 6-MP	None
Observation period, mo	231	103
Outcome	Alive	Alive
Fraction of mutant alleles, % (pyrosequencing)		
Nail (whole)	24	12.5 (average)
Nail (left hand)	ND	26
Nail (right hand)	ND	13
Nail (left foot)	ND	8
Nail (right foot)	ND	3
Buccal smear cells	43	21
Hair bulbs	5	ND
Family studies		
Father	Wild-type	Wild-type
Mother	Wild-type	Wild-type
Sibling	ND	Wild-type

Hb indicates hemoglobin; 6-MP, 6-mercaptopurine; and ND, not done.

Results and discussion

DNA sequencing for JMML-associated genes (ie, *NRAS*, *KRAS*, *PTPN11*, and *CBL*) was performed (Figure 1 and Table 1). In Patient 1, the *NRAS* G12D mutation was identified in BM-MNCs at the time of diagnosis of both JMML and MDS. We identified the same G12D mutation in DNA derived from buccal smear cells and nails of both hands; however, the sequence profile of the nails showed a low signal for the mutant allele compared with signal of blood cells. In Patient 2, the *NRAS* G12S mutation was identified in DNA from BM-MNCs, buccal smear cells, and nails of the left hand. However, the sequence profiles of buccal smear cells and nails of the left hand showed a low signal for the mutant variant. No mutation was detected in DNA from the PB-MNCs of the patient's parents or sibling.

We used pyrosequencing to quantify the fraction of mutated alleles in DNA samples from different somatic tissues (Figure 1 and Table 1). The frequency of mutated alleles varied by tissue type as follows. For Patient 1: BM-MNCs, 50%; nails, 24%; buccal smear cells, 43%; and hair bulbs, 5%. For Patient 2: buccal smear cells, 21%; nails of left hand, 26%; nails of right hand, 13%; nails of left foot, 8%; and nails of right foot, 3%. We cloned the PCR product of *NRAS* exon 2 from the nails of Patient 1 and picked up 15 clones. The clones were sequenced. Four of the 15 clones (27%) contained the mutant allele, which is consistent with the results of pyrosequencing analysis (24% mutant allele). Because the confirmed detection level by pyrosequencing technique was above 5%, results with a low percentage (< 5%) of mutant allele (ie, hair bulbs in Patient 1) should be interpreted with caution.[13,14]

We diagnosed 2 JMML patients as having somatic mosaicism of *NRAS* mutations: G12D for Patient 1 and G12S for Patient 2. The diagnoses were based on negative familial studies and mutational allele quantification analyses that showed diversity in the chimeric mutational status of different somatic tissues. Although DNA from buccal smear cells might be contaminated with WBCs, we also identified mutations in DNA from the nail tissue, which is known to be a good biologic material without contamination from hematopoietic cells, in both patients. These data suggest that a portion of the *NRAS*-mutated somatic cells were derived from one cell that acquired the mutation at a very early developmental stage. Although both somatic and germline mutations of RAS pathway genes (ie, *PTPN11*, *NRAS*, *NF1*, and *CBL*) are found in some JMML patients,[3,8-11] somatic mosaicism for these genes has never been reported. To the best of our knowledge, the present study is

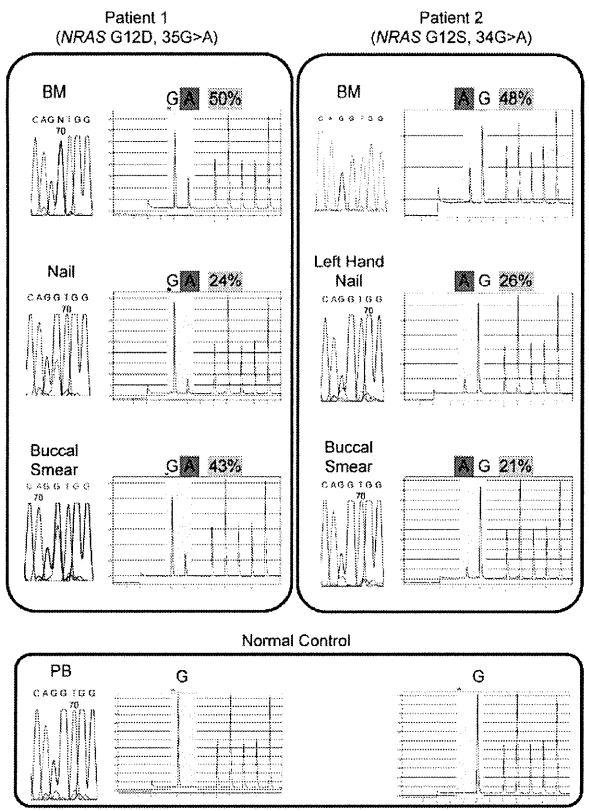

Figure 1. Direct sequencing and quantitative mutational analysis of *NRAS* in JMML patients. *NRAS* mutations are detected by direct sequencing and quantified by pyrosequencing. Direct sequencing identified oncogenic *NRAS* mutations: for Patient 1, G12D, 35G > A; for Patient 2, G12S, 34G > A) in BM-MNCs at diagnosis of JMML and in the nails and buccal smear cells. Quantification by pyrosequencing revealed that the fractions of mutated allele varied among different tissue types. For Patient 1: BM, 50%; nail, 24%; and buccal smear, 43%. For Patient 2: BM, 48%; left-hand nail, 26%; and buccal smear, 21%.

the first report of JMML patients with somatic mosaicism of mutations in RAS pathway genes.

Germline RAS pathway mutations are often associated with dysmorphic features similar to Noonan syndrome or its associated diseases. Correspondingly, JMML patients with germline *NRAS* or *CBL* mutations exhibit characteristic dysmorphic features.[3,10] Although our patients did not show any dysmorphic or developmental abnormalities, they should receive careful medical follow-up, especially for the occurrence of other cancers, because of the oncogenic nature of the mutations.

In general, JMML is a rapidly fatal disorder if left untreated.[8] However, recent clinical genotype-phenotype analyses have revealed heterogeneity in their clinical course. We and other researchers have reported that patients with *PTPN11* mutations have a worse prognosis than patients with other gene mutations, including *NRAS* and *KRAS*.[15,16] Both of the JMML patients in the present study with somatic mosaicism of oncogenic *NRAS* mutations have had a mild and self-limiting clinical course. We analyzed nails of other 3 JMML patients with RAS mutations who experienced aggressive clinical course and none showed somatic mosaicism (data not shown). In analogy to the mild phenotype of JMML patients with germline mutations in *PTPN11*, we speculate that JMML patients with somatic mosaicism of RAS genes might have a mild clinical course. We are planning to confirm these observations in larger cohort.

Acknowledgments

The authors thank Ms Yoshie Miura, Ms Yuko Imanishi, and Ms Hiroe Namizaki for their valuable assistance with sample preparation and clerical work.

Authorship

Contribution: S.D. and H.M. designed and conducted the research, analyzed the data, and wrote the manuscript; A.S., M.M.-E., M. Sato, H.K., A.K., M. Sotomatsu, and Y.H. treated the patients; Y.T., Y.F.-H., K.Y., H.H., H.K., N.Y., H.S., A.N., X.W., O.I., Y.X., N.N., M.T., A.H., and K.K. conducted the research; and S.K. designed the research, analyzed the data, and wrote the manuscript.

Conflict-of-interest disclosure: The authors declare no competing financial interests.

Correspondence: Seiji Kojima, Department of Pediatrics, Nagoya University Graduate School of Medicine, 65 Tsuruma-cho, Showa-ku, Nagoya 466-8550, Japan; e-mail: kojimas@med.nagoya-u.ac.jp.

References

1. Flotho C, Kratz CP, Niemeyer CM. How a rare pediatric neoplasia can give important insights into biological concepts: a perspective on juvenile myelomonocytic leukemia. *Haematologica*. 2007; 92(11):1441-1446.
2. Muramatsu H, Makishima H, Jankowska AM, et al. Mutations of an E3 ubiquitin ligase c-Cbl but not TET2 mutations are pathogenic in juvenile myelomonocytic leukemia. *Blood*. 2010;115(10): 1969-1975.
3. Niemeyer CM, Kang MW, Shin DH, et al. Germline CBL mutations cause developmental abnormalities and predispose to juvenile myelomonocytic leukemia. *Nat Genet*. 2010;42(9):794-800.
4. Cotterman CW. Somatic mosaicism for antigen A2. *Acta Genet Stat Med*. 1956;6(4):520-521.
5. Gripp KW, Stabley DL, Nicholson L, Hoffman JD, Sol-Church K. Somatic mosaicism for an HRAS mutation causes Costello syndrome. *Am J Med Genet A*. 2006;140(20):2163-2169.
6. Sol-Church K, Stabley DL, Demmer LA, et al. Male-to-male transmission of Costello syndrome: G12S HRAS germline mutation inherited from a father with somatic mosaicism. *Am J Med Genet A*. 2009;149A(3):315-321.
7. Girisha KM, Lewis LE, Phadke SR, Kutsche K. Costello syndrome with severe cutis laxa and mosaic HRAS G12S mutation. *Am J Med Genet A*. 2010;152A(11):2861-2864.
8. Niemeyer CM, Arico M, Basso G, et al. Chronic myelomonocytic leukemia in childhood: a retrospective analysis of 110 cases. European Working Group on Myelodysplastic Syndromes in Childhood (EWOG-MDS). *Blood*. 1997;89(10): 3534-3543.
9. Tartaglia M, Niemeyer CM, Fragale A, et al. Somatic mutations in PTPN11 in juvenile myelomonocytic leukemia, myelodysplastic syndromes and acute myeloid leukemia. *Nat Genet*. 2003; 34(2):148-150.
10. De Filippi P, Zecca M, Lisini D, et al. Germ-line mutation of the NRAS gene may be responsible for the development of juvenile myelomonocytic leukaemia. *Br J Haematol*. 2009;147(5):706-709.
11. Side LE, Emanuel PD, Taylor B, et al. Mutations of the NF1 gene in children with juvenile myelomonocytic leukemia without clinical evidence of neurofibromatosis, type 1. *Blood*. 1998;92(1): 267-272.
12. Pinkel D. Differentiating juvenile myelomonocytic leukemia from infectious disease [letter]. *Blood*. 1998;91(1):365-367.
13. Fakhrai-Rad H, Pourmand N, Ronaghi M. Pyrosequencing: an accurate detection platform for single nucleotide polymorphisms. *Hum Mutat*. 2002;19(5):479-485.
14. Ogino S, Kawasaki T, Brahmandam M, et al. Sensitive sequencing method for KRAS mutation detection by Pyrosequencing. *J Mol Diagn*. 2005; 7(3):413-421.
15. Bresolin S, Zecca M, Flotho C, et al. Gene expression-based classification as an independent predictor of clinical outcome in juvenile myelomonocytic leukemia. *J Clin Oncol*. 2010; 28(11):1919-1927.
16. Yoshida N, Yagasaki H, Xu Y, et al. Correlation of clinical features with the mutational status of GM-CSF signaling pathway-related genes in juvenile myelomonocytic leukemia. *Pediatr Res*. 2009;65(3):334-340.

From bloodjournal.hematologylibrary.org at MEDICAL LIBRARY OF NAGOYA UNIV on January 10, 2013. For personal use only.

The EMBO Journal (2012) 00, 1–13 | © 2012 European Molecular Biology Organization | All Rights Reserved 0261-4189/12
www.embojournal.org

THE EMBO JOURNAL

Histone chaperone activity of Fanconi anemia proteins, FANCD2 and FANCI, is required for DNA crosslink repair

Koichi Sato[1,7], Masamichi Ishiai[2,7], Kazue Toda[1], Satoshi Furukoshi[1], Akihisa Osakabe[1], Hiroaki Tachiwana[1], Yoshimasa Takizawa[1], Wataru Kagawa[1], Hiroyuki Kitao[2,3], Naoshi Dohmae[4], Chikashi Obuse[5], Hiroshi Kimura[6], Minoru Takata[2,*] and Hitoshi Kurumizaka[1,*]

[1]Laboratory of Structural Biology, Graduate School of Advanced Science and Engineering, Waseda University, Tokyo, Japan, [2]Laboratory of DNA Damage Signaling, Department of Late Effects Studies, Radiation Biology Center, Kyoto University, Kyoto, Japan, [3]Graduate School of Medical Sciences, Department of Molecular Oncology, Kyushu University, Fukuoka, Japan, [4]RIKEN Advanced Science Institute, Saitama, Japan, [5]Graduate School of Life Science, Hokkaido University, Hokkaido, Japan and [6]Graduate School of Frontier Biosciences, Osaka University, Osaka, Japan

Fanconi anaemia (FA) is a rare hereditary disorder characterized by genomic instability and cancer susceptibility. A key FA protein, FANCD2, is targeted to chromatin with its partner, FANCI, and plays a critical role in DNA crosslink repair. However, the molecular function of chromatin-bound FANCD2-FANCI is still poorly understood. In the present study, we found that FANCD2 possesses nucleosome-assembly activity *in vitro*. The mobility of histone H3 was reduced in FANCD2-knockdown cells following treatment with an interstrand DNA crosslinker, mitomycin C. Furthermore, cells harbouring FANCD2 mutations that were defective in nucleosome assembly displayed impaired survival upon cisplatin treatment. Although FANCI by itself lacked nucleosome-assembly activity, it significantly stimulated FANCD2-mediated nucleosome assembly. These observations suggest that FANCD2-FANCI may regulate chromatin dynamics during DNA repair.

The EMBO Journal advance online publication, 24 July 2012; doi:10.1038/emboj.2012.197

Subject Categories: genome stability & dynamics; chromatin & transcription

Keywords: DNA repair; FANCD2; FANCI; Fanconi anaemia; histone chaperone

*Corresponding authors. M Takata, Laboratory of DNA Damage Signaling, Radiation Biology Center, Kyoto University, Yoshida-konoe, Sakyo-ku, Kyoto 606-8501, Japan. Tel.: +81 75 753 7563; Fax: +81 75 753 7565; E-mail: mtakata@house.rbc.kyoto-u.ac.jp
or H Kurumizaka, Laboratory of Structural Biology, Graduate School of Advanced Science and Engineering, Waseda University, 2-2 Wakamatsu-cho, Shinjuku-ku, Tokyo 162-8480, Japan. Tel.: +81 3 5369 7315; Fax: +81 3 5367 2820; E-mail: kurumizaka@waseda.jp
[7]These authors contributed equally to this work

Received: 17 June 2012; accepted: 3 July 2012

Introduction

Fanconi anaemia (FA) is a rare hereditary disorder characterized by skeletal abnormalities, progressive bone marrow failure, and genomic instability accompanied by cancer susceptibility (Venkitaraman, 2004; Niedernhofer *et al*, 2005; Taniguchi and D'Andrea, 2006; Wang, 2007). FA-mutant cells are highly sensitive to interstrand DNA crosslinking reagents, which induce stalled replication forks, suggesting that FA proteins promote the stabilization and restarting of the replisome (Thompson *et al*, 2005; Wang, 2007).

Thirteen genes, *FANCA*, *-B*, *-C*, *-D1* (*BRCA2*), *-D2*, *-E*, *-F*, *-G*, *-I*, *-J* (*BRIP1*), *-L*, *-M*, and *-N* (*PALB2*), corresponding to individual FA complementation groups, have been cloned (Thompson *et al*, 2005; Wang, 2007; Kee and D'Andrea, 2010; Garner and Smogorzewska, 2011; Kitao and Takata, 2011). In addition, homozygous Rad51C mutations have recently been identified in a family with an FA-like disorder, as the *FANCO* gene (Vaz *et al*, 2010), and *SLX4* has been confirmed as the *FANCP* gene (Crossan *et al*, 2011; Kim *et al*, 2011; Stoepker *et al*, 2011). These FA gene products constitute a common DNA damage response pathway that is often referred to as the 'FA pathway'. In this pathway, eight proteins, FANCA, -B, -C, -E, -F, -G, -L, and -M, and three FANCA-associated polypeptides (FAAPs) form the FA core E3 ligase complex (Garcia-Higuera *et al*, 2001; Wang, 2007; Ali *et al*, 2012; Kim *et al*, 2012; Leung *et al*, 2012). On the other hand, FANCD2 and FANCI associate with each other to form a different complex, called the ID complex (Sims *et al*, 2007; Smogorzewska *et al*, 2007).

Upon DNA damage during S-phase, multiple phosphorylations of FANCI trigger the monoubiquitination of FANCD2 and FANCI by the FA core complex (Ishiai *et al*, 2008). The monoubiquitinated ID complex is then targeted to the chromatin, where it plays a critical role in DNA-repair pathways, such as homologous recombination and translesion synthesis (Matsushita *et al*, 2005; Thompson *et al*, 2005; Yamamoto *et al*, 2005; Wang, 2007; Kee and D'Andrea, 2010; Garner and Smogorzewska, 2011; Kitao and Takata, 2011). Recent studies indicated that monoubiquitinated FANCD2 (and FANCI) recruit the FAN1 nuclease, which possesses endo- and exonuclease activities, providing a partial explanation for their roles in DNA repair (Kratz *et al*, 2010; MacKay *et al*, 2010; Smogorzewska *et al*, 2010; Yoshikiyo *et al*, 2010). Monoubiquitinated FANCD2 also reportedly recruits SLX4 (Garner and Smogorzewska, 2011; Yamamoto *et al*, 2011), which is considered to function as a scaffold that interacts with the other nucleases, SLX1, XPF, and MUS81 (Fekairi *et al*, 2009; Svendsen *et al*, 2009; Yamamoto *et al*, 2011). Furthermore, a recent report found that FANCD2 itself might have exonuclease activity (Pace *et al*, 2010). However, whether chromatin-bound FANCD2 and FANCI have any additional functions remains to be determined.

The nucleosome is the fundamental repeating unit of chromatin (Wolffe, 1998). Four core histones, H2A, H2B, H3, and H4, are the protein components of the nucleosome. H2A forms a specific dimer with H2B (H2A/H2B dimer), and H3 forms a specific dimer with H4 (H3/H4 dimer). During nucleosome assembly, two H3/H4 dimers (H3/H4 tetramer) are first deposited on DNA, forming a tetrasome, in which the DNA is wrapped around the H3/H4 tetramer. Two H2A/H2B dimers are then incorporated into the tetrasome to form the mature nucleosome, in which about 150 base pairs of DNA are wrapped around a histone octamer, containing two each of the H2A/H2B and H3/H4 dimers. In cells, nucleosomes are dynamically assembled and disassembled during the replication, transcription, recombination, and repair processes, and such nucleosome dynamics are accomplished with the aid of histone chaperones and/or ATP-dependent chromatin remodelling factors (Avvakumov *et al*, 2011).

In the present study, we purified the human and chicken FANCD2 proteins, and found that FANCD2 possesses nucleosome-assembly activity *in vitro*. We also purified FANCI, and showed that it significantly stimulated FANCD2-mediated nucleosome assembly, although FANCI itself lacked nucleosome-assembly activity. A histone-binding domain was mapped in the chicken FANCD2 C-terminal region (residues 1268–1439). The FANCD2 mutants, in which either the histone-binding domain was deleted or the Arg1336 and Lys1346 residues were replaced by Ala, were significantly defective in nucleosome assembly *in vitro*, and cells bearing these mutants displayed impaired survival upon cisplatin treatment *in vivo*. Furthermore, a disease-related mutation, human FANCD2(R302W) (Timmers *et al*, 2001), compromised histone dynamics, and the corresponding chicken FANCD2(R305W) also showed impaired histone chaperone activity. These data suggest that the histone chaperone activity of FANCD2 is crucial for the histone dynamics and the DNA crosslink repair in cells.

Results

Human FANCD2 promotes nucleosome assembly

In a proteome analysis to search for proteins in HeLa cell extracts that bind to the histone H3/H4 complex (Supplementary Figure S1), we unexpectedly detected human FANCD2 (hFANCD2) as a candidate interacting protein. Indeed, hFANCD2 was efficiently captured from a HeLa cell extract, using H3/H4 beads (Figure 1A). We purified hFANCD2 as a recombinant protein expressed in insect cells (Supplementary Figure S2A), and confirmed that purified hFANCD2 also bound to H3/H4 (Figure 1B). The hFANCD2-H3/H4 binding was also detected in the presence of DNaseI (Figure 1B, lane 5), indicating that the interaction is not mediated by DNA contamination. These results indicated that hFANCD2 directly binds to H3/H4, which prompted us to examine its nucleosome-assembly activity.

We tested hFANCD2-mediated nucleosome assembly by a topological assay, using relaxed circular DNA in the presence of topoisomerase (Figure 1C). The extent of nucleosome formation was assessed by analysing the superhelicity of circular DNA fractionated through an agarose gel, because negative supercoils are introduced when nucleosomes are formed. As shown in Figure 1C, the number of superhelical turns in the DNA substrate increased with greater amounts of hFANCD2. The faster migration of the DNA substrate was not due to DNA degradation (Supplementary Figure S2B). Therefore, hFANCD2 actually promoted nucleosome assembly *in vitro*. We next performed the nucleosome-assembly assay with a short DNA fragment, to directly detect the nucleosomes by an electrophoretic mobility shift assay. hFANCD2 stimulated the nucleosome assembly in this assay (Figure 1D, lanes 6–9). The nucleosome-assembly activity of hFANCD2 was slightly lower than that of human Nap1, which is a prominent nucleosome-assembly protein (Figure 1D). These biochemical results suggest that FANCD2 may regulate chromatin reorganization during DNA repair in higher eukaryotes.

Chromatin-bound FANCD2 is known to be monoubiquitinated, and the ubiquitin moiety may function to recruit its associated nucleases (Fekairi *et al*, 2009; Svendsen *et al*, 2009; Kratz *et al*, 2010; MacKay *et al*, 2010; Smogorzewska *et al*, 2010; Yoshikiyo *et al*, 2010; Yamamoto *et al*, 2011). Therefore, we tested whether FANCD2 monoubiquitination affects the nucleosome-assembly activity. For this purpose, we utilized the chicken FANCD2 protein (cFANCD2) (Yamamoto *et al*, 2005), which was bacterially expressed and purified to homogeneity (Supplementary Figure S2C). We then prepared monoubiquitinated cFANCD2, using purified components for the conjugation (i.e., FANCL, UBE2T, E1, and ubiquitin; Supplementary Figure S2D–F). As we previously reported, the cFANCD2 monoubiquitination was robustly enhanced in the presence of DNA (Sato *et al*, 2012), and about 40% of cFANCD2 was monoubiquitinated in this study (Supplementary Figure S2F). This monoubiquitinated cFANCD2 fraction was purified, and was subjected to the topological assay. However, we did not find a clear difference in the nucleosome-assembly activities between the fractions containing monoubiquitinated cFANCD2 and the monoubiquitination-deficient cFANCD2(K563R) mutant (Supplementary Figure S2G). Therefore, the monoubiquitination does not affect the activity. However, this could be due to the incomplete monoubiquitination of cFANCD2. Therefore, we prepared the monoubiquitination-mimicking version of FANCD2, by genetically fusing FANCD2(K563R) with ubiquitin to create FANCD2(K563R)-Ub (Supplementary Figure S2H), which is known to complement the DNA-repair-defective phenotype in the *FANCD2*$^{-/-}$ DT40 cells (Matsushita *et al*, 2005). We found that purified FANCD2(K563R)-Ub possessed similar histone-binding and nucleosome-assembly activities to those of cFANCD2 (Supplementary Figure S2I and J). These results suggested that the FANCD2 monoubiquitination may not be directly involved in the nucleosome assembly.

The C-terminal region of FANCD2 is responsible for interacting with histone H3/H4 and for promoting nucleosome assembly

To gain further insights into the molecular mechanism and the functional relevance of the nucleosome-assembly activity of FANCD2, we first searched for the FANCD2 region that interacts with the H3/H4 complex. We subjected cFANCD2 to limited proteolysis, and two fragments, cFANCD2(1-1167) and cFANCD2(1-1389), were identified (Figure 2A). These fragments lacked the acidic region, which is composed of the C-terminal 50 amino-acid residues of FANCD2. In addition, FANCD2(1268X), which also lacks the C-terminal region, is present in FA patients (FA Mutation Database, http://www.rockefeller.edu/fanconi/mutate/), suggesting the functional

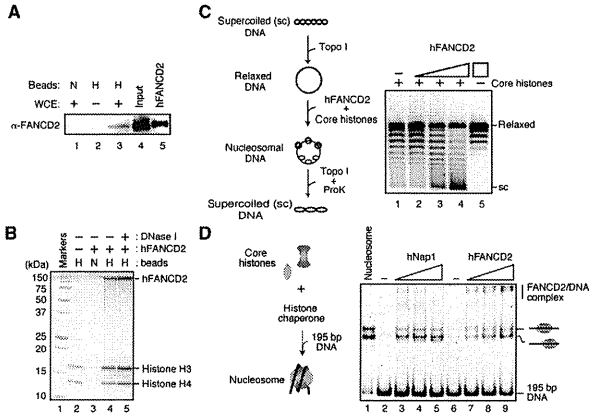

Figure 1 hFANCD2 promotes nucleosome assembly. (**A**) The H3/H4-conjugated beads were incubated with a HeLa WCE, and the endogenous FANCD2 bound to the beads was detected by western blotting with an anti-FANCD2 monoclonal antibody (α-FANCD2). N and H indicate the control Affi-Gel 10 beads and the H3/H4-conjugated beads, respectively. Input WCE (30 μg of protein) and hFANCD2 (125 ng) were applied in lanes 4 and 5, respectively. (**B**) The H3/H4 beads were incubated with purified hFANCD2 in the absence or presence of DNaseI, washed with buffer, and mixed with two-fold SDS sample buffer. The proteins bound to the beads were analysed by 15% SDS–PAGE. (**C**) Topological assay. A schematic diagram of topological assay is shown in the left panel. Nucleosomes were reconstituted on the relaxed plasmid DNA by hFANCD2 (0.2, 0.5, and 0.9 μM), in the presence of wheat germ topoisomerase I. After deproteinization, the topoisomers were separated by agarose gel electrophoresis. Highly supercoiled and relaxed DNAs are denoted as 'sc' and 'relaxed', respectively. (**D**) Nucleosome-assembly assay. A schematic diagram of the nucleosome-assembly assay is shown in the left panel. Nucleosomes were reconstituted on the linear 195 base-pair DNA by hNap1 (0.4, 0.8, and 1.6 μM) or hFANCD2 (0.2, 0.4, and 0.8 μM). Nucleosomes positioned at the edge and centre of the 195-bp DNA are indicated by cartoons on the right side of the panel.

importance of the FANCD2 C-terminal region. As histone chaperones are generally acidic, we investigated whether this acidic C-terminal region is essential for histone binding. The C-terminal deletion mutants, cFANCD2(1-1167), cFANCD2(1-1267), and cFANCD2(1-1389), were expressed as GFP-tagged forms in HEK293T cells, and their H3/H4-binding activity was examined by a pull-down assay, using the H3/H4 beads. We found that cFANCD2(1-1167) and cFANCD2(1-1267) displayed diminished H3/H4 binding (Figure 2B, lanes 3 and 4). In contrast, cFANCD2(1-1389) retained residual H3/H4-binding activity (Figure 2B, lane 2). Consistently, cFANCD2(1-1167) and cFANCD2(1-1267) showed significant defects in nucleosome assembly (Figure 2C, lanes 13–17 and 18–22, and D; Supplementary Figure S3A). cFANCD2(1-1389) was completely proficient in the nucleosome-assembly activity under low protein concentration conditions (Figure 2C, lanes 8–12, and D; Supplementary Figure S3B). These observations suggest that the C-terminal region of FANCD2 (amino acids 1268–1389) is important for interacting with H3/H4 and for promoting nucleosome assembly. It should be noted that cFANCD2(1-1389) was defective in nucleosome assembly under high protein concentration conditions (Figure 2C, lanes 10–11, and D; Supplementary Figure S3C). This may reflect the biochemical property of cFANCD2(1-1389), which tends to form large protein–DNA aggregates that are unable to enter an agarose gel during electrophoresis (Supplementary Figure S3D).

Since the cFANCD2 C-terminal deletion may induce the improper folding of the cFANCD2 structure, we next performed the H3/H4-binding and nucleosome-assembly experiments with cFANCD2 point mutants. Based on the amino-acid conservation among the human, mouse, chicken, frog, fish, and fly FANCD2 proteins, we mutated the conserved amino-acid residues, which might be functionally important (Figure 2A). We found that the FANCD2(R1336A/K1346A) mutant, in which the Arg1336 and Lys1346 residues are replaced by Ala, was significantly defective in nucleosome assembly *in vitro*, while another mutant, cFANCD2(D1350A/E1365A/E1382A), in which the Asp1350, Glu1365, and Glu1382 residues are replaced by Ala, did not affect the nucleosome-assembly activity (Figure 2A, E, and F; Supplementary Figure S3E). Consistently, the histone-binding activity was substantially reduced in cFANCD2(R1336A/K1346A) (Figure 2B lane 11), but not in cFANCD2(D1350A/E1365A/E1382A) (Figure 2B, lane 10). These results strongly support the conclusion that FANCD2 promotes nucleosome assembly through its C-terminal histone-binding domain.

Finally, we tested the histone binding of the C-terminal cFANCD2 fragments, cFANCD2(669-1439) and cFANCD2(953-1439), which contain the C-terminal amino-acid residues 669-1439 and 953-1439, respectively (Figure 2A). These cFANCD2 fragments were identified by a protease mapping experiment. As expected, the cFANCD2(669-1439) and cFANCD2(953-1439) fragments both efficiently bound to histones (Figure 2B, lanes 5 and 6). Surprisingly, cFANCD2(953-1439), which contained only one-third of cFANCD2, promoted nucleosome assembly (Figure 2C, lanes 23–27, and D). Therefore, we concluded that the histone-binding domain is located in the C-terminal region of FANCD2.

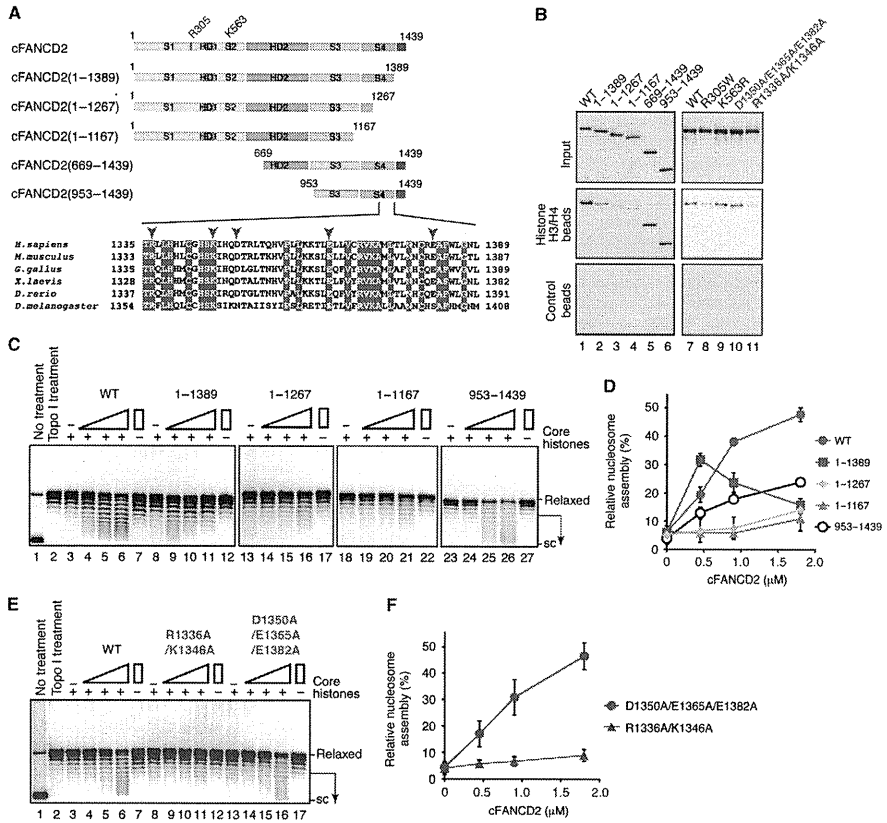

Figure 2 The C-terminal region of FANCD2 is responsible for histone binding and nucleosome assembly. (**A**) Schematic representations of full-length cFANCD2, and the cFANCD2(1-1389), cFANCD2(1-1267), cFANCD2(1-1167), cFANCD2(669-1439), and cFANCD2(953-1439) deletion mutants. The cFANCD2 domains, solenoid 1, helical domain 1, solenoid 2, helical domain 2, solenoid 3, and solenoid 4, are denoted as S1, HD1, S2, HD2, S3, and S4, respectively (Joo *et al*, 2011). The FANCD2 C-terminal acidic region is coloured red. The amino-acid sequences of the C-terminal regions of the *Homo sapiens*, *Mus musculus*, *Gallus gallus*, *Xenopus laevis*, *Danio rerio*, and *Drosophila melanogaster* FANCD2 proteins are aligned. The highly conserved residues are coloured red. The mutated residues in cFANCD2(R1336A/K1346A) and cFANCD2(D1350A/E1365A/E1382A) are indicated by orange and purple arrowheads, respectively. (**B**) The H3/H4 beads were incubated with extracts of HEK293T cells, producing either GFP-tagged cFANCD2, cFANCD2(1-1389), cFANCD2(1-1267), cFANCD2(1-1167), cFANCD2(669-1439), cFANCD2(953-1439), cFANCD2(R305W), cFANCD2(K563R), cFANCD2(D1350A/E1365A/E1382A), or cFANCD2(R1336A/K1346A). Proteins bound to the beads were detected by western blotting with an anti-chFANCD2 (polyclonal) antibody. The bottom panel indicates negative control experiments with beads lacking histones. (**C**) Nucleosomes were reconstituted on the relaxed plasmid DNA by cFANCD2 (lanes 3–7), cFANCD2(1-1389) (lanes 8–12), cFANCD2(1-1267) (lanes 13–17), cFANCD2(1-1167) (lanes 18–22), and cFANCD2(953-1439) (lanes 23–27) in the presence of wheat germ topoisomerase I. After deproteinization, the topoisomers were separated by agarose gel electrophoresis with ethidium bromide staining. The cFANCD2 concentrations were 0, 0.45, 0.90, and 1.8 μM. Highly supercoiled and relaxed DNAs are denoted as 'sc' and 'relaxed', respectively. (**D**) Graphic representation of nucleosome-assembly activities of the cFANCD2 mutants shown in **C**. Representative images are shown in **C**. The supercoiled DNA fractions were generated by nucleosome assembly in the presence of cFANCD2, and the intensities of the bands indicated by the arrows in **C** were quantitated by an LAS-4000 Image Analyser (GE Healthcare). Means of three independent experiments are shown with s.d.'s. (**E**) Nucleosomes were reconstituted on the relaxed plasmid DNA by cFANCD2 (lanes 3–7), cFANCD2(R1336A/K1346A) (lanes 8–12), and cFANCD2(D1350A/E1365A/E1382A) (lanes 13–17) in the presence of wheat germ topoisomerase I. The cFANCD2 concentrations were 0, 0.45, 0.90, and 1.8 μM. Highly supercoiled and relaxed DNAs are denoted as 'sc' and 'relaxed', respectively. (**F**) Graphical representation of the nucleosome-assembly activities of the cFANCD2 mutants shown in **E**. Representative images are shown in **E**. The supercoiled DNA fractions were generated by nucleosome assembly in the presence of cFANCD2, and the intensities of the bands indicated by the arrows in **E** were quantitated by an LAS-4000 Image Analyser (GE Healthcare). Means of three independent experiments are shown with s.d.'s.

FANCD2 mediates histone mobilization in living cells in a DNA damage-dependent manner

To determine whether FANCD2 plays a role in histone dynamics in living cells during DNA repair, we knocked down hFANCD2 in HeLa cells expressing histone H3-GFP (Kimura and Cook, 2001), using small inhibitory RNA (siRNA). Three days after the transfection of the specific siRNA, the level of hFANCD2 had decreased substantially, to <10% of the normal level (Supplementary Figure S4A and B). Using these cells, the mobility of H3 was analysed by fluorescence recovery after photobleaching (FRAP) (Kimura *et al*, 2006). The recovery kinetics (the curve shapes) of the exchanging fractions were similar in the hFANCD2-knockdown and control cells (Figure 3A), suggesting that hFANCD2 does not play a major role in H3 assembly or exchange under normal conditions. As FA-mutant cells display significant sensitivity to interstrand DNA crosslinking reagents, such as mitomycin C (MMC) (Niedernhofer *et al*, 2005; Thompson *et al*, 2005; Wang, 2007; Kee and D'Andrea, 2010; Garner and Smogorzewska, 2011; Kitao and Takata, 2011), we next tested the effect of MMC on the H3 mobility in the hFANCD2-knockdown HeLa cells. Interestingly, the recovery of H3-GFP in the hFANCD2-knockdown cells was clearly slower in the presence of MMC (Figure 3B). Similar results were obtained with a different FANCD2-specific siRNA (Supplementary Figure S4C). The slower H3-GFP exchange observed in the MMC-treated FANCD2-knockdown cells could be due to a different cell cycle distribution, since the FA-deficient cells may be arrested at S and/or G2 due to the deficiency of DNA crosslink repair. We therefore performed FRAP experiments in cells stably expressing both H3-GFP and mCherry-tagged PCNA, which shows characteristic patterns representing replication and repair foci (Leonhardt *et al*, 2000). We first examined the mobility of H3-GFP in different cell cycle stages under the normal growth conditions. The H3-GFP mobility in PCNA foci-positive (S-phase) cells did not differ from that in PCNA foci-negative cells (Figure 3C). In the presence of MMC, the PCNA foci-positive cells were indeed enriched by the hFANCD2 knockdown, but the mobility of H3-GFP was still slower than that in the MMC-treated PCNA foci-positive control cells (Figure 3D; Supplementary Figure S4D). Therefore, the reduced histone H3 mobility in the MMC-treated hFANCD2-knockdown cells does not appear to be attributable to a difference in the cell cycle phase. Furthermore, the slower H3-GFP recovery in the presence of MMC was also detected in the hFANCA-knockdown cells, in which the damage-dependent focus formation of hFANCD2 on chromosomes was significantly inhibited (Supplementary Figure S4E–H). These data suggest that hFANCD2 may mediate nucleosome assembly and/or histone exchange in human cells, in a damage-dependent manner.

The C-terminal histone-binding region of FANCD2 is important for the DNA repair mediated by the FA pathway

To determine whether the histone assembly activity levels of the FANCD2 mutants *in vitro* correlate with their DNA-repair activities *in vivo*, we expressed them in *FANCD2*$^{-/-}$ DT40 cells, and exposed the cells to cisplatin in a colony survival assay. As shown in Figure 4A, full-length cFANCD2, cFANCD2(1-1389), and cFANCD2(D1350A/E1365A/E1382A) rescued the cisplatin-sensitive phenotype of the *cFANCD2*$^{-/-}$ cells, in contrast to cFANCD2(1-1167), cFANCD2(1-1267),

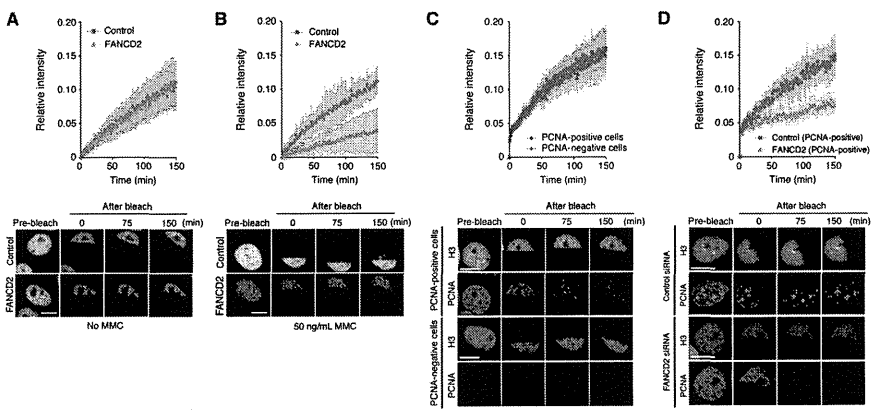

Figure 3 Histone H3 mobility is decreased in FANCD2-knockdown cells in the presence of a DNA crosslinking reagent. (**A**, **B**) FRAP with HeLa cells. Three days after the transfection of hFANCD2-siRNA or control RNA, the mobility of histone H3-GFP was analysed by bleaching one-half of a nucleus in the absence (**A**) or presence (**B**) of 50 ng/ml MMC for 12–18 h. The mean of the relative fluorescence intensity with the s.d. (n = 10–11) and examples are shown. (**C**) FRAP with HeLa cells stably expressing mCherry-PCNA. Three days after the transfection of control RNA, the mobility of histone H3-GFP was analysed in the absence of MMC. The PCNA foci-positive (S-phase) cells were identified by the characteristic mCherry-PCNA distribution. The mean of the relative fluorescence intensity with the s.d. (n = 10–14) and examples are shown. (**D**) FRAP with MMC-treated HeLa cells expressing H3-GFP and mCherry-PCNA in S-phase. Three days after the transfection of hFANCD2-siRNA or control RNA, the mobility of histone H3-GFP in the PCNA foci-positive (S-phase) cells was analysed in the presence of 50 ng/ml MMC. The mean of the relative fluorescence intensity with the s.d. (n = 10–18) and examples are shown. Bars: 10 μm.

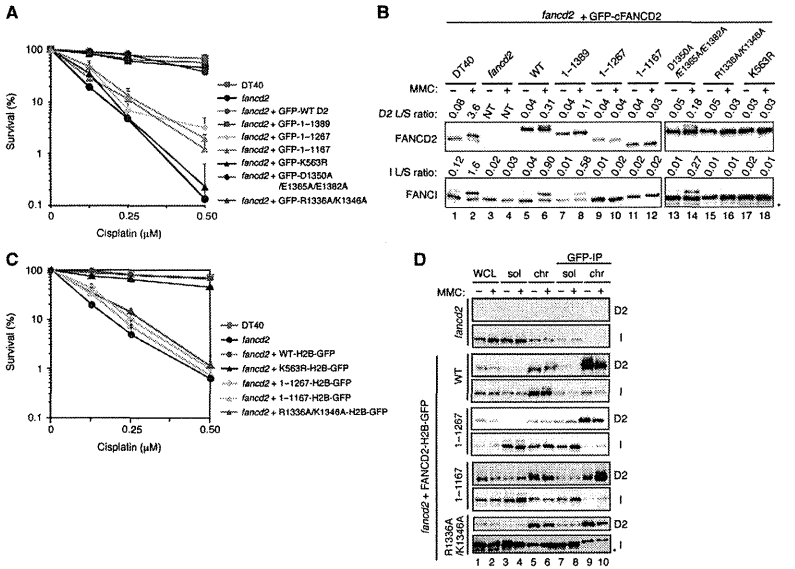

Figure 4 DNA-repair defects in the cFANCD2 C-terminal mutants. (**A**) Colony survival assay of the *cFANCD2*$^{-/-}$ DT40 cells expressing GFP fusions with the wild-type (WT) and indicated cFANCD2 mutants in the presence of cisplatin. The mean and s.d. of measurements performed in triplicate are shown. (**B**) FANCD2/FANCI monoubiquitination in *cFANCD2*$^{-/-}$ cells expressing the indicated cFANCD2 mutants. Cells were treated with or without MMC, and the WCEs were subjected to western blotting. The bands detected just above the original bands (S-forms) correspond to the monoubiquitinated forms (L-forms) of cFANCD2 and cFANCI (lanes 2, 6, 8, and 14). The L-form and S-form bands were quantitated with the Image J software, and the L/S ratios are indicated just above each panel. An asterisk indicates the non-specific bands. ND: not detectable. (**C**) Colony survival assay of the *cFANCD2*$^{-/-}$ cells expressing H2B-GFP fusions with the WT and indicated cFANCD2 mutants in the presence of cisplatin. The mean and s. d. of measurements performed in triplicate are shown. (**D**) Chromatin targeting of cFANCD2 (WT)-H2B, cFANCD2(1-1167)-H2B, cFANCD2(1-1267)-H2B, and cFANCD2(R1336A/K1346A)-H2B. Negative control experiments in the absence of exogenously expressed cFANCD2 are shown in the top panel. The *cFANCD2*$^{-/-}$ cells expressing the indicated proteins were treated with MMC (500 ng/ml, 6 h) or left untreated and then fractionated. Each fraction was separated by SDS–PAGE, and western blotting was performed using anti-cFANCD2 and anti-cFANCI antibodies. An asterisk indicates the non-specific band.

and cFANCD2(R1336A/K1346A). To ensure the chromatin targeting of these cFANCD2 mutants, we repeated this assay with the cFANCD2 mutants expressed as fusions with histone H2B, since cFANCD2(1-1167), cFANCD2(1-1267), and cFANCD2(R1336A/K1346A) were not monoubiquitinated (Figure 4B), probably due to the weakened interaction with FANCL, which was identified as the catalytic E3 subunit for FANCD2 monoubiquitination (Meetei *et al*, 2003) (Supplementary Figure S5A). We confirmed that the fusion of H2B to cFANCD2 and cFANCD2(1-1267) did not affect their nucleosome-assembly activities (Supplementary Figure S5B–E). Although substantial amounts of cFANCD2(1-1167)-H2B, cFANCD2(1-1267)-H2B, and cFANCD2(R1336A/K1346A)-H2B were detected at the chromatin (Figure 4D), the mutants still could not complement the cisplatin sensitivity of *cFANCD2*$^{-/-}$ cells, in contrast to the H2B fusion proteins with the full-length cFANCD2 and cFANCD2(K563R), bearing a point mutation at the monoubiquitination site (K563R) (Figure 4C) (Matsushita *et al*, 2005). These results strongly suggest that the nucleosome-assembly activity, which depends on the C-terminal region of FANCD2, might be crucial for the DNA repair mediated by the FA pathway. Notably, these cFANCD2 mutants were able to interact with the cFANCI protein in chromatin, as detected by anti-GFP immunoprecipitation followed by western blotting (Figure 4D), and as further supported by the results of *in vitro* binding experiments (Supplementary Figure S7F–H).

A disease-related FA mutant, human FANCD2(R302W), and its chicken counterpart, cFANCD2(R305W), are monoubiquitinated but do not facilitate histone exchange

As shown in Figure 4B, the C-terminally deleted or point FANCD2 mutants, which were defective in nucleosome assembly, were also defective in monoubiquitination, probably due to their weakened interactions with FANCL (Supplementary Figure S5A). This suggested that the histone-binding and FANCL-binding regions may partially overlap. To provide evidence that the FANCD2 histone-chaperone activity functions in DNA repair independently of its monoubiquitination, a FANCD2 mutant, in which the histone-chaperone and monoubiquitination activities are separated, would be useful.

We reasoned that such mutations might be found outside the putative histone-binding site. We found that the chicken FANCD2 R305W mutation (Arg305 to Trp), which corresponds to a disease-related mutation (human FANCD2 R302W) in FA (Timmers *et al*, 2001), is such a separation mutation. cFANCD2(R305W) exhibited reduced histone binding (Figure 2B, lane 8), and was defective in the nucleosome-assembly activity (Figure 5A and B). In contrast, cFANCD2(R305W) was proficient in its monoubiquitination (Figure 5C) and chromatin-targeting activities (Supplementary Figure S6A). Interestingly, cFANCD2(R305W) was moderately defective in the repair of DNA damage induced by cisplatin (Figure 5D), although its binding to cFANCI was proficient *in vivo* (Supplementary Figure S6A) and *in vitro* (Supplementary Figure S7E). The DNA-repair deficiency was also observed when H2B-fused cFANCD2(R305W) was expressed in the *cFANCD2*$^{-/-}$ cells (Figure 5E). These results indicated that the DNA-repair defect observed in the *cFANCD2*$^{-/-}$ cells expressing cFANCD2(R305W) may be accounted for by the defective histone chaperone activity of cFANCD2(R305W). Therefore, the histone chaperone activity of FANCD2 may be required in the steps after the FANCD2 monoubiquitination and chromatin targeting, during DNA repair by the FA pathway (Figure 8B).

To test whether the histone chaperone activity of FANCD2 functions in histone dynamics in living cells, we expressed mCherry-tagged hFANCD2, hFANCD2(R302W), or hFANCD2 (K561R) in H3-GFP-expressing HeLa cells, in which the endogenous hFANCD2 was knocked down by siRNA (Supplementary Figure S6B). We compared the H3-GFP mobility between mCherry-positive and -negative cells. The mobility of H3-GFP was efficiently restored with the expression of wild-type (WT) hFANCD2 (Figure 6A), but not with the monoubiquitination-deficient hFANCD2(K561R) mutant (Figure 6B, top panel), consistent with its chromatin-targeting deficiency (diffusing within the nucleus; Figure 6B, bottom panels). Interestingly, hFANCD2(R302W) also failed to restore the H3-GFP mobility (Figure 6C, top panel), although its chromatin targeting was not defective (forming nuclear foci like the WT hFANCD2; Figure 6C, bottom panels). Together with the DNA-repair deficiency of the *cFANCD2*$^{-/-}$ cells expressing cFANCD2(R305W), these results support the view that the histone-chaperone activity of FANCD2 is important in the DNA repair by the FA pathway. It should be noted that the VU008 patient cell line, which has the hFANCD2(R302W) mutation, produces the mutant hFANCD2 protein at extremely low levels (Timmers *et al*, 2001). Therefore, both defective histone-chaperone activity

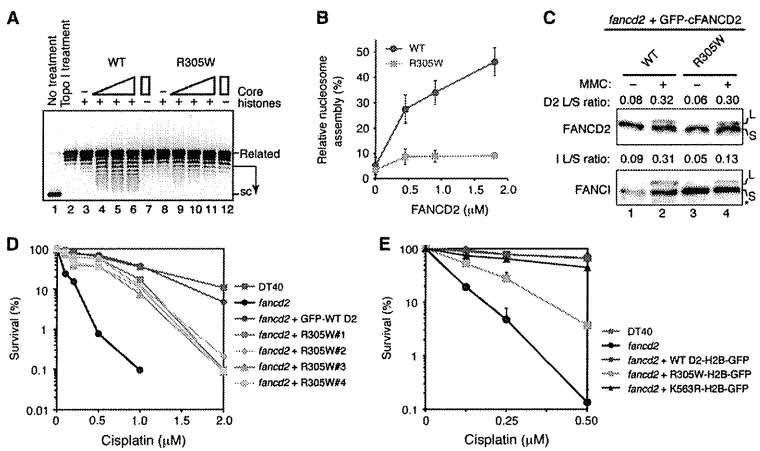

Figure 5 An FA-related mutant, cFANCD2(R305W), is defective in nucleosome-assembly activity and DNA repair. (**A**) Nucleosomes were reconstituted on the relaxed plasmid DNA by cFANCD2 (lanes 3–7) and cFANCD2(R305W) (lanes 8–12), in the presence of wheat germ topoisomerase I. After deproteinization, the topoisomers were separated by agarose gel electrophoresis. The cFANCD2 concentrations were 0, 0.45, 0.90, and 1.8 μM. Highly supercoiled and relaxed DNAs are denoted as 'sc' and 'relaxed', respectively. (**B**) Graphical representation of the nucleosome-assembly activity of the cFANCD2(R305W) mutants. Representative images are shown in **A**. The supercoiled DNA fractions were generated by nucleosome assembly in the presence of cFANCD2 (indicated by arrows in **A**), and the intensities of the bands indicated by the arrows in **A** were quantitated by an LAS-4000 Image Analyser (GE Healthcare). Means of three independent experiments are shown with s.d.'s. (**C**) FANCD2/FANCI monoubiquitination in *cFANCD2*$^{-/-}$ cells expressing the wild-type (WT) FANCD2 or cFANCD2(R305W). Cells were treated with or without MMC, and the WCEs were subjected to western blotting. The bands detected just above the original bands (S-forms) correspond to the monoubiquitinated forms (L-forms) of cFANCD2 and cFANCI (lanes 2 and 4). The L-form and S-form bands were quantitated with the Image J software, and the L/S ratios are indicated just above each panel. An asterisk indicates the non-specific band. (**D**) Colony survival assay of the cFANCD DT40 cells expressing GFP fusions with the wild type (WT) and cFANCD2(R305W), in the presence of cisplatin. Four independent DT40 cells expressing cFANCD2(R305W) were tested and plotted. (**E**) Colony survival assay of the *cFANCD2*$^{-/-}$ DT40 cells expressing H2B-GFP fusions with the WT and cFANCD2(R305W), in the presence of cisplatin. The mean and s.d. of measurements performed in triplicate are shown.

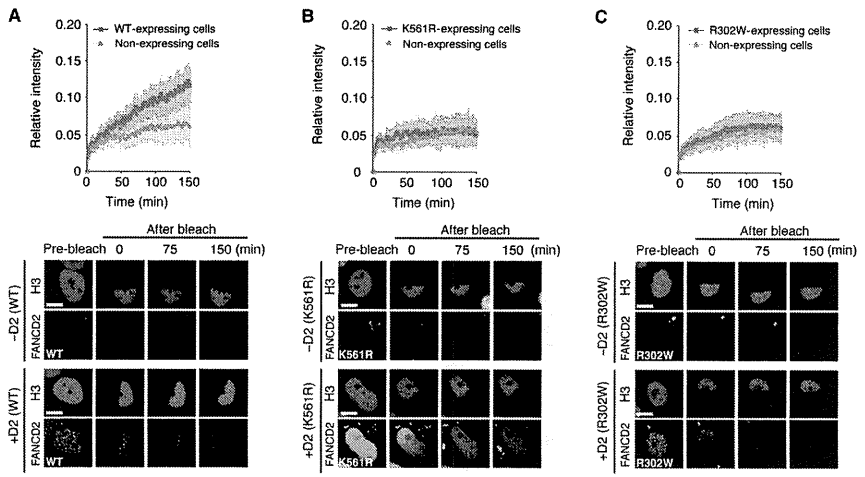

Figure 6 An FA-related mutant, human FANCD2(R302W), is defective in facilitating histone exchange. (**A–C**) FRAP with HeLa cells expressing H3-GFP and mCherry fusions with hFANCD2 (WT) (**A**), hFANCD2(K561R) (**B**), and hFANCD2(R302W) (**C**). After the depletion of endogenous hFANCD2 by siRNA, mCherry-hFANCD2, hFANCD2(K561R), or -hFANCD2(R302W) was expressed. In these cells, the mobility of histone H3-GFP was analysed in the presence of 50 ng/ml MMC for 12–18 h. The mean of the relative fluorescence intensity with the s.d. ($n = 10$–12) and examples are shown. Bars: 10 μm.

and instability of hFANCD2(R302W) protein may be potential causes of the FA phenotype in this patient.

FANCI stimulates nucleosome assembly by FANCD2

Finally, we examined the involvement of FANCI in nucleosome assembly, using purified chicken FANCI (cFANCI) (Supplementary Figure S7A and B), which could form a stable complex with cFANCD2 (Figure 7A). Although FANCI shares significant homology with FANCD2 (Sims *et al*, 2007; Smogorzewska *et al*, 2007), purified cFANCI alone did not efficiently promote nucleosome assembly (Figure 7B). However, cFANCI clearly stimulated the cFANCD2-mediated nucleosome assembly at low cFANCD2 concentrations, at which cFANCD2 itself did not promote detectable levels of nucleosome assembly (Figure 7C and D). cFANCI did not form a complex with the major histone chaperone Nap1, and did not stimulate its nucleosome assembly (Supplementary Figure S7C and D), suggesting that it may specifically stimulate the cFANCD2-mediated nucleosome assembly. In addition, cFANCI stimulated the nucleosome-assembly activity of cFANCD2(1-1389), which retained H3/H4-binding ability, but not that of cFANCD2(1-1267) (Supplementary Figure S7I). Therefore, the ID complex may facilitate nucleosome reorganization during DNA repair.

Discussion

In the present study, we found that the purified FANCD2 protein promotes nucleosome assembly *in vitro*, and that its partner, FANCI, significantly stimulates this activity. We also discovered that the C-terminal region of FANCD2 is critical for the nucleosome-assembly activity, and showed that the FANCD2 deletion and point mutants are defective in both nucleosome assembly *in vitro* and tolerance to cisplatin treatment *in vivo*. These findings provide novel insights into the function of the ID complex in chromatin.

The crystal structure of the mouse ID complex revealed that FANCD2 is composed of seven subdomains, solenoid 1 (S1), helical domain 1 (HD1), solenoid 2 (S2), helical domain 2 (HD2), solenoid 3 (S3), solenoid 4 (S4), and the C-terminal acidic region (Joo *et al*, 2011). In the present study, we mapped the histone-binding region within the S4 domain of FANCD2. The FANCD2 S4 domain is separate from the FANCI-binding surface, and is largely accessible (Joo *et al*, 2011). In the S4 domain, the cFANCD2 Arg1336 and Lys1346 residues are perfectly conserved among the human, mouse, chicken, frog, fish, and fly FANCD2 proteins (Figure 2A), and are located on the concave surface (Figure 8A; Joo *et al*, 2011). Our mutational analysis revealed that the cFANCD2 Arg1336 and Lys1346 residues are essential for nucleosome assembly *in vitro* and cisplatin resistance *in vivo*. In the crystal structure, the side chains of the mouse FANCD2 Arg1334 and Lys1344 residues, corresponding to the cFANCD2 Arg1336 and Lys1346 residues, respectively, are completely exposed to the solvent on the concave surface (Figure 8A). Therefore, the concave surface of the FANCD2 S4 domain may be its histone-binding region.

In cFANCD2, Arg1336 and Lys1346 are positively charged residues, which are considered to be less important for the histone binding of the acidic histone chaperone, Asf1 (English *et al*, 2006; Natsume *et al*, 2007). However, the involvement of positively charged residues in histone

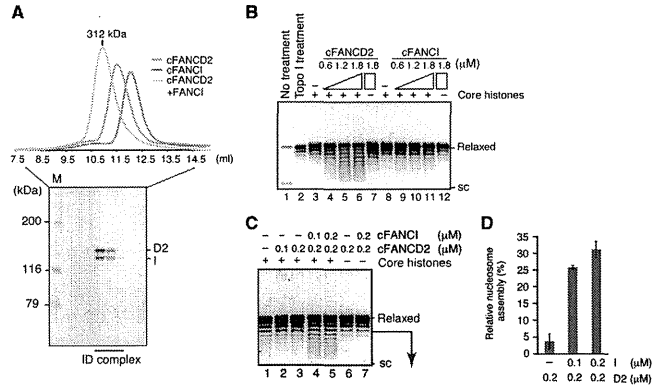

Figure 7 FANCI stimulates the FANCD2-mediated nucleosome assembly. (**A**) Gel filtration analysis of cFANCI–cFANCD2 complex formation. The SDS–PAGE analysis of the cFANCI–cFANCD2 fractions is shown below the gel filtration profiles. (**B**, **C**) Nucleosomes were reconstituted with relaxed plasmid DNA and cFANCD2 and/or cFANCI in the presence of wheat germ topoisomerase I. After deproteinization, the topoisomers were separated by agarose gel electrophoresis. The protein concentrations used in the assay are indicated at the top of the panels. Highly supercoiled and relaxed DNAs are denoted as 'sc' and 'relaxed', respectively. (**D**) Graphical representation of the experiments shown in **C**, lanes 3–5. The supercoiled DNA fractions generated by nucleosome assembly in the presence of cFANCD2 and cFANCI (indicated by arrows in **C**) were quantitated. Means of three independent experiments are shown with s.d.'s.

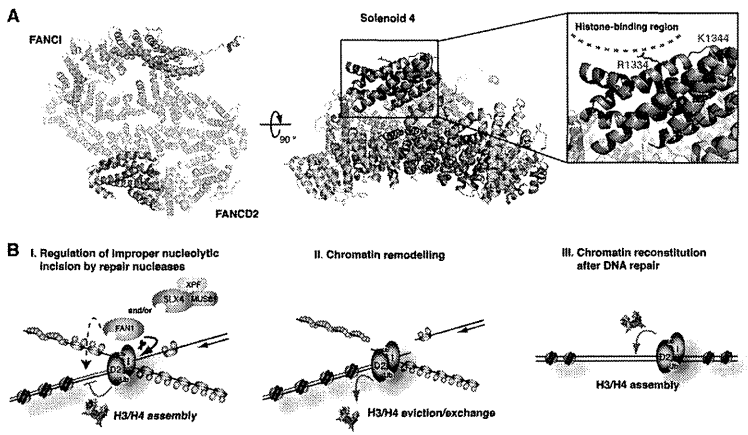

Figure 8 Models for the FANCD2 function in the FA pathway. (**A**) Locations of the Arg1334 and Lys1344 residues in the mouse FANCD2 structure. Structure of the mouse ID complex (PDB ID: 3S4W; Joo *et al*, 2011). The FANCD2 and FANCI subunits are coloured grey and light blue, respectively. The FANCD2 Arg1334 and Lys1344 residues (red), corresponding to the cFANCD2 Arg1336 and Lys1346 residues, respectively, are located on the concave surface of the FANCD2 Solenoid 4 (S4) domain (dark grey). (**B**) Three possible functions of the histone chaperone activity of the ID complex. (I) After the chromatin binding and monoubiquitination of the ID complex, the nucleosomes assembled by the ID complex on newly synthesized DNA may suppress the improper nucleolytic digestion by the repair nucleases, such as FAN1 and the SLX4 nuclease complex, which are recruited by the monoubiquitinated ID complex. (II) Chromatin remodelling mediated by the ID complex and FANCD2-associated chromatin modifiers may facilitate the RAD51-mediated homologous recombination reaction in chromatin. (III) The nucleosome-assembly activity of the ID complex may be required for chromatin reconstitution after DNA repair. RAD51 and RPA are coloured red and green, respectively. Histone octamers are shown in brown.

binding has been reported in the histone chaperone HJURP, which is the specific chaperone for the histone H3 variant, CENP-A (Dunleavy *et al*, 2009; Foltz *et al*, 2009). In the complex of HJURP with histone H4 and CENP-A, polar interactions exist between the negatively charged Glu96 of CENP-A and the two positively charged Arg32 and Lys39 residues of HJURP, and also between Glu107 of CENP-A and Arg28 of HJURP (Hu *et al*, 2011). Interestingly, the Glu96 and Glu107 residues of CENP-A are both conserved in histone H3 (Tachiwana *et al*, 2011a). Therefore, the histone-binding mechanism of FANCD2 may be similar to that of HJURP.

In the present study, we found that cFANCD2(R305W) was clearly defective in reversing the cisplatin sensitivity of the *FANCD2*$^{-/-}$ DT40 cells, but was proficient in its monoubiquitination *in vivo*. Interestingly, cFANCD2(R305W) was significantly defective in both the histone-binding and nucleosome-assembly activities. In addition, the corresponding human FANCD2(R302W) mutant could not rescue the decreased histone H3 mobility in the FANCD2-knockdown cells. These findings indicate that the histone-chaperone activity of FANCD2 is actually involved in the DNA crosslink repair by the FA pathway, and strongly suggest that FANCD2 regulates nucleosome dynamics after its monoubiquitination. The C-terminal cFANCD2 mutants tested in this study showed more severe cisplatin sensitivity than cFANCD2(R305W), *even when localized in the chromatin by the H2B fusion.* The residual histone-chaperone activity of cFANCD2 (R305W), which was barely detectable in the present nucleosome formation assay, may partially complement the cisplatin sensitivity of the *cFANCD2*$^{-/-}$ cells. In the crystal structure of mouse FANCD2, the side chain of the corresponding Arg300 directly hydrogen bonds with Asp379 (Joo *et al*, 2011), suggesting that the Arg300–Asp379 interaction may be important in the tertiary structure of the protein. Therefore, the Arg to Trp substitution found in cFANCD2(R305W) or hFANCD2(R302W) may cause a large structural change, which may allosterically impair the histone-binding activity of FANCD2.

FANCI–FANCD2 is reportedly required for nucleolytic incisions *in a replicating plasmid carrying an interstrand cross*-link in a frog egg extract (Knipscheer *et al*, 2009). One can envision that the ID complex-mediated chromatin remodelling may regulate the incision step by promoting the recruitment of nucleases (Figure 8B, I) (e.g., FAN1, Mus81, and XPF) (Nomura *et al*, 2007; Bhagwat *et al*, 2009; Fekairi *et al*, 2009; Svendsen *et al*, 2009; Hicks *et al*, 2010; Kratz *et al*, 2010; MacKay *et al*, 2010; Smogorzewska *et al*, 2010; Yoshikiyo *et al*, 2010; Yamamoto *et al*, 2011). In this step, the proper incision by the repair nucleases may occur on the single-stranded DNA region (Figure 8B, I, arrowhead), while the improper digestion of intact DNA strands may be restricted by the nucleosomes formed by the ID complex (Figure 8B, I, dashed line). Second, in the FA pathway, *homologous recombination repair may be promoted after* FANCD2 assembly into chromatin. The nucleosome remodelling by the ID complex may facilitate the DNA recombination reaction mediated by RAD51, which is the key protein for homologous recombinational repair (Figure 8B, II). Finally, the histone assembly activity of the ID complex may simply be important for chromatin reformation, following crosslink removal and DNA repair (Figure 8B, III). In addition to the direct interaction of the ID complex with histones, presented here, several chromatin modifiers have been suggested to interact with FA proteins. For example, a histone acetyltransferase, TIP60, reportedly interacts with FANCD2 (Hejna *et al*, 2008). Thus, the function of FANCD2 may be tightly coupled with those of other chromatin remodelling factors in chromatin dynamics, to facilitate DNA crosslink repair.

Materials and methods

Purifications of FANCD2, FANCI, FANCL, UBE2T, and Nap1

Experimental procedures are described in Supplementary Materials and Methods. The protein concentration was determined by the Bradford method (Bradford, 1976), using bovine serum albumin as the standard protein.

Purification of recombinant human H3/H4 and H2A/H2B complexes

Human histones H2A, H2B, H3, and H4 were overexpressed in *Escherichia coli* cells as His_6-tagged proteins, as described (Tanaka *et al*, 2004; Tachiwana *et al*, 2008). The purification and preparation of the histone H3/H4 and H2A/H2B complexes were performed as previously described (Tachiwana *et al*, 2010, 2011b). The His_6-tag was removed during the purification steps.

Proteome analysis

The purified recombinant human histone H3/H4 complex was covalently conjugated with Affi-Gel 10 beads (Bio-Rad), according to the manufacturer's protocol. Briefly, the histone H3/H4 beads were incubated with a chromatin extract from HeLa cells at 4°C. The beads were washed with 10 mM PIPES buffer (pH 7.0), containing 1 mM $MgCl_2$, 1 mM EDTA, 0.01% Triton X-100, 300 mM sucrose, and 0.1 M NaCl. The proteins bound to the beads were fractionated by SDS–PAGE. Each lane was cut into nine pieces, and was further treated with trypsin. To identify the peptide fragments, the samples were analysed by liquid chromatography/tandem mass spectrometry, as previously described (Nozawa *et al*, 2010). The raw data files were analysed by the Mascot software (Matrix Science).

Pull-down assay with histone-conjugated beads

The histone H3/H4 complex was covalently conjugated with Affi-Gel 10 beads (Bio-Rad), according to the manufacturer's protocol. The histone H3/H4 beads were incubated with a HeLa whole-cell extract (WCE) (3 mg of protein), and the beads were washed three times with 100 μl of washing buffer, containing 50 mM Tris–HCl (pH 7.5), 200 mM NaCl, 5 mM EDTA, 0.5% Nonidet P-40, 1 mM PMSF, and Protease Inhibitor Cocktail (Nacalai Tesque). The hFANCD2 that copelleted with the histone H3/H4 beads was fractionated by 8% SDS–PAGE, and was detected by western blotting with the hFANCD2-specific mouse monoclonal antibody (FI17, Santa Cruz Biotechnology, Inc.).

For the recombinant hFANCD2-binding assay, the histone H3/H4 beads (15 μl) were incubated with purified hFANCD2, with or without 10 U of DNaseI (TOYOBO), at 23°C for 120 min. The beads were then washed three times with 100 μl of 10 mM PIPES-KOH buffer (pH 7.0), containing 0.5 M NaCl, 0.3 M sucrose, 1 mM $MgCl_2$, and 0.01% Triton X-100. The proteins bound to the beads were separated by 15% SDS–PAGE, and were visualized by Coomassie Brilliant Blue staining.

For the cFANCD2-binding assay, 293T cells were transiently transfected with GFP-cFANCD2-mutant plasmids, using Lipofectamine2000 (Invitrogen). Cells were disrupted in lysis buffer (Seki *et al*, 2007), and after the lysate was incubated with the histone H3/H4 beads (7.5 μl) at 4°C for 3 h, the beads were washed four times with lysis buffer. The proteins were separated by 6% SDS–PAGE, and were detected by western blotting with an anti-GFP Ab (Clontech).

Topological assay for nucleosome formation

Experimental procedures are described in Supplementary Materials and Methods.

Gel-shift assay for nucleosome formation

The H2A/H2B complex (8 ng/μl) and the H3/H4 complex (8 ng/μl) were pre-incubated with hFANCD2 or hNap1 at 23°C for 10 min. The nucleosome-assembly reaction was initiated by the addition of the 195 bp DNA (8 ng/μl) containing the *Lytechinus variegates* 5S ribosomal RNA gene (Osakabe *et al*, 2010) in a 10 μl reaction mixture, containing 20 mM Tris–HCl (pH 8.0), 140 mM NaCl, 7% glycerol, and 1 mM dithiothreitol. The reaction was continued at 23°C for 60 min, followed by a further incubation at 42°C for 60 min to eliminate the non-specific DNA binding by free histones. The samples were then separated by 6% PAGE in 0.2× TBE buffer

(18 mM Tris base, 18 mM boric acid, and 0.4 mM EDTA). DNA was visualized by ethidium bromide staining.

Pull-down assay with GST-cFANCL and cFANCD2

Purified cFANCD2 (6 μg) and GST-cFANCL (5 μg) were incubated at 30°C for 60 min in a 100 μl reaction mixture, containing 20 mM Tris–HCl (pH 8.0), 10% glycerol, 200 mM NaCl, and 5 mM 2-mercaptoethanol. Glutathione Sepharose 4B beads (5 μl) were added to the reaction mixtures, which were gently mixed at 4°C for 60 min. The beads were then washed three times with 1 ml of wash buffer, containing 20 mM Tris–HCl (pH 8.0), 0.4 M NaCl, 10% glycerol, 5 mM 2-mercaptoethanol, and 0.05% Triton X-100. The proteins bound to the beads were separated by 7% SDS–PAGE, and were visualized by Coomassie Brilliant Blue staining.

In vitro FANCD2 monoubiquitination and purification of monoubiquitinated FANCD2

Experimental procedures are described in Supplementary Materials and Methods.

Gel-shift assay

Circular ϕX174 dsDNA (100 ng) was mixed with cFANCD2 (0.45–1.8 μM) or cFANCD2(1-1389) (0.45–1.8 μM) in 10 μl of reaction buffer, containing 22 mM Tris–HCl (pH 8.0), 70 mM NaCl, 7% glycerol, 2 mM $MgCl_2$, and 2.5 mM dithiothreitol. The samples were incubated at 37°C for 15 min, and were then analysed by 0.8% agarose gel electrophoresis in TAE buffer. DNA was visualized by ethidium bromide staining.

siRNA transfection, immunoblotting, and FRAP

The FANCD2-specific Stealth RNAs ((no. 1, HSS103525, 5′-AAUGAACGCUCUUUAGCAGACAUGG-3′, for Figures 3 and 6, and Supplementary Figure S3; and no. 2, HSS103527, 5′-AAUAGACGACAACUUAUCCAUCACC-3′, for Supplementary Figure S3; Invitrogen), a FANCA-specific Stealth RNA (5′-AAGGGUCAAGAGGGAAAAAUA-3′, for Supplementary Figure S4; Invitrogen), and the control RNA (Negative Control Medium; Invitrogen) were introduced into HeLa cells expressing histone H3-GFP by Lipofectamine2000 (Invitrogen), as described (Kimura *et al*, 2006). Total cellular proteins were prepared 0–4 days after the RNA introduction, separated by 8% SDS–PAGE, and immunoblotted with a mouse monoclonal antibody directed against either FANCD2 (1:250; FI17, Santa Cruz Biotechnology, Inc.), α-tubulin (1:1000; Sigma) as a loading control, or an antibody against FANCA (1:1000; rabbit polyclonal, Bethyl Laboratories, Inc.). Secondary detection was performed with a sheep anti-mouse IgG, horseradish peroxidase-linked species-specific $F(ab')_2$ fragment (GE Healthcare; 1:500 for FANCD2 and 1:1000 for α-tubulin), or a sheep anti-rabbit IgG, horseradish peroxidase-linked species-specific $F(ab')_2$ fragment (GE Healthcare; 1:1000 for FANCA). The signals were detected by chemiluminescence (Western Lightning Plus; Perkin Elmer).

To generate HeLa cells expressing both H3-GFP and mCherry-PCNA, cells expressing H3-GFP (blasticidin resistance; Kimura and Cook, 2001) and mCherry-PCNA (puromycin resistance; generated using pMX-puro-based expression vector carrying mCherry-PCNA; Leonhardt *et al*, 2000; Kitamura *et al*, 2003) were fused using polyethylene glycol (Roche; Kimura and Cook, 2001), and single colonies were selected in the presence of 1 μg/ml blasticidin and 0.5 μg/ml puromycin.

FRAP was performed 3–4 days after siRNA transfection as described (Kimura *et al*, 2006), using a confocal microscope (FV-1000; Olympus) with a × 60 UPlanSApo NA = 1.35 lens. Three confocal images of a field containing 4–10 nuclei were collected (800 × 800 pixels, zoom 3, scan speed 2 μs/pixel, pinhole 800 μm, Kalman filtration for four scans, LP505 emission filter, and 0.1% transmission of 488-nm Ar laser), one half of each nucleus was bleached using 75% transmission of 488 nm and 100% of 514 nm (two iterations), and images were obtained using the original setting at 1 min intervals.

For the complementation experiments, RNAi-resistant *hFANCD2* genes were constructed by introducing silent mutations in the FANCD2-specific Stealth RNA (no. 1) target sequence (5′-TCTGCTAAAGAG-3′) as follows: 5′-TCCGCCAAGGAA-3′. HeLa cells expressing histone H3-GFP were transfected with the FANCD2-specific Stealth RNAs (no. 1) to knockdown the endogenous hFANCD2. The next day, the cells were transfected with the RNAi-resistant mCherry-*hFANCD2*, mCherry-*hFANCD2(R302W)*, or mCherry-*hFANCD2(K561R)* gene, using the FuGENE system (Promega), and were further grown for 2 days before FRAP. After FRAP, the glass-bottom dish was processed for immunofluorescence.

The fluorescence intensity of the bleached area was measured using Image J 1.39u (W Rasband; http://rsb.info.nih.gov/ij/). After subtracting the background, the intensity was normalized to the initial intensity before bleaching.

Immunofluorescence

For immunofluorescence, HeLa cells expressing histone H3-GFP were grown on a glass-bottom dish (Mat-tek), transfected with Stealth RNA, and fixed with 4% paraformaldehyde at 3 days after transfection. The fixed cells were permeabilized and stained using mouse anti-FANCD2 (1:250) and goat Cy3-conjugated anti-mouse IgG (1:500; Jackson Immunoresearch). When mCherry-*hFANCD2* was transfected, goat Cy5-conjugated anti-mouse IgG (1:500; Jackson Immunoresearch) was used as the secondary antibody. For double staining with FANCA, rabbit anti-FANCA (1:100; Bethyl Laboratories, Inc.) and goat Cy5-conjugated anti-rabbit IgG (1:500; Jackson Immunoresearch) are also used. DNA was counterstained with DAPI. The fluorescence images were obtained using a confocal microscope (Olympus FV-1000 with a × 60 UPlanSApo NA = 1.35 oil-immersion objective lens; or Carl Zeiss LSM510 with a × 40 C-Apo NA = 1.2 water-immersion objective lens).

Generation of the FANCD2$^{-/-}$ DT40 cells producing the FANCD2 mutants

Plasmids for the cFANCD2-mutant fusions were constructed in the pcDNA3.1-based GFP or histone H2B-GFP expression vector, by inserting FANCD2 fragments using the Gateway system (Invitrogen). To obtain stably expressing clones, these plasmids were transfected into *FANCD2*-deficient DT40 cells (Yamamoto *et al*, 2005), and the clones expressing the fusions were identified by measuring the GFP fluorescence with a FACSCalibur (Becton Dickinson), as described (Yamamoto *et al*, 2003; Ishiai *et al*, 2004).

Cisplatin sensitivity assay

Sensitivity to cisplatin (Nihon-Kayaku) was assayed by colony formation, in medium containing 1.4% methylcellulose and the indicated dosage of cisplatin (Yamamoto *et al*, 2003; Ishiai *et al*, 2004).

Cell fractionation and detection of FANCD2/FANCI proteins

The indicated cells were either treated with MMC (500 ng/ml for 6 h) or left untreated, and were fractionated into soluble and chromatin fractions, as described previously (Matsushita *et al*, 2005; Ishiai *et al*, 2008). Pull-down assays of cFANCD2-H2B-GFP proteins were performed using anti-GFP beads (MBL). The proteins were separated by 6% SDS–PAGE, and were detected by western blotting. The anti-chicken FANCD2 and FANCI antibodies were obtained by immunizing rabbits with the bacterially expressed His fusion protein with full-length chicken FANCD2 and the GST fusion protein with chicken FANCI (amino acids 1–251), respectively.

Gel filtration analysis

The purified cFANCD2 and cFANCI proteins were analysed by Superdex 200 HR 10/30 (GE Healthcare) gel filtration chromatography. The elution buffer contained 20 mM Tris–HCl (pH 8.0), 200 mM NaCl, 10% glycerol, and 1 mM DTT.

Supplementary data

Supplementary data are available at *The EMBO Journal* Online (http://www.embojournal.org).

Acknowledgements

We would like to thank Emi Uchida for expert technical assistance, and M Cristina Cardoso, Toshio Kitamura, and Shin-ya Isobe for materials. This work was supported in part by Grants-in-Aid from the Japanese Society for the Promotion of Science (JSPS), and the Ministry of Education, Culture, Sports, Science and Technology (MEXT), Japan. H Kurumizaka was also supported by the Waseda Research Institute for Science and Engineering, the Sagawa Foundation for Promotion of Cancer Research, and NOVARTIS Foundation (Japan) for the Promotion of Science. MI was supported by the Ichiro Kanehara Foundation and the Mochida Memorial Foundation for Medical and Pharmaceutical Research.

Author contributions: KS, KT, SF, YT, AO, HT, and WK purified FANCD2, FANCI, and histones, and KS and KT performed biochemical analyses. MI, H Kitao, and MT performed genetic and cell biological analyses. KS and H Kimura performed FRAP analyses. KS and ND performed domain analysis of FANCD2 by mass spectroscopy. AO, HT, and CO performed proteome analysis of histone-binding proteins. H Kurumizaka and MT conceived, designed, and supervised all of the work, and KS and H Kurumizaka wrote the paper. All of the authors discussed the results and commented on the manuscript.

Conflict of interest

The authors declare that they have no conflict of interest.

References

Ali AM, Pradhan A, Singh TR, Du C, Li J, Wahengbam K, Grassman E, Auerbach AD, Pang Q, Meetei AR (2012) FAAP20: a novel ubiquitin-binding FA nuclear core-complex protein required for functional integrity of the FA-BRCA DNA repair pathway. *Blood* **119:** 3285–3294

Avvakumov N, Nourani A, Côté J (2011) Histone chaperones: modulators of chromatin marks. *Mol Cell* **41:** 502–514

Bhagwat N, Olsen AL, Wang AT, Hanada K, Stuckert P, Kanaar R, D'Andrea A, Niedernhofer LJ, McHugh PJ (2009) XPF-ERCC1 participates in the Fanconi anemia pathway of cross-link repair. *Mol Cell Biol* **29:** 6427–6437

Bradford MM (1976) A rapid and sensitive method for the quantitation of microgram quantities of protein utilizing the principle of protein-dye binding. *Anal Biochem* **72:** 248–254

Crossan GP, van der Weyden L, Rosado IV, Langevin F, Gaillard PH, McIntyre RE; Sanger Mouse Genetics Project, Gallagher F, Kettunen MI, Lewis DY, Brindle K, Arends MJ, Adams DJ, Patel KJ (2011) Disruption of mouse Slx4, a regulator of structure-specific nucleases, phenocopies Fanconi anemia. *Nat Genet* **43:** 147–152

Dunleavy EM, Roche D, Tagami H, Lacoste N, Ray-Gallet D, Nakamura Y, Daigo Y, Nakatani Y, Almouzni G (2009) HJURP is a cell-cycle-dependent maintenance and deposition factor of CENP-A at centromeres. *Cell* **137:** 485–497

English CM, Adkins MW, Carson JJ, Churchill ME, Tyler JK (2006) Structural basis for the histone chaperone activity of Asf1. *Cell* **127:** 495–508

Fekairi S, Scaglione S, Chahwan C, Taylor ER, Tissier A, Coulon S, Dong MQ, Ruse C, Yates 3rd JR, Russell P, Fuchs RP, McGowan CH, Gaillard PH (2009) Human SLX4 is a Holliday junction resolvase subunit that binds multiple DNA repair/recombination endonucleases. *Cell* **138:** 78–89

Foltz DR, Jansen LET, Bailey AO, Yates JR, Bassett EA, Wood S, Black BE, Cleveland DW (2009) Centromere-specific assembly of CENP-A nucleosomes is mediated by HJURP. *Cell* **137:** 472–484

Garcia-Higuera I, Taniguchi T, Ganesan S, Meyn MS, Timmers C, Hejna J, Grompe M, D'Andrea AD (2001) Interaction of the Fanconi anemia proteins and BRCA1 in a common pathway. *Mol Cell* **7:** 249–262

Garner E, Smogorzewska A (2011) Ubiquitylation and the Fanconi anemia pathway. *FEBS Lett* **585:** 2853–2860

Hejna J, Holtorf M, Hines J, Mathewson L, Hemphill A, Al-Dhalimy M, Olson SB, Moses RE (2008) Tip60 is required for DNA interstrand cross-link repair in the Fanconi anemia pathway. *J Biol Chem* **283:** 9844–9851

Hicks JK, Chute CL, Paulsen MT, Ragland RL, Howlett NG, Guéranger Q, Glover TW, Canman CE (2010) Differential roles for DNA polymerases eta, zeta, and REV1 in lesion bypass of intrastrand versus interstrand DNA cross-links. *Mol Cell Biol* **30:** 1217–1230

Hu H, Liu Y, Wang M, Fang J, Huang H, Yang N, Li Y, Wang J, Yao X, Shi Y, Li G, Xu RM (2011) Structure of a CENP-A-histone H4 heterodimer in complex with chaperone HJURP. *Genes Dev* **25:** 901–906

Ishiai M, Kimura M, Namikoshi K, Yamazoe M, Yamamoto K, Arakawa H, Agematsu K, Matsushita N, Takeda S, Buerstedde JM, Takata M (2004) DNA cross-link repair protein SNM1A interacts with PIAS1 in nuclear focus formation. *Mol Cell Biol* **24:** 10733–10741

Ishiai M, Kitao H, Smogorzewska A, Tomida J, Kinomura A, Uchida E, Saberi A, Kinoshita E, Kinoshita-Kikuta E, Koike T, Tashiro S, Elledge SJ, Takata M (2008) FANCI phosphorylation functions as a molecular switch to turn on the Fanconi anemia pathway. *Nat Struct Mol Biol* **15:** 1138–1146

Joo W, Xu G, Persky NS, Smogorzewska A, Rudge DG, Buzovetsky O, Elledge SJ, Pavletich NP (2011) Structure of the FANCI-FANCD2 complex: insights into the Fanconi anemia DNA repair pathway. *Science* **333:** 312–316

Kee Y, D'Andrea AD (2010) Expanded roles of the Fanconi anemia pathway in preserving genomic stability. *Genes Dev* **24:** 1680–16943

Kim H, Yang K, Dejsuphong D, D'Andrea AD (2012) Regulation of Rev1 by the Fanconi anemia core complex. *Nat Struct Mol Biol* **19:** 164–170

Kim Y, Lach FP, Desetty R, Hanenberg H, Auerbach AD, Smogorzewska A (2011) Mutations of the *SLX4* gene in Fanconi anemia. *Nat Genet* **43:** 142–146

Kimura H, Cook PR (2001) Kinetics of core histones in living human cells: little exchange of H3 and H4 and some rapid exchange of H2B. *J Cell Biol* **153:** 1341–1353

Kimura H, Takizawa N, Allemand E, Hori T, Iborra FJ, Nozaki N, Muraki M, Hagiwara M, Krainer AR, Fukagawa T, Okawa K (2006) A novel histone-exchange factor, protein phosphatase 2Cγ, mediates the exchange and dephosphorylation of H2A-H2B. *J Cell Biol* **175:** 389–400

Kitamura T, Koshino Y, Shibata F, Oki T, Nakajima H, Nosaka T, Kumagai H (2003) Retrovirus-mediated gene transfer and expression cloning: powerful tools in functional genomics. *Exp Hematol* **31:** 1007–1014

Kitao H, Takata M (2011) Fanconi anemia: a disorder defective in the DNA damage response. *Int J Hematol* **93:** 417–424

Knipscheer P, Räschle M, Smogorzewska A, Enoiu M, Ho TV, Schärer OD, Elledge SJ, Walter JC (2009) The Fanconi anemia pathway promotes replication-dependent DNA interstrand cross-link repair. *Science* **326:** 1698–1701

Kratz K, Schöpf B, Kaden S, Sendoel A, Eberhard R, Lademann C, Cannavó E, Sartori AA, Hengartner MO, Jiricny J (2010) Deficiency of FANCD2-associated nuclease KIAA1018/FAN1 sensitizes cells to interstrand crosslinking agents. *Cell* **142:** 77–88

Leonhardt H, Rahn HP, Weinzierl P, Sporbert A, Cremer T, Zink D, Cardoso MC (2000) Dynamics of DNA replication factories in living cells. *J Cell Biol* **149:** 271–280

Leung JW, Wang Y, Fong KW, Huen MS, Li L, Chen J (2012) Fanconi anemia (FA) binding protein FAAP20 stabilizes FA complementation group A (FANCA) and participates in interstrand cross-link repair. *Proc Natl Acad Sci USA* **109:** 4491–4496

MacKay C, Déclais AC, Lundin C, Agostinho A, Deans AJ, MacArtney TJ, Hofmann K, Gartner A, West SC, Helleday T, Lilley DM, Rouse J (2010) Identification of KIAA1018/FAN1, a DNA repair nuclease recruited to DNA damage by monoubiquitinated FANCD2. *Cell* **142:** 65–76

Matsushita N, Kitao H, Ishiai M, Nagashima N, Hirano S, Okawa K, Ohta T, Yu DS, McHugh PJ, Hickson ID, Venkitaraman AR, Kurumizaka H, Takata M (2005) A FancD2-monoubiquitin fusion reveals hidden functions of Fanconi anemia core complex in DNA repair. *Mol Cell* **19:** 841–847

Meetei AR, de Winter JP, Medhurst AL, Wallisch M, Waisfisz Q, van de Vrugt HJ, Oostra AB, Yan Z, Ling C, Bishop CE, Hoatlin ME, Joenje H, Wang W (2003) A novel ubiquitin ligase is deficient in Fanconi anemia. *Nat Genet* **35:** 165–170

Natsume R, Eitoku M, Akai Y, Sano N, Horikoshi M, Senda T (2007) Structure and function of the histone chaperone CIA/ASF1 complexed with histones H3 and H4. *Nature* **446:** 338–341

Niedernhofer LJ, Lalai AS, Hoeijmakers JHJ (2005) Fanconi anemia (cross)linked to DNA repair. *Cell* **123:** 1191–1198

Nomura Y, Adachi N, Koyama H (2007) Human Mus81 and FANCB independently contribute to repair of DNA damage during replication. *Genes Cells* **12:** 1111–1122

Nozawa RS, Nagao K, Masuda HT, Iwasaki O, Hirota T, Nozaki N, Kimura H, Obuse C (2010) Human POGZ modulates dissociation of HP1alpha from mitotic chromosome arms through Aurora B activation. *Nat Cell Biol* **12:** 719–727

Osakabe A, Tachiwana H, Matsunaga T, Shiga T, Nozawa RS, Obuse C, Kurumizaka H (2010) Nucleosome formation activity of human somatic nuclear autoantigenic sperm protein (sNASP). *J Biol Chem* **285:** 11913–11921

Pace P, Mosedale G, Hodskinson MR, Rosado IV, Sivasubramaniam M & Patel KJ (2010) Ku70 corrupts DNA repair in the absence of the Fanconi anemia pathway. *Science* **329:** 219–223

Sato K, Toda K, Ishiai M, Takata M, Kurumizaka H (2012) DNA robustly stimulates FANCD2 monoubiquitylation in the complex with FANCI. *Nucleic Acids Res* **40:** 4553–4561

Seki S, Ohzeki M, Uchida A, Hirano S, Matsushita N, Kitao H, Oda T, Yamashita T, Kashihara N, Tsubahara A, Takata M, Ishiai M (2007) A requirement of FancL and FancD2 monoubiquitination in DNA repair. *Genes Cells* **12:** 299–310

Sims AE, Spiteri E, Sims 3rd RJ, Arita AG, Lach FP, Landers T, Wurm M, Freund M, Neveling K, Hanenberg H, Auerbach AD, Huang TT (2007) FANCI is a second monoubiquitinated member of the Fanconi anemia pathway. *Nat Struct Mol Biol* **14:** 564–567

Smogorzewska A, Desetty R, Saito TT, Schlabach M, Lach FP, Sowa ME, Clark AB, Kunkel TA, Harper JW, Colaiácovo MP, Elledge SJ (2010) A genetic screen identifies FAN1, a Fanconi anemia-associated nuclease necessary for DNA interstrand crosslink repair. *Mol Cell* **39:** 36–47

Smogorzewska A, Matsuoka S, Vinciguerra P, McDonald 3rd ER, Hurov KE, Luo J, Ballif BA, Gygi SP, Hofmann K, D'Andrea AD, Elledge SJ (2007) Identification of the FANCI protein, a monoubiquitinated FANCD2 paralog required for DNA repair. *Cell* **129:** 289–301

Stoepker C, Hain K, Schuster B, Hilhorst-Hofstee Y, Rooimans MA, Steltenpool J, Oostra AB, Eirich K, Korthof ET, Nieuwint AW, Jaspers NG, Bettecken T, Joenje H, Schindler D, Rouse J, de Winter JP (2011) SLX4, a coordinator of structure-specific endonucleases, is mutated in a new Fanconi anemia subtype. *Nat Genet* **43:** 138–141

Svendsen JM, Smogorzewska A, Sowa ME, O'Connell BC, Gygi SP, Elledge SJ, Harper JW (2009) Mammalian BTBD12/SLX4 assembles a Holliday junction resolvase and is required for DNA repair. *Cell* **138:** 63–77

Tachiwana H, Kagawa W, Osakabe A, Kawaguchi K, Shiga T, Hayashi-Takanaka Y, Kimura H, Kurumizaka H (2010) Structural basis of instability of the nucleosome containing a testis-specific histone variant, human H3T. *Proc Natl Acad Sci USA* **107:** 10454–10459

Tachiwana H, Kagawa W, Shiga T, Osakabe A, Miya Y, Saito K, Hayashi-Takanaka Y, Oda T, Sato M, Park S-Y, Kimura H, Kurumizaka H (2011a) Crystal structure of the human centromeric nucleosome containing CENP-A. *Nature* **476:** 232–235

Tachiwana H, Osakabe A, Kimura H, Kurumizaka H (2008) Nucleosome formation with the testis-specific histone H3 variant, H3t, by human nucleosome assembly proteins in vitro. *Nucleic Acids Res* **36:** 2208–2218

Tachiwana H, Osakabe A, Shiga T, Miya Y, Kimura H, Kagawa W, Kurumizaka H (2011b) Structures of human nucleosomes containing major histone H3 variants. *Acta Cryst D* **67**(Pt 6): 578–583

Tanaka Y, Tawaramoto-Sasanuma M, Kawaguchi S, Ohta T, Yoda K, Kurumizaka H, Yokoyama S (2004) Expression and purification of recombinant human histones. *Methods* **33:** 3–11

Taniguchi T, D'Andrea AD (2006) Molecular pathogenesis of Fanconi anemia: recent progress. *Blood* **107:** 4223–4233

Thompson LH, Hinz JM, Yamada NA, Jones NJ (2005) How Fanconi anemia proteins promote the four Rs: replication, recombination, repair, and recovery. *Environ Mol Mutagen* **45:** 128–142

Timmers C, Taniguchi T, Hejna J, Reifsteck C, Lucas L, Bruun D, Thayer M, Cox B, Olson S, D'Andrea AD, Moses R, Grompe M (2001) Positional cloning of a novel Fanconi anemia gene, *FANCD2*. *Mol Cell* **7:** 241–248

Vaz F, Hanenberg H, Schuster B, Barker K, Wiek C, Erven V, Neveling K, Endt D, Kesterton I, Autore F, Fraternali F, Freund M, Hartmann L, Grimwade D, Roberts RG, Schaal H, Mohammed S, Rahman N, Schindler D, Mathew CG (2010) Mutation of the *RAD51C* gene in a Fanconi anemia-like disorder. *Nat Genet* **42:** 406–409

Venkitaraman AR (2004) Tracing the network connecting BRCA and Fanconi anaemia proteins. *Nat Rev Cancer* **4:** 435–445

Wang W (2007) Emergence of a DNA-damage response network consisting of Fanconi anaemia and BRCA proteins. *Nat Rev Genet* **8:** 735–748

Wolffe A (1998) *Chromatin: Structure and Function*. 3rd ednSan Diego, California, USA: Academic Press

Yamamoto K, Hirano S, Ishiai M, Morishima K, Kitao H, Namikoshi K, Kimura M, Matsushita N, Arakawa H, Buerstedde JM, Komatsu K, Thompson LH, Takata M (2005) Fanconi anemia protein FANCD2 promotes immunoglobulin gene conversion and DNA repair through a mechanism related to homologous recombination. *Mol Cell Biol* **25:** 34–43

Yamamoto K, Ishiai M, Matsushita N, Arakawa H, Lamerdin JE, Buerstedde JM, Tanimoto M, Harada M, Thompson LH, Takata M (2003) Fanconi anemia FANCG protein in mitigating radiation- and enzyme-induced DNA double-strand breaks by homologous recombination in vertebrate cells. *Mol Cell Biol* **23:** 5421–5430

Yamamoto KN, Kobayashi S, Tsuda M, Kurumizaka H, Takata M, Kono K, Jiricny J, Takeda S, Hirota K (2011) Involvement of SLX4 in interstrand cross-link repair is regulated by the Fanconi anemia pathway. *Proc Natl Acad Sci USA* **108:** 6492–6496

Yoshikiyo K, Kratz K, Hirota K, Nishihara K, Takata M, Kurumizaka H, Horimoto S, Takeda S, Jiricny J (2010) KIAA1018/FAN1 nuclease protects cells against genomic instability induced by interstrand cross-linking agents. *Proc Natl Acad Sci USA* **107:** 21553–21557

Extensive gene deletions in Japanese patients with Diamond-Blackfan anemia

Madoka Kuramitsu,[1] Aiko Sato-Otsubo,[2] Tomohiro Morio,[3] Masatoshi Takagi,[3] Tsutomu Toki,[4] Kiminori Terui,[4] RuNan Wang,[4] Hitoshi Kanno,[5] Shouichi Ohga,[6] Akira Ohara,[7] Seiji Kojima,[8] Toshiyuki Kitoh,[9] Kumiko Goi,[10] Kazuko Kudo,[11] Tadashi Matsubayashi,[12] Nobuo Mizue,[13] Michio Ozeki,[14] Atsuko Masumi,[1] Haruka Momose,[1] Kazuya Takizawa,[1] Takuo Mizukami,[1] Kazunari Yamaguchi,[1] Seishi Ogawa,[2] Etsuro Ito,[4] and Isao Hamaguchi[1]

[1]Department of Safety Research on Blood and Biological Products, National Institute of Infectious Diseases, Tokyo, Japan; [2]Cancer Genomics Project, Graduate School of Medicine, The University of Tokyo, Tokyo, Japan; [3]Department of Pediatrics and Developmental Biology, Graduate School of Medicine, Tokyo Medical and Dental University, Bunkyo-ku, Tokyo, Japan; [4]Department of Pediatrics, Hirosaki University Graduate School of Medicine, Hirosaki, Japan; [5]Department of Transfusion Medicine and Cell Processing, Tokyo Women's Medical University, Tokyo, Japan; [6]Department of Pediatrics, Graduate School of Medical Sciences, Kyushu University, Fukuoka, Japan; [7]First Department of Pediatrics, Toho University School of Medicine, Tokyo, Japan; [8]Department of Pediatrics, Nagoya University Graduate School of Medicine, Nagoya, Japan; [9]Department of Hematology/Oncology, Shiga Medical Center for Children, Shiga, Japan; [10]Department of Pediatrics, School of Medicine, University of Yamanashi, Yamanashi, Japan; [11]Division of Hematology and Oncology, Shizuoka Children's Hospital, Shizuoka, Japan; [12]Department of Pediatrics, Seirei Hamamatsu General Hospital, Shizuoka, Japan; [13]Department of Pediatrics, Kushiro City General Hospital, Hokkaido, Japan; and [14]Department of Pediatrics, Graduate School of Medicine, Gifu University, Gifu, Japan

Fifty percent of Diamond-Blackfan anemia (DBA) patients possess mutations in genes coding for ribosomal proteins (RPs). To identify new mutations, we investigated large deletions in the RP genes *RPL5*, *RPL11*, *RPL35A*, *RPS7*, *RPS10*, *RPS17*, *RPS19*, *RPS24*, and *RPS26*. We developed an easy method based on quantitative-PCR in which the threshold cycle correlates to gene copy number. Using this approach, we were able to diagnose 7 of 27 Japanese patients (25.9%) possessing mutations that were not detected by sequencing. Among these large deletions, similar results were obtained with 6 of 7 patients screened with a single nucleotide polymorphism array. We found an extensive intragenic deletion in *RPS19*, including exons 1-3. We also found 1 proband with an *RPL5* deletion, 1 patient with an *RPL35A* deletion, 3 with *RPS17* deletions, and 1 with an *RPS19* deletion. In particular, the large deletions in the *RPL5* and *RPS17* alleles are novel. All patients with a large deletion had a growth retardation phenotype. Our data suggest that large deletions in RP genes comprise a sizable fraction of DBA patients in Japan. In addition, our novel approach may become a useful tool for screening gene copy numbers of known DBA genes. (*Blood*. 2012;119(10): 2376-2384)

Introduction

Diamond-Blackfan anemia (DBA; MIN# 105650) is a rare congenital anemia that belongs to the inherited BM failure syndromes, generally presenting in the first year of life. Patients typically present with a decreased number of erythroid progenitors in their BM.[1] A main feature of the disease is red cell aplasia, but approximately half of patients show growth retardation and congenital malformations in the craniofacial, upper limb, cardiac, and urinary systems. Predisposition to cancer, in particular acute myeloid leukemia and osteogenic sarcoma, is also characteristic of the disease.[2]

Mutations in the *RPS19* gene were first reported in 25% of DBA patients by Draptchinskaia et al in 1999.[3] Since that initial finding, many genes that encode large (RPL) or small (RPS) ribosomal subunit proteins were found to be mutated in DBA patients, including *RPL5* (approximately 21%), *RPL11* (approximately 9.3%), *RPL35A* (3.5%), *RPS7* (1%), *RPS10* (6.4%), *RPS17* (1%), *RPS24* (2%), and *RPS26* (2.6%).[4-7] To date, approximately half of the DBA patients analyzed have had a mutation in one of these genes. Konno et al screened 49 Japanese patients and found that 30% (12 of 49) carried mutations.[8] In addition, our data showed that 22 of 68 DBA patients (32.4%) harbored a mutation in ribosomal protein (RP) genes (T.T., K.T., R.W., and E.I., unpublished observation, April 16, 2011). These abnormalities of RP genes cause defects in ribosomal RNA processing, formation of either the large or small ribosome subunit, and decreased levels of polysome formation,[4-6,9-12] which is thought to be one of the mechanisms for impairment of erythroid lineage differentiation.

Although sequence analyses of genes responsible for DBA are well established and have been used to identify new mutations, it is estimated that approximately half of the mutations remain to be determined. Because of the difficulty of investigating whole allele deletions, there have been few reports regarding allelic loss in DBA, and they have only been reported for *RPS19* and *RPL35A*.[3,6,13] However, a certain percentage of DBA patients are thought to have a large deletion in RP genes. Therefore, a detailed analysis of allelic loss mutations should be conducted to determine other RP genes that might be responsible for DBA.

In the present study, we investigated large deletions using our novel approach for gene copy number variation analysis based on quantitative-PCR and a single nucleotide polymorphism (SNP) array. We screened Japanese DBA patients and found 7 patients with a large deletion in an allele in *RPL5*, *RPL35A*, *RPS17*, or *RPS19*. Interestingly, all of these patients with a large deletion had a phenotype of growth retardation, including short stature and

Submitted July 24, 2011; accepted November 15, 2011. Prepublished online as *Blood* First Edition paper, January 18, 2012; DOI 10.1182/blood-2011-07-368662.

The online version of this article contains a data supplement.

The publication costs of this article were defrayed in part by page charge payment. Therefore, and solely to indicate this fact, this article is hereby marked "advertisement" in accordance with 18 USC section 1734.

From bloodjournal.hematologylibrary.org at MEDICAL LIBRARY OF NAGOYA UNIV on February 6, 2013. For personal use only.

Table 1. Primers used for synchronized quantitative-PCR (s-q-PCR) of RPL proteins

Gene	Primer name	Sequence	Primer name	Sequence	Size, bp
RPL5	L5-02F	CTCCCAAAGTGCTTGAGATTACAG	L5-02R	CACCTTTTCCTAACAAATTCCCAAT	132
	L5-05F	AGCCCTCCAACCTAGGTGACA	L5-05R	GAATTGGGATGGGCAAGAACT	102
	L5-17F	TGAACCCTTGCCCTAAAACATG	L5-17R	TCTTGGTCAGGCCCTGCTTA	105
	L5-19F	ATTGTGCAAACTCGATCACTAGCT	L5-19R	GTGTCTGAGGCTAACACATTTCCAT	103
	L5-21F	GTGCCACTCTCTTGGACAAACTG	L5-21R	CATAGGGCCAAAAGTCAAATAGAAG	102
	L5-28F	TCCACTTTAGGTAGGCGAAACC	L5-28R	TCAGATTTGGCATGTACCTTTCA	102
RPL11	L11-06F	GCACCCACATGGCTTAAAGG	L11-6R	CAACCAACCCATAGGCCAAA	102
	L11-20F	GAGCCCCCTTTCTCAGATGATA	L11-20R	CATGAACTTGGGCTCTGAATCC	109
	L11-22F	TATGTGCAGATAAGAGGGCAGTCT	L11-22R	ATACAGATAAGGAAACTGAGGCAGATT	98
RPL19	L19-02F	TGGCCTCTCATAAAGGAAATCTCT	L19-02R	GGAATGCAGGCAAGTTACTCTGTT	103
	L19-08F	TTTGAAGGCAAGAAATAAGTTCCA	L19-08R	AGCACATCACAGAGTCCAAATAGG	107
	L19-16F	GGTTAGTTGAAGCAGGAGCCTTT	L19-16R	TGCTAGGGAGACAGAAGCACATC	102
	L19-19F	GGACCAGTAGTTGTGACATCAGTTAAG	L19-19R	CCCATTTGTAACCCCCACTTG	106
RPL26	L26-03F	TCCAAAGAGCTGAGACAGAAGTACA	L26-03R	TCCATCAAGACAACGAGAACAAGT	102
	L26-16F	TTTGAGAATGCTTGAGAGAAGGAA	L26-16R	TTCCAGCACATGTAAAATCAAGGA	102
	L26-18F	ATGTTTTAATAAGCCCTCCAGTTGA	L26-18R	GAGAACAGCAAGTTGAAAGGTTCA	102
	L26-20F	GGGCTTTGCTTGATCACTCTAGA	L26-20R	AGGGAGCCCGAAAACATTTAC	104
RPL35A	L35A-01F	TGTGGCTTCTATTTTGCGTCAT	L35A-01R	GGAATTACCTCCTTTATTGCTTACAAG	121
	L35A-07F	TTTCCGTTCTGTCTATTGCTGTGT	L35A-07R	GAACCCTGAGTGGAGGATGTTC	113
	L35A-17F	GCCCACAACCTCCAGAGAATC	L35A-17R	GGATCACTTGAGGCCAGGAAT	104
	L35A-18F	TTAGGTGGGCTTTTCAGTCTCAA	L35A-18R	ATCTCCTGATTCCCCAACTTTGT	102
RPL36	L36-02F	CCGCTCTACAAGTGAAGAAATTCTG	L36-02R	CTCCCTCTGCCTGTGAAATGA	102
	L36-04F	TGCGTCCTGCCAGTGTTG	L36-04R	GGGTAGCTGTGAGAACCAAGGT	105
	L36-17F	CCCCTTGAAAGGACAGCAGTT	L36-17R	TTGGACACCAGGCACAGACTT	114

Table 2. Primers used for s-q-PCR of RPS proteins

Gene	Primer name	Sequence	Primer name	Sequence	Size, bps
RPS7	S7-11F	GCGCTGCCAGATAGGAAATC	S7-11R	TTAGGGAGCTGCCTTACATATGG	102
	S7-12F	ACTGGCAGTTCTGTGATGCTAAGT	S7-12R	ACTCTTGCTCATCTCCAAAACCA	102
	S7-16F	GTGTCTGTGCCAGAAAGCTTGA	S7-16R	GAACCATGCAAAAGTGCCAATAT	112
RPS10	S10-03F	CTACGGTTTTGTGTGGGTCACTT	S10-03R	CATCTGCAAGAAGGAGACGATTG	102
	S10-15F	GTTGGCCTGGAGTCGTGATTT	S10-15R	ATTCCAAGTGCACCATTTCCTT	101
	S10-17F	AATGGTGTTTAGGCCAACGTTAC	S10-17R	TTTGAACAGTGGTTTTTGTGCAT	100
RPS14	S14-03F	GAATTCCAAACCCTTCTGCAAA	S14-03R	TTGCTTCATTTACTCCTCAAGACATT	104
	S14-05F	ACAACCAGCCCTCTACCTCTTTT	S14-05R	GGAAGACGCCGGCATTATT	102
	S14-06F	CGCCTCTACCTCGCCAAAC	S14-06R	GGGATCGGTGCTATTGTTATTCC	102
	S14-09F	GCCATCATGCCGAAACATACT	S14-09R	AACGCGCCACAGGAGAGA	102
	S14-13F	ATCAGGTGGAGCACAGGAAAAC	S14-13R	GCGAGGGAGCTGCTTGATT	111
	S14-15F	AGAAGTTTTAGTGAGGCAGAAATGAGA	S14-15R	TCCCCTGGCTATTAAATGAAACC	102
	S14-19F	GATGAATTGTCCTTTCCTCCATTC	S14-19R	TAGGCGGAAACCAAAAATGCT	102
RPS15	S15-11F	CTCAGCTAATAAAGGCGCACATG	S15-11R	CCTCACACCACGAACCTGAAG	108
	S15-15F	GGTTGGAGAACATGGTGAGAACTA	S15-15R	CACATCCCTGGGCCACTCT	108
RPS17	S17-03F	ACTGCTGTCGTGGCTCGATT	S17-03R	GATGACCTGTTCTTCTGGCCTTA	121
	S17-05F	GAAAACAGATACAAATGGCATGGT	S17-05R	TGCCTCCCACTTTTCCAGAGT	114
	S17-12F	CTATGTGTAGGAGGTCCCAGGATAG	S17-12R	CCACCTGGTACTGAGCACATGT	102
	S17-16F	TAGCGGAAGTTGTGTGCATTG	S17-16R	CAAGAACAGAAGCAGCCAAGAG	102
	S17-18F	TGGCTGAATCTGCCTGCTT	S17-18R	GCCTTGTATGTACCTGGAAATGG	103
	S17-20F	GGGCCCTTCACAAATGTTGA	S17-20R	GCAAAACTCTGTCCCTTTGAGAA	101
RPS19	S19-24F	CCATCCCAAGAATGCACACA	S19-24R	CGCCGTAGCTGGTACTCATG	120
	S19-28F	GACACACCTGTTGAGTCCTCAGAGT	S19-28R	GCTTCTATTAACTGGAGCACACATCT	114
	S19-36F	CTCTTGAGGGTGGTCTGGAAAT	S19-36R	GTCTTTGCGGGTTCTTCCTCTAC	102
	S19-40F	GGAACGGTGTCAGGATTCAAG	S19-40R	AGCGGCTGTACACCAGAAATG	101
	S19-44F	CTGAGGTTGAGTGTCCCATTTCT	S19-44R	GCACCGGGCCTCTGTTATC	104
	S19-57F	CAGGGACACAGTGCTGAGAAACT	S19-57R	TGAGATGTCCCATTTTCACTATTGTT	101
	S19-58F	CATGATGTTAGCTCCGTTGCATA	S19-58R	ATTTTGGGAAGAGTGAAGCTTAGGT	102
	S19-62F	GCAACAGAGCGAGACTCCATTT	S19-62R	AGCACTTTTCGGCACTTACTTCA	102
	S19-65F	ACATTTCCCAGAGCTGACATGA	S19-65R	TCGGGACACCTAGACCTTGCT	102
RPS24	S24-17F	CGACCACGTCTGGCTTAGAGT	S24-17R	CCTTCATGCCCAACCAAGTC	101
	S24-20F	ACAAGTAAGCATCATCACCTCGAA	S24-20R	TTTCCCTCACAGCTATCGTATGG	105
	S24-32F	GGGAAATGCTGTGTCCACATACT	S24-32R	CTGGTTTCATGGCTCCAGAGA	105
RPS26	S26-03F	CGCAGCAGTCAGGGACATTT	S26-03R	AAGTTGGGCGAAGGCTTTAAG	104
	S26-05F	ATGGAGGCCGTCTAGTTTGGT	S26-05R	TGCCTACCCTGAACCTTGCT	102
RPS27A	S27A-09F	GCTGGAGTGCATTCGCTTGT	S27A-09R	CACGCCTGTAATCCCCACTAA	102
	S27A-12F	CAGGCTTGGTGTGCTGTGACT	S27A-12R	ACGTCCATCTTCCAGCTGCTT	103
	S27A-18F	GGGTTTTTCCTGTTTGGTATTTGA	S27A-18R	AAAGGCCAGCTTTGCAAGTG	111
	S27A-22F	TTACCATATTGCCAGTCTTTCCATT	S27A-22R	TTCATATGCATTTGCACAAACTGT	106

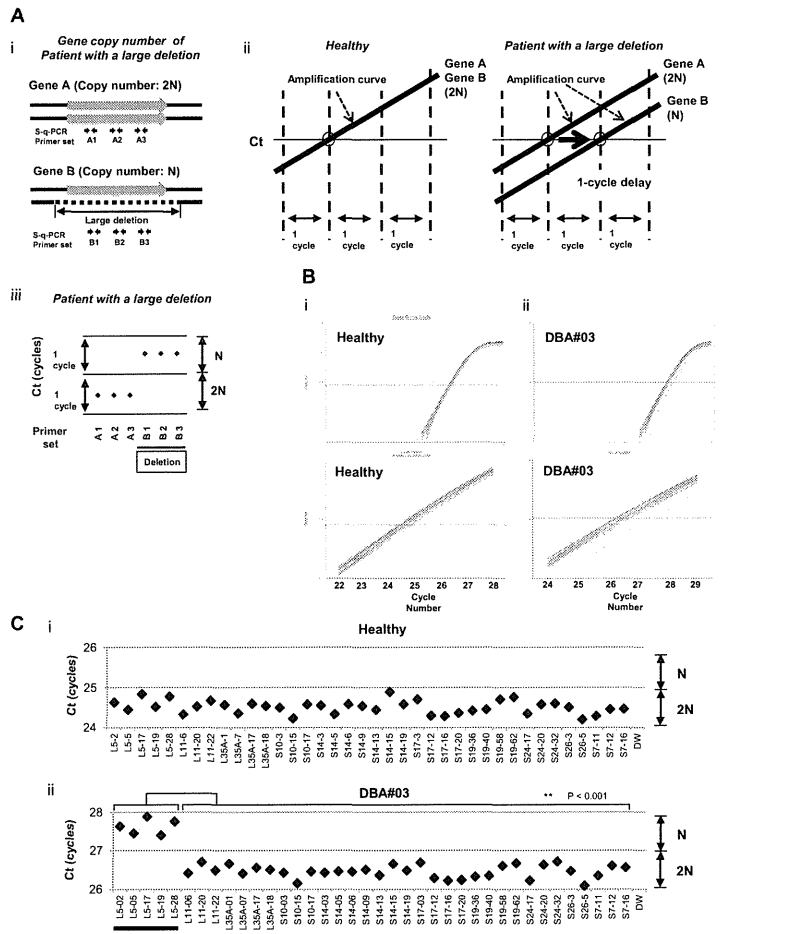

Figure 1. s-q-PCR can determine a large gene deletion in DBA. (A) Concept of the DBA s-q-PCR assay. The difference in gene copy number between a healthy sample and that with a large deletion is 2-fold (i). When all genomic s-q-PCR for genes of interest synchronously amplify DNA fragments, a 2-fold difference in the gene copy number is detected by a 1-cycle difference of the Ct scores of the s-q-PCR amplification curves (ii). Also shown is a dot plot of the Ct scores (iii). (B) Results of the amplification curves of s-q-PCR performed with a healthy person (i) and a DBA patient (patient 3; ii). The top panel shows the results of PCR cycles; the bottom panel is an extended graph of the PCR cycles at logarithmic amplification. (C) Graph showing Ct scores of s-q-PCR. If all specific primer sets for DBA genes show a 1-cycle delay relative to each other, this indicates a large deletion in the gene. Gene primer sets with a large deletion are underlined in the graph. $^{**}P < .001$.

small-for-gestational age (SGA), which suggests that this is a characteristic of DBA patients with a large gene deletion in Japan.

Methods

Patient samples

Genomic DNA was extracted using the GenElute Blood Genomic DNA Kit (Sigma-Aldrich) according to the manufacturer's protocol. Clinical manifestation of patients from a Japanese DBA genomic library are listed elsewhere or are as reported by Konno et al.[8] The study was approved by the institutional review board at the National Institute of Infectious Diseases and Hirosaki University.

DBA gene copy number assay by s-q-PCR

For s-q-PCR, primers were designed using Primer Express Version 3.0 software (Applied Biosystems). Primers are listed in Tables 1 and 2. Genomic DNA in water was denatured at 95°C for 5 minutes and immediately cooled on ice. The composition of the s-q-PCR mixture was as follows: 5 ng of denatured genomic DNA, 0.4mM forward and reverse primers, 1× SYBR Premix Ex Taq II (Takara), and 1× ROX reference dye II (Takara) in a total volume of 20 μL (all experiments were performed in duplicate). Thermal cycling was performed using the Applied Biosystems 7500 fast real-time PCR system. Briefly, the PCR mixture was denatured at 95°C for 30 seconds, followed by 35 cycles of 95°C for 5 seconds, 60°C for 34 seconds, and then dissociation curve measurement. Threshold cycle (Ct) scores were determined as the average of duplicate samples. The technical errors of Ct scores in the triplicate analysis were within 0.2 cycles (supplemental Figure 1, available on the *Blood* Web site; see the Supplemental Materials link at the top of the online article). The sensitivity and specificity of this method was evaluated with 15 healthy samples. Any false positive was not observed in all primer sets in all healthy samples (supplemental Figure 2). We performed direct sequencing of the s-q-PCR products. The results of the sequence analysis were searched for using BLAST to confirm uniqueness. Sequence data were obtained from GenBank (http://www.ncbi.nlm.nih.gov/gene/) and Ensemble Genome Browser (http://uswest.ensembl.org).

Genomic PCR

Genomic PCR was performed using KOD FX (Toyobo) according to the manufacturer's step-down PCR protocol. Briefly, the PCR mixture contained 20 ng of genomic DNA, 0.4mM forward and reverse primers, 1mM dNTP, 1× KOD FX buffer, and 0.5 U KOD FX in a total volume of 25 μL in duplicate. Primers are given in supplemental Figure 3 and Table 2. PCR mixtures were denatured at 94°C for 2 minutes, followed by 4 cycles of 98°C for 10 seconds, 74°C for 12 minutes, followed by 4 cycles of 98°C for 10 seconds, 72°C for 12 minutes followed by 4 cycles of 98°C for 10 seconds, 70°C for 12 minutes, followed by 23 cycles of 98°C for 10 seconds and 68°C for 12 minutes. PCR products were loaded on 0.8% agarose gels and detected by LAS-3000 (Fujifilm).

DNA sequencing analysis

The genomic PCR product was purified by the GenElute PCR clean-up kit (Sigma-Aldrich) according to the manufacturer's instructions. Direct sequencing was performed using the BigDye Version 3 sequencing kit. Sequences were read and analyzed using a 3120x genetic analyzer (Applied Biosystems).

SNP array-based copy number analysis

SNP array experiments were performed according to the standard protocol of GeneChip Human Mapping 250K Nsp arrays (Affymetrix). Microarray data were analyzed for determination of the allelic-specific copy number using the CNAG program, as described previously.[14] All microarray data are available at the EGA database (www.ebi.ac.uk/ega) under accession number EGAS00000000105.

Results

Construction of a convenient method for RP gene copy number analysis based on s-q-PCR

We focused on the heterozygous large deletions in DBA-responsible gene. The difference in copy number of genes between a mutated DBA allele and the intact allele was 2-fold (N and 2N; Figure 1Ai). If each PCR can synchronously amplify DNA fragments when the template genomic DNA used is of normal karyotype, it is possible to conveniently detect a gene deletion with a 1-cycle delay in s-q-PCR analysis (Figure 1Aii-iii).

Table 3. Summary of mutations and the mutation rate observed in Japanese DBA patients

Gene	Sequencing analysis
RPS19	10
RPL5	6
RPL11	3
RPS17	1
RPS10	1
RPS26	1
RPL35A	0
RPS24	0
RPS14	0
Mutations, n (%)	22 (32.4%)
Total analyzed, N	68

To apply this strategy for allelic analysis of DBA, we prepared primers for 16 target genes, *RPL5*, *RPL11*, *RPL35A*, *RPS10*, *RPS19*, *RPS26*, *RPS7*, *RPS17*, *RPS24*, *RPL9*, *RPL19*, *RPL26*, *RPL36*, *RPS14*, *RPS15*, and *RPS27A*, under conditions in which the Ct of s-q-PCR would occur within 1 cycle of that of the other primer sets (Tables 1 and 2). At the same time, we defined the criteria of a large deletion in our assay as follows. If multiple primer sets for one gene showed a 1-cycle delay from the other gene-specific primer set at the Ct score, we assumed that this represented a large deletion. As shown in Figure 1Bii and 1Cii, the specific primer sets for *RPL5* (L5-02, L5-05, L5-17, L5-19, and L5-28) detected a 1-cycle delay with respect to the mutated allele of patient 3. This assessment could be verified by simply confirming the difference of the cycles with the s-q-PCR amplification curves.

Study of large gene deletions in a Japanese DBA genomic DNA library

Sixty-eight Japanese DBA patients were registered and blood genomic DNA was collected at Hirosaki University. All samples were first screened for mutations in *RPL5*, *L11*, *L35A*, *S10*, *S14*, *S17*, *S19*, and *S26* by sequencing. Among these patients, 32.4% (22 of 68) had specific DBA mutations (Table 3 and data not shown). We then screened for large gene deletions in 27 patients from the remaining 46 patients who did not possess mutations as determined by sequencing (Table 4).

When we performed the s-q-PCR DBA gene copy number assay, 7 of 27 samples displayed a 1-cycle delay of Ct scores: 1 patient had *RPL5* (patient 14), 1 had *RPL35A* (patient 71), 3 had *RPS17* (patients 3, 60, 62), and 2 had *RPS19* (patients 24 and 72; Figure 2 and Table 4). Among these patients, the large deletions in the *RPL5* and *RPS17* genes are the first reported cases of allelic deletions in DBA. From these results, we estimate that a sizable number of Japanese DBA patients have a large deletion.

Based on our findings, the rate of large deletions was approximately 25.9% (7 of 27) in a category of unspecified gene mutations. Such mutations have typically gone undetected by conventional sequence analysis. We could not find any additional gene deletions in the analyzed samples.

Confirmation of the gene copy number for DBA genes by genome-wide SNP array

We performed genome-wide copy number analysis of the 27 DBA patients with a SNP array to confirm our s-q-PCR results. SNP array showed that patient 3 had a large deletion in

Table 4. Characteristics of DBA patients tested

Patient no.	Age at diagnosis	Sex	Hb, g/dL	Large deletion by s-q-PCR	Large deletion by SNP array	Inheritance	Malformations	Response to first steroid therapy
Patients with a large deletion in RP genes								
3*†	1 y	M		RPL5	RPL5	Sporadic	Short stature, thumb anomalies	Response
14*	5 y	M	5.5	RPS17	RPS17	Sporadic	White spots, short stature	Response
24*†	1 mo	F	5.5	RPS19	ND	Sporadic	Short stature, SGA	Response
60*†	2 mo	F	2.4	RPS17	RPS17	Sporadic	SGA	NT
62*†	1 mo	F	6.2	RPS17	RPS17	Sporadic	Small ASD, short stature, SGA	Response
71	0 y	M	5.3	RPL35A	RPL35A	Sporadic	Thumb anomalies, synostosis of radius and ulna, Cohelia Lange-like face, cleft palate, underdescended testis, short stature, cerebellar hypoplasia, fetal hydrops	NT
72†	0 y	M	2	RPS19	RPS19	Sporadic	Thumb anomalies, flat thenar, testicular hypoplasia, fetal hydrops, short stature, learning disability	No
Patients without a large deletion in RP genes								
5*	1 y	F	3.1	ND	ND	Sporadic	ND	Response
15*	1 mo	F	1.6	ND	ND	Sporadic	ND	Response
21*	1 y	F	2.6	ND	ND	Sporadic	ND	Response
26*	1 y 1 mo	F	8	ND	ND	Sporadic	Congenital hip dislocation, spastic quatriplegia, hypertelorism, nystagmus, short stature, learning disability	Response
33*	2 mo	F	1.3	ND	ND	Sporadic	ND	Response
36*	0 y	M	8.2	ND	ND	Familial	ND	Response
37*	4 y	M	6.1	ND	ND	Sporadic	Hypospadias, underdescended testis, SGA	NT
45*	5 d	M	5.1	ND	ND	Sporadic	Short stature, microcephaly, mental retardation, hypogammaglobulinemia	Poor
50*	2 m	F	3.4	ND	ND	Familial	ND	Response
61*	9 m	M	4	ND	ND	Sporadic	ND	Response
63*	0 y	M	6.8	ND	ND	Sporadic	Micrognathia, hypertelorism, short stature	Response
68	1 y 4 mo	M	5.9	ND	ND	Sporadic	ND	NT (CR)
69	1 y	M	9.3	ND	ND	Sporadic	ND	Response
76	0 y	M	4	ND	ND	Sporadic	ND	Response
77	0 y	M	7.8	ND	ND	Familial	Short stature	No
83	9 mo	F	3	ND	ND	Sporadic	ND	NT
90	10 mo	M	9	ND	ND	Sporadic	ND	No
91	0 y	F	3.8	ND	ND	Sporadic	ND	Response
92	2 mo	M	3.7	ND	ND	Sporadic	ASD, PFO, melanosis, underdescended testis, SGA, short stature	Response
93	11 mo	M	2.2	ND	ND	Sporadic	White spots, senile face, corneal opacity, underdescended testis, syndactyly, ectrodactyly, flexion contracture, extension contracture	Response

ND indicates not detected; NT, not tested; CR, complete remission; ASD, atrial septal defect; and PFO, persistent foramen ovale.
*Status data of Japanese probands 3 to 63 is from a report by Konno et al.[8]
†Large deletions of the parents of 5 DBA patients (3, 24, 60, 62, and 72) were analyzed by s-q-PCR, but there were no deletions in DBA genes in any of the 5 pairs of parents.

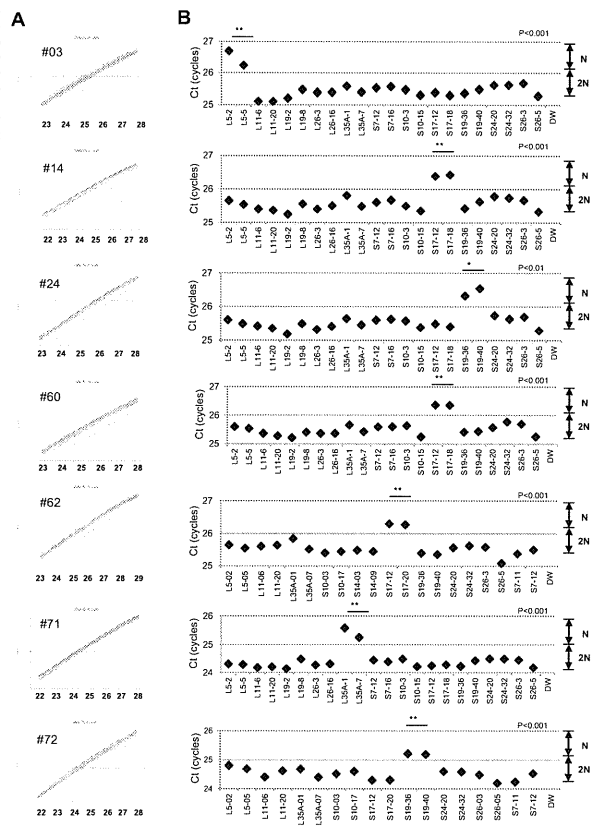

Figure 2. Detection of 7 mutations with a large deletion in DBA patients. Genomic DNA of 27 Japanese DBA patients with unknown mutations were subjected to the DBA gene copy number assay. (A) Amplification curve of s-q-PCR of a mutation with a large deletion. The deleted gene can be easily distinguished. (B) Ct score (cycles) of representative s-q-PCR with DBA genomic s-q-PCR primers. Results of the 2 gene-specific primer pairs indicated in the graph are representative of at least 2 sets for each gene-specific primer (carried out in the same run). $^{**}P < .001$; $^{*}P < .01$

chromosome 1 (ch1) spanning 858 kb (Figure 3A); patient 71 had a large deletion in ch3 spanning 786 kb (Figure 3B); patients 14, 60, and 62 had a large deletion in ch15 spanning 270 kb, 260 kb, and 330 kb, respectively (Figure 3C); and patient 72 had a large deletion in ch19 spanning 824 kb (Figure 3D). However, there were no deletions detected in ch19 in patient 24 (Figure 3D). Genes estimated to reside within a large deletion are listed in supplemental Table 1. Consistent with these s-q-PCR results, 6 of 7 large deletions were detected and confirmed as deleted regions, and these large deletions contained *RPL5*, *RPL35A*, *RPS17*, and *RPS19* (Table 4 and supplemental Table 1). Other large deletions in RP genes were not detected by this analysis. From these results, we conclude that the synchronized multiple PCR amplification method has a detection sensitivity comparable to that of SNP arrays.

Detailed examination of a patient with intragenic deletion in the RPS19 allele (patient 24)

Interestingly, for patient 24, in whom we could not detect a large deletion by SNP array at s-q-PCR gene copy number analysis, 2 primer sets for *RPS19* showed a 1-cycle delay (RPS19-36 and RPS19-40), but 2 other primer pairs (RPS19-58 and RPS19-62) did not show this delay (Figure 4A). We attempted to determine the deleted region in detail by testing more primer sets on *RPS19*. We tested a total of 9 primer sets for *RPS19* (Figure 4B) and examined the gene copy numbers. Surprisingly, 4 primer sets (S19-24, S19-36, S19-40, and S19-44) for intron 3 of *RPS19* indicated a 1-cycle delay, but the other primers for *RPS19* located on the 5′untranslated region (5′UTR), intron 3, or 3′UTR did not show this delay (S19-57, S19-58, S19-28, S19-62, and S19-65; Figure 4B-C). These results suggest that the intragenic deletion occurred in the *RPS19* allele. To confirm this deleted region precisely, we performed genomic PCR on *RPS19*, amplifying a region from the 5′UTR to intron 3 (Figure

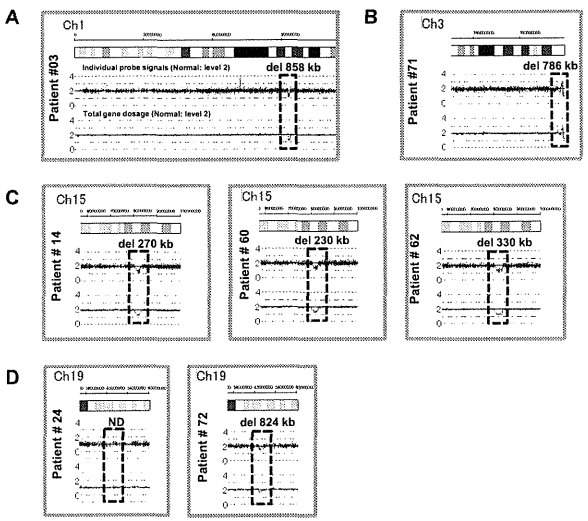

Figure 3. Results of SNP genomic microarray (SNP-chip) analysis. Genomic DNA of 27 Japanese DBA patients with unknown mutations was examined using a SNP array. Six patients had large deletions in their chromosome (ch), which included one DBA-responsible gene. Patient 3 has a large deletion in ch1 (A), patient 71 has a deletion in ch3 (B), patients 14, 60, and 62 have deletions in ch15 (C), and patient 72 has a deletion in ch19 (D).

4B). In patient 24, we observed an abnormally sized PCR product at a low molecular weight by agarose gel electrophoresis (Figure 4D). We did not detect a wild-type PCR product from the genomic PCR. This finding is probably because PCR tends to amplify smaller molecules more easily. However, we did detect a PCR fragment at the correct size using primers located in the supposedly deleted region. These bands were thought to be from the products of a wild-type allele. Sequencing of the mutant band revealed that intragenic recombination occurred at a homologous region of 27 nucleotides, from −1400 to −1374 in the 5′ region, to +5758 and +5784 in intron 3, which resulted in the loss of 7157 base pairs in the *RPS19* gene (Figure 4E). The deleted region contains exons 1, 2, and 3, and therefore the correct *RPS19* mRNA could not be transcribed.

Genotype-phenotype analysis and DBA mutations in Japan

Patients with a large deletion in DBA genes had common phenotypes (Table 4). Malformation with growth retardation (GR), including short stature or SGA, were observed in all 7 patients. In patients who had a mutation found by sequencing, half had GR (11 of 22; status data of DBA patients with mutations found by sequencing are not shown). GR may be a distinct phenotypic feature of large deletion mutations in Japanese DBA patients. Familial mutations were analyzed for parents for 5 DBA patients with a large deletion (patients 3, 24, 60, 62, and 72) by s-q-PCR. There are no large deletions in all 5 pairs of parents in DBA-responsible genes. Four of the 7 patients responded to steroid therapy. We have not observed significant phenotypic differences between patients with extensive deletions and other patients with regard to blood counts, responsiveness to treatment, or other malformations.

Discussion

Many studies have reported RP genes to be responsible for DBA. However, mutations have not been determined for approximately half of DBA patients analyzed. There are 2 possible reasons for this finding. One possibility is that patients have other genes responsible for DBA, and the other is that patients have a complicated set of mutations in RP genes that are difficult to detect. In the present study, we focused on the latter possibility because we have found fewer Japanese DBA patients with RP gene mutations (32.4%) compared with another cohort study of 117 DBA patients and 9 RP genes (approximately 52.9%).[4] With our newly developed method, we identified 7 new mutations with a large deletion in *RPL5*, *RPL35A*, *RPS17*, and *RPS19*.

The frequency of a large deletion was approximately 25.9% (7 of 27) in our group of patients who were not found to have mutations by genomic sequencing. Therefore, total RP gene mutations were confirmed in 42.6% of these Japanese patients (Table 5). Interestingly, mutations in *RPS17* have been observed at a high rate (5.9%) in Japan relative to that in other countries (1%).[5,15,16] Although the percentage of DBA mutations differs among different ethnic groups,[8,17-19] a certain portion of large deletions in DBA-responsible genes are likely to be determined in other countries by new strategies.

In the present study, we analyzed patient data to determine genotype-phenotype relations. To date, large deletions have been reported with RPS19 and RPL35A in DBA patients.[3,6,13] *RPS19* large deletions/translocations have been reported in 12 patients, and *RPL35A* large deletions have been reported in 2 patients.[19] GR in patients with a large deletion has been observed previously with *RPS19* translocations,[3,19-21] but it was not found in 2 patients with *RPL35A* deletion.[6] Interestingly, all of our patients with a large deletion had a phenotype

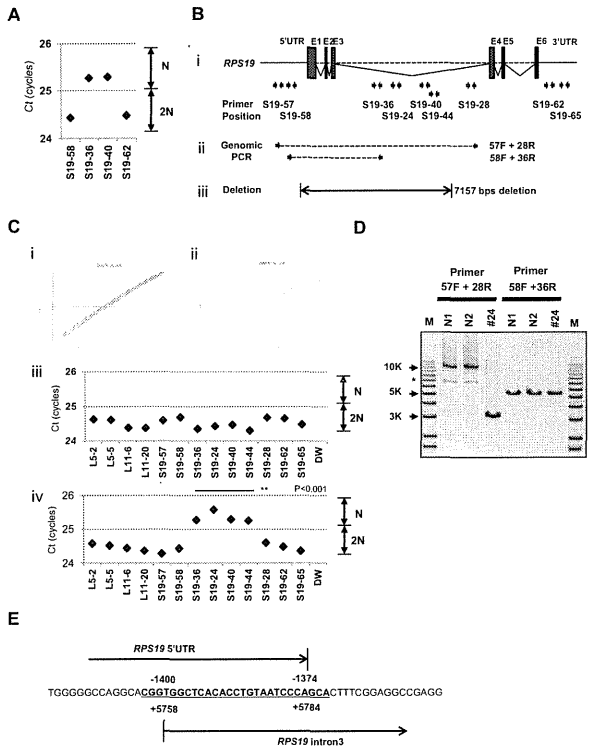

Figure 4. Result of s-q-PCR gene copy number assay for patient 24. (A) Results of s-q-PCR gene copy number assay for *RPS19* with 4 primer sets. (Bi) The *RPS19* gene copy number was analyzed with 9 specific primer sets for *RPS19* that span from the 5′UTR to the 3′UTR. (ii) Primer positions of genomic PCR for *RPS19*. (iii) Region determined to be an intragenic deletion in *RPS19*. (C) Results of gene copy number assay for *RPS19* show a healthy person (i,iii) and a DBA patient (ii,iv), and Ct results are shown (iii-iv). Patient 24 showed a "1-cycle delay" with primers located in the intron 3 region, but other primer sets were normal. (D) Results of genomic PCR amplification visualized by agarose gel electrophoresis to determine the region of deletion. N1 and N2 are healthy samples. *Nonspecific band. (E) Results from the genomic sequence of the 3-kb DNA band from genomic PCR on patient 24 showing an intragenic recombination from −1400 to 5784 (7157 nt) in *RPS19*. **$P < .001$.

of GR, including short stature and SGA, which suggests that this is a characteristic of DBA with a large gene deletion in Japan. Our study results suggest the possibility that GR is associated with extensive deletion in Japanese patients. Although further case studies will be needed to confirm this possibility, screening of DBA samples using our newly developed method will help to advance our understanding of the broader implications of the mutations and the correlation with the DBA genotype-phenotype.

Table 5. Total mutations in Japanese DBA patients, including large gene deletions

Gene	Mutation rate
RPS19	12(17.6%)
RPL5	7(10.3%)
RPL11	3 (4.4%)
RPS17	4 (5.9%)
RPS10	1 (1.5%)
RPS26	1 (1.5%)
RPL35A	1 (1.5%)
RPS24	0
RPS14	0
Mutations, n (%)	29(42.6%)
Total analyzed, N	68

Copy number variation analysis of DBA has been performed by linkage analysis, and the *RPS19* gene was first identified as a DBA-susceptibility gene. Comparative genomic hybridization array technology has also been used to detect DBA mutations in *RPL35A*, and multiplex ligation-dependent probe amplification has been used for *RPS19* gene deletion analysis.[3,6,13,22] However, these analyzing systems have problems in mutation screening. Linkage analysis is not a convenient tool to screen for multiple genetic mutations, such as those in DBA, because it requires a high level of proficiency. Although comparative genomic hybridization technology is a powerful tool with which to analyze copy number comprehensively, this method requires highly specialized equipment and analyzing software, which limits accessibility for researchers. Whereas quantitative PCR–based methods for copy number variation analysis are commercially available (TaqMan), they require a standard curve for each primer set, which limits the number of genes that can be loaded on a PCR plate. To address this issue, a new method of analysis is needed. By stringent selection of PCR primers, the s-q-PCR method enables analysis of many DBA genes in 1 PCR plate and the ability to immediately distinguish a large deletion using the s-q-PCR amplification curve. In our study, 6 of 7 large deletions in the RP gene detected by s-q-PCR were confirmed by SNP arrays (Figure 3). Interestingly, we detected

1 large intragenic deletion in *RPS19*, which was not detected by the SNP array. This agreement between detection results suggests that the s-q-PCR copy number assay could be useful for detecting large RP gene deletions.

In the present study, 7 DBA patients carried a large deletion in the RP genes. This type of mutation could be underrepresented by sequencing analysis, although in the future, genome sequencing might provide a universal platform for mutation and deletion detection. We propose that gene copy number analysis for known DBA genes, in addition to direct sequencing, should be performed to search for a novel responsible gene for DBA. Although at present, it may be difficult to observe copy numbers on all 80 ribosomal protein genes in one s-q-PCR assay, our method allows execution of gene copy number assays for several target genes in 1 plate. Because our method is quick, easy, and low cost, it could become a conventional tool for detecting DBA mutations.

Acknowledgments

The authors thank Momoka Tsuruhara, Kumiko Araki, and Keiko Furuhata for their expert assistance.

This work was partially supported by grants-in-aid for scientific research from the Ministry of Education, Culture, Sports, Science and Technology of Japan, and by Health and Labor Sciences research grants (Research on Intractable Diseases) from the Ministry of Health, Labor and Welfare of Japan.

Authorship

Contribution: M.K. designed and performed the research, analyzed the data, and wrote the manuscript; A.S-O. and S. Ogawa performed the SNP array analysis; T.M., M.T., and M.O designed the study; T.T, K. Terui, and R.W. analyzed the mutations and status data; H.K., S. Ohga, A.O., S.K., T.K., K.G., K.K., T.M., and N.M. analyzed the status data; A.M., H.M., K. Takizawa, T.M., and K.Y., performed the research and analyzed the data; E.I. and I.H. designed the study and analyzed the data; and all authors wrote the manuscript.

Conflict-of-interest disclosure: The authors declare no competing financial interests.

Correspondence: Isao Hamaguchi, MD, PhD, Department of Safety Research on Blood and Biological Products, National Institute of Infectious Diseases, 4-7-1, Gakuen, Musashimurayama, Tokyo 208-0011, Japan; e-mail: 130hama@nih.go.jp; or Etsuro Ito, MD, PhD, Department of Pediatrics, Hirosaki University Graduate School of Medicine, 5 Zaifucho, Hirosaki, Aomori 036-8562, Japan; e-mail: eturou@cc.hirosaki-u.ac.jp.

References

1. Hamaguchi I, Flygare J, Nishiura H, et al. Proliferation deficiency of multipotent hematopoietic progenitors in ribosomal protein S19 (RPS19)-deficient diamond-Blackfan anemia improves following RPS19 gene transfer. *Mol Ther.* 2003;7(5 pt 1):613-622.
2. Vlachos A, Ball S, Dahl N, et al. Diagnosing and treating Diamond Blackfan anaemia: results of an international clinical consensus conference. *Br J Haematol.* 2008;142(6):859-876.
3. Draptchinskaia N, Gustavsson P, Andersson B, et al. The gene encoding ribosomal protein S19 is mutated in Diamond-Blackfan anaemia. *Nat Genet.* 1999;21(2):169-175.
4. Doherty L, Sheen MR, Vlachos A, et al. Ribosomal protein genes RPS10 and RPS26 are commonly mutated in Diamond-Blackfan anemia. *Am J Hum Genet.* 2010;86(2):222-228.
5. Gazda HT, Sheen MR, Vlachos A, et al. Ribosomal protein L5 and L11 mutations are associated with cleft palate and abnormal thumbs in Diamond-Blackfan anemia patients. *Am J Hum Genet.* 2008;83(6):769-780.
6. Farrar JE, Nater M, Caywood E, et al. Abnormalities of the large ribosomal subunit protein, Rpl35a, in Diamond-Blackfan anemia. *Blood.* 2008;112(5):1582-1592.
7. Gazda HT, Grabowska A, Merida-Long LB, et al. Ribosomal protein S24 gene is mutated in Diamond-Blackfan anemia. *Am J Hum Genet.* 2006; 79(6):1110-1118.
8. Konno Y, Toki T, Tandai S, et al. Mutations in the ribosomal protein genes in Japanese patients with Diamond-Blackfan anemia. *Haematologica.* 2010;95(8):1293-1299.
9. Robledo S, Idol RA, Crimmins DL, Ladenson JH, Mason PJ, Bessler M. The role of human ribosomal proteins in the maturation of rRNA and ribosome production. *RNA.* 2008;14(9):1918-1929.
10. Léger-Silvestre I, Caffrey JM, Dawaliby R, et al. Specific Role for Yeast Homologs of the Diamond Blackfan Anemia-associated Rps19 Protein in Ribosome Synthesis. *J Biol Chem.* 2005;280(46): 38177-38185.
11. Choesmel V, Fribourg S, Aguissa-Toure AH, et al. Mutation of ribosomal protein RPS24 in Diamond-Blackfan anemia results in a ribosome biogenesis disorder. *Hum Mol Genet.* 2008;17(9):1253-1263.
12. Flygare J, Aspesi A, Bailey JC, et al. Human RPS19, the gene mutated in Diamond-Blackfan anemia, encodes a ribosomal protein required for the maturation of 40S ribosomal subunits. *Blood.* 2007;109(3):980-986.
13. Quarello P, Garelli E, Brusco A, et al. Multiplex ligation-dependent probe amplification enhances molecular diagnosis of Diamond-Blackfan anemia due to RPS19 deficiency. *Haematologica.* 2008; 93(11):1748-1750.
14. Yamamoto G, Nannya Y, Kato M, et al. Highly sensitive method for genomewide detection of allelic composition in nonpaired, primary tumor specimens by use of affymetrix single-nucleotide-polymorphism genotyping microarrays. *Am J Hum Genet.* 2007;81(1):114-126.
15. Song MJ, Yoo EH, Lee KO, et al. A novel initiation codon mutation in the ribosomal protein S17 gene (RPS17) in a patient with Diamond-Blackfan anemia. *Pediatr Blood Cancer.* 2010;54(4):629-631.
16. Cmejla R, Cmejlova J, Handrkova H, Petrak J, Pospisilova D. Ribosomal protein S17 gene (RPS17) is mutated in Diamond-Blackfan anemia. *Hum Mutat.* 2007;28(12):1178-1182.
17. Cmejla R, Cmejlova J, Handrkova H, et al. Identification of mutations in the ribosomal protein L5 (RPL5) and ribosomal protein L11 (RPL11) genes in Czech patients with Diamond-Blackfan anemia. *Hum Mutat.* 2009;30(3):321-327.
18. Quarello P, Garelli E, Carando A, et al. Diamond-Blackfan anemia: genotype-phenotype correlations in Italian patients with RPL5 and RPL11 mutations. *Haematologica.* 2010;95(2):206-213.
19. Boria I, Garelli E, Gazda HT, et al. The ribosomal basis of Diamond-Blackfan Anemia: mutation and database update. *Hum Mutat.* 2010;31(12):1269-1279.
20. Campagnoli MF, Garelli E, Quarello P, et al. Molecular basis of Diamond-Blackfan anemia: new findings from the Italian registry and a review of the literature. *Haematologica.* 2004;89(4):480-489.
21. Willig TN, Draptchinskaia N, Dianzani I, et al. Mutations in ribosomal protein S19 gene and diamond blackfan anemia: wide variations in phenotypic expression. *Blood.* 1999;94(12):4294-4306.
22. Gustavsson P, Garelli E, Draptchinskaia N, et al. Identification of microdeletions spanning the Diamond-Blackfan anemia locus on 19q13 and evidence for genetic heterogeneity. *Am J Hum Genet.* 1998;63(5):1388-1395.

Brief report

Identification of *TRIB1* R107L gain-of-function mutation in human acute megakaryocytic leukemia

Takashi Yokoyama,[1] Tsutomu Toki,[2] Yoshihiro Aoki,[2] Rika Kanezaki,[2] Myoung-ja Park,[3] Yohei Kanno,[1] Tomoko Takahara,[1] Yukari Yamazaki,[1] Etsuro Ito,[2] Yasuhide Hayashi,[3] and Takuro Nakamura[1]

[1]Division of Carcinogenesis, Cancer Institute, Japanese Foundation for Cancer Research, Tokyo, Japan; [2]Department of Pediatrics, Hirosaki University Graduate School of Medicine, Hirosaki, Japan; and [3]Department of Hematology/Oncology, Gunma Children's Medical Center, Gunma, Japan

***Trib1* has been identified as a myeloid oncogene in a murine leukemia model. Here we identified a *TRIB1* somatic mutation in a human case of Down syndrome–related acute megakaryocytic leukemia. The mutation was observed at well-conserved arginine 107 residue in the pseudokinase domain. This R107L mutation remained in leukocytes of the remission stage in which *GATA1* mutation disappeared, suggesting the *TRIB1* mutation is an earlier genetic event in leukemogenesis. The bone marrow transfer experiment showed that acute myeloid leukemia development was accelerated by transducing murine bone marrow cells with the R107L mutant in which enhancement of ERK phosphorylation and C/EBPα degradation by Trib1 expression was even greater than in those expressing wild-type. These results suggest that TRIB1 may be a novel important oncogene for Down syndrome–related acute megakaryocytic leukemia. (*Blood.* 2012; 119(11):2608-2611)**

Introduction

The Down syndrome (DS) patients are predisposed to developing myeloid leukemia, and those patients frequently exhibit *GATA1* mutations.[1] However, it is proposed that the *GATA1* mutation is important for transient leukemia in DS but not sufficient for full-blown leukemia, suggesting that additional genetic alterations are needed.[1] Therefore, it is important to search the subsequent genetic changes for DS-related leukemia (ML-DS) to predict malignant transformation and prognosis of the patients.

Trib1 has been identified as a myeloid oncogene that cooperates with *Hoxa9* and *Meis1* in murine acute myeloid leukemia (AML).[2] As a member of the tribbles family of proteins, TRIB1 interacts with MEK1 and enhances ERK phosphorylation.[2,3] Moreover, TRIB1 promotes degradation of C/EBP family transcription factors, including C/EBPα, an important tumor suppressor for AML, and we observed that degradation of C/EBPα by Trib1 is mediated by its interaction with MEK1.[4] Thus, TRIB1 plays an important role in the development of AML by modulating both the RAS/MAPK pathway and C/EBPα function together with Trib2 that has also been identified as a myeloid-transforming gene.[5] Potential involvement of *TRIB1* in human leukemia has been reported in cases of AML with 8q34 amplification in which both *c-MYC* and *TRIB1* are included in the amplicon.[6] The enhancing effect of TRIB1 on the MAPK signaling suggests that TRIB1 alterations may be related to AML cases, which do not show any mutations in the pathway members, such as FLT3, c-Kit, or Ras. In this report, we identified a novel somatic mutation of *TRIB1* in a case of human acute megakaryocytic leukemia developed in DS (DS-AMKL). Retrovirus-mediated gene transfer followed by bone marrow transfer indicated that the mutation enhanced leukemogenic activity and MAPK phosphorylation by TRIB1.

Methods

Patients

TRIB1 mutations have been investigated in 12 cases of transient leukemia (TL), 5 of DS-AMKL, and 4 cell lines of DS-AML. Peripheral blood leukocytes of TL and bone marrow cells of DS-AMKL were used as sources for the molecular analysis. This study was approved by the Ethics Committee of Hirosaki University Graduate School of Medicine, and all clinical samples were obtained with informed consent from the parents of all patients, in accordance with the Declaration of Helsinki.

Patient 84 showed trisomy 21 and extensive leukocytosis at birth. Hematologic findings revealed the white blood cell count to be 148 × 10^9/L, including 87% myeloblasts, a hemoglobin level of 19.4 g/dL, and a platelet count of 259 × 10^9/L. Patent ductus arteriosus and atrial septal defect have been pointed out. Based on the hematologic data and the chromosomal abnormality, the patient was diagnosed as DS-related TL. The hematologic abnormality was then improved, but 8 months later 3% of 6.9 × 10^9/L white blood cells became myeloblasts (Figure 1A). A karyotype analysis of bone marrow cells revealed 48, XY,+8,+21 in 3 of 20 cells. In addition, *GATA1* mutation was detected at nt 113 from A to G, resulting in loss of the first methionine.[7] He was diagnosed as AMKL at this time, and his disease was in remission by subsequent chemotherapy.

PCR and sequencing

The entire coding region of human *TRIB1* cDNA of patients' samples was amplified using Taq polymerase (Promega) and specific primer pairs (the sequences of the primers are available on request). The genomic DNA samples of patient 84 were also analyzed. The sequence analysis of *GATA1* was performed as described previously.[7] After checking the PCR products by agarose gel electrophoresis, the products were purified and directly sequenced.

Submitted December 12, 2010; accepted January 6, 2012. Prepublished online as *Blood* First Edition paper, January 31, 2012; DOI 10.1182/blood-2010-12-324806.

The online version of this article contains a data supplement.

The publication costs of this article were defrayed in part by page charge payment. Therefore, and solely to indicate this fact, this article is hereby marked "advertisement" in accordance with 18 USC section 1734.

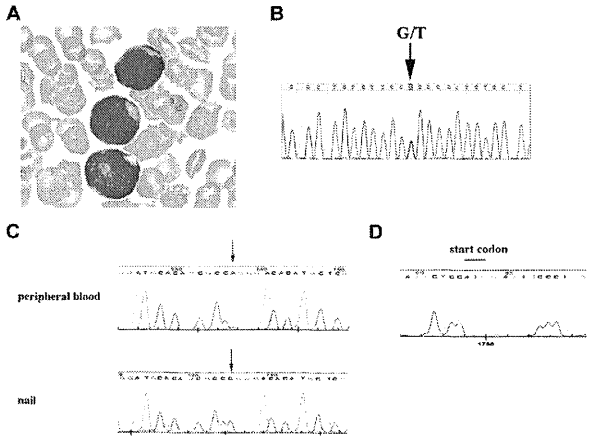

Figure 1. *TRIB1* R107L mutation identified in DS-related leukemias. (A) Giemsa staining of the case 84 peripheral blood smear diagnosed as AMKL. The image was acquired using a BX40 microscope equipped with a 100×/1.30 NA oil objective (Olympus) and a C-4040 digital camera (Olympus). (B) Fluorescent dye sequencing chromatographs of *TRIB1* genotyping by direct sequencing of the case 84 using a cDNA sample as a template. The vertical arrow indicates mixed G and T signals at codon 107. (C) Fluorescent dye sequencing chromatographs of *TRIB1* of peripheral blood leukocytes (top) or nail (bottom) in the same case at the complete remission stage. The red arrows indicate that the mutation remains in leukocytes but not in nail. The reverse strand sequences are shown. (D) *GATA1* sequence. The start codon that was mutated in AMKL[7] is normal in the peripheral blood leukocytes at the remission stage.

Retroviral infection of murine bone marrow cells and bone marrow transfer

Bone marrow cells were prepared from 8-week-old female C57Bl/6J mice 5 days after injection of 150 mg/kg body weight of 5-fluorouracil (Kyowa Hakko Kogyo). Retroviral infection of bone marrow cells and bone marrow transfer experiments were performed as described.[2] Transduction efficiencies evaluated by flow cytometric techniques were comparable between wild-type (WT; 5.3%) and R107L (3.4%). Animals were housed, observed daily, and handled in accordance with the guidelines of the animal care committee at Japanese Foundation for Cancer Research. All the diseased mice were subjected to autopsy and analyzed morphologically, and the blood was examined by flow cytometric techniques. The mice were diagnosed as positive for AML according to the classification of the Bethesda proposal.[8] The survival rate of each group was evaluated using the Kaplan-Meier method, and differences between survival curves were compared using the log-rank test.

Immunoblotting

Immunoblotting was performed using cell lysates in RIPA buffer as described.[4] Anti-p44/42 ERK (Cell Signaling Technologies), anti-phospho-p44/42 ERK (Cell Signaling Technologies), anti-C/EBPα (Santa Cruz Biotechnology), anti-FLAG (Sigma-Aldrich), and anti-GAPDH (Hy Test Ltd) antibodies were used.

Results and discussion

The important role of TRIB1 on the MAPK signaling suggests that *TRIB1* alterations may occur in some AML cases, which do not show overlapping mutations in the pathway members, such as FLT3, KIT, or RAS. Therefore, we tried to search mutations of *TRIB1* in cases of ML-DS and TL in which such mutations are infrequent.[9] In a case of DS-AMKL (case 84), a nucleotide change from guanine to thymine has been identified at 902 that results in amino acid alteration from arginine 107 (R107) to leucine (Figure 1B). The sequence changes were confirmed by subcloning the PCR product into the TA-type plasmid vector (data not shown). The nucleotide change was not observed in the DNA sample derived from the nail of the same patient at all (Figure 1C), indicating that this change is a somatic mutation. Interestingly, the mutation was retained in the peripheral blood sample in the complete remission stage in which the GATA1 mutation completely disappeared (Figure 1C-D). These results indicate that the *TRIB1* mutation precedes the onset of TL and the *GATA1* mutation, and suggest that *TRIB1* mutation occurred at the hematopoietic stem cell level and that the clone retaining the *TRIB1* mutation survived after chemotherapy. In case 84, there was no mutation for *FLT3* exons 14, 15, and 20, *PTPN11* exons 3 and 13, *KRAS* exons 2, 3, and 5, and *KIT* exons 8, 11, and 17 by the high-resolution melt analysis (data not shown).

An additional mutation was found in a case of TL (case 109) at the nucleotides 805 and 806 from GC to AT, which results in amino acid conversion from alanine (A75) to isoleucine (supplemental Figure 1, available on the *Blood* Web site; see the Supplemental Materials link at the top of the online article). *TRIB1* expression in DS-related and DS-unrelated leukemias was examined by real-time quantitative RT-PCR (supplemental Figure 2).

R107 is located within a psuedokinase domain of TRIB1 that is considered as a functionally core domain of TRIB family proteins.[10] Sequence comparison among 3 TRIB family proteins as well as tribbles homologs in other organisms revealed that the R107 is well conserved in mammalian TRIB1 and TRIB2,[10] suggesting that this arginine residue is evolutionary conserved and may be related to an important function. On the other hand, A75 is located outside of the pseudokinase domain, not conserved between human and mouse, or other tribbles homologs. Moreover, the N-terminal domain containing A75 is dispensable for the leukemogenic activity of Trib1.[4] Therefore, we tried to investigate whether the R107L mutation could affect the leukemogenic activity of *TRIB1*.

R107L was introduced into the murine *Trib1* cDNA by site-directed mutagenesis. Both WT and R107L cDNAs were subcloned into the pMYs-IRES-GFP retroviral vector and were used for retrovirus-mediated gene transfer followed by bone marrow transfer according to the method previously described.[1] All the mice

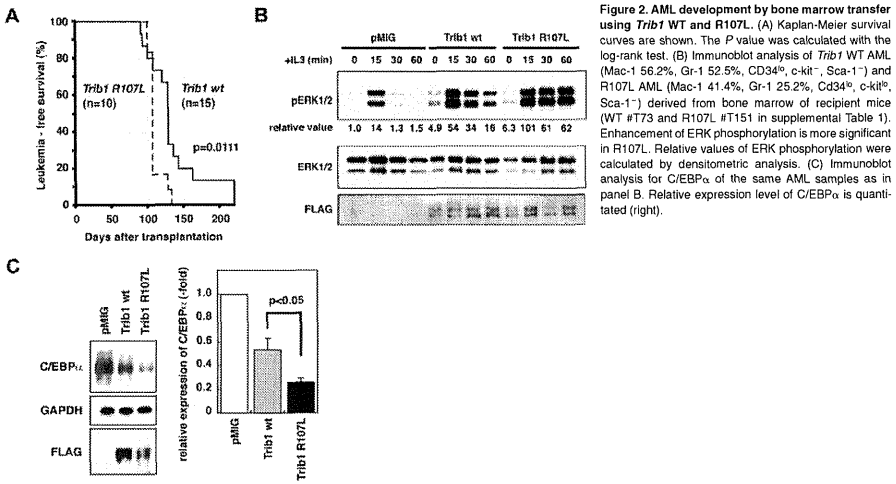

Figure 2. AML development by bone marrow transfer using *Trib1* WT and R107L. (A) Kaplan-Meier survival curves are shown. The *P* value was calculated with the log-rank test. (B) Immunoblot analysis of *Trib1* WT AML (Mac-1 56.2%, Gr-1 52.5%, CD34^{lo}, c-kit^{-}, Sca-1^{-}) and R107L AML (Mac-1 41.4%, Gr-1 25.2%, Cd34^{lo}, c-kit^{lo}, Sca-1^{-}) derived from bone marrow of recipient mice (WT #T73 and R107L #T151 in supplemental Table 1). Enhancement of ERK phosphorylation is more significant in R107L. Relative values of ERK phosphorylation were calculated by densitometric analysis. (C) Immunoblot analysis for C/EBPα of the same AML samples as in panel B. Relative expression level of C/EBPα is quantitated (right).

transplanted with bone marrow cells expressing WT (n = 15) or R107L (n = 12) developed AML (Figure 2A). The mean survival time was shorter in the recipients with R107L-expressing bone marrow cells (110 days) than those with WT (136 days; Figure 2A). The difference was significant (P = .0111, log-rank test). The result indicates that the R107L mutation enhances the leukemogenic activity of TRIB1. These results also suggest that *TRIB1* mutation might cooperate with *GATA1* mutation in the genesis of DS-AMKL, and that trisomy 21, *TRIB1*, and *GATA1* mutations occurred consecutively, which contributed to the multistep leukemogenic process.

We have shown that TRIB1 interacts with MEK1 and enhances phosphorylation of ERK.[2] The R107L mutant enhanced ERK phosphorylation more extensively than WT (Figure 2B) in AML cells derived from bone marrow of recipient mice, and more significant degradation of C/EBPα was induced by the R107L mutant (Figure 2C). These findings might be correlated to the enhanced leukemogenic activity of the mutant. Both R107L and WT proteins could interact with MEK1, having the binding motif in their C-termini. The residue 107 is located at subdomain II of the pseudokinase domain.[11] The mutation may affect conformation of the domain and may promote the MEK1 function on ERK, although additional studies are required to address the possibility. A recent study demonstrates that Trib1 and Trib2 failed to show ERK phosphorylation in 32D cells.[12] The different response to Trib1 between primary leukemic cells and the cell line might depend on the cellular context and/or combination of additional mutations. The AML phenotypes were somewhat varied in each case and Mac-1–positive/Gr-1–negative AMLs were more remarkable in WT than in R107L, although the difference was not statistically significant (supplemental Figures 3-4; supplemental Table 1). The current study underscores the role of TRIB1 in human leukemogenesis and the significance of the R107L mutation in its function. Further sequence analysis of tribbles family genes in a larger cohort will emphasize the importance of R107L and/or additional mutations of *TRIB1* in leukemic patients.

Acknowledgments

This work was supported by KAKENHI (Grant-in-Aid for Scientific Research) on Priority Areas Integrative Research Toward the Conquest of Cancer (E.I. and T.N.) and the Ministry of Education, Culture, Sports, Science and Technology of Japan (Young Scientists, T.Y.).

Authorship

Contribution: T.Y., E.I., Y.H., and T.N. designed and performed the research and wrote the manuscript; T. Toki, Y.A., R.K., and M.-j.P. performed the research; and Y.K., T. Takahara, and Y.Y. contributed to the bone marrow transplantation analysis.

Conflict-of-interest disclosure: The authors declare no competing financial interests.

Correspondence: Takuro Nakamura, Division of Carcinogenesis, Cancer Institute, Japanese Foundation for Cancer Research, 3-8-31 Ariake, Koto-ku, Tokyo 135-8550, Japan; e-mail: takuro-ind@umin.net.

References

1. Shimizu R, Engel JD, Yamamoto M. GATA1-related leukaemias. *Nat Rev Cancer.* 2008;8(4):279-287.
2. Jin G, Yamazaki Y, Takuwa M, et al. Trib1 and Evi1 cooperate with Hoxa and Meis1 in myeloid leukemogenesis. *Blood.* 2007;109(9):3998-4005.
3. Kiss-Toth E, Bagstaff SM, Sung HY, et al. Human Tribbles, a protein family controlling mitogen-activated protein kinase cascades. *J Biol Chem.* 2004;279(41):42703-42708.
4. Yokoyama T, Kanno Y, Yamazaki Y, et al. Trib1 links the MEK/ERK pathway in myeloid leukemogenesis. *Blood.* 2010;116(15):2768-2775.
5. Keeshan K, He Y, Wouters BJ, et al. Tribbles homolog 2 inactivates C/EBPalpha and causes acute myelogenous leukemia. *Cancer Cell.* 2006;10(5):401-411.
6. Storlazzi CT, Fioretos T, Surace C, et al. MYC-containing double minutes in hematologic malignancies: evidence in favor of the episome model and exclusion of MYC as the target gene. *Hum Mol Genet.* 2006;15(6):933-942.
7. Kanezaki R, Toki T, Terui K, et al. Down syndrome and GATA1 mutations in transient abnormal myeloproliferative disorder: mutation classes correlate with progression to myeloid leukemia. *Blood.* 2010;116(22):4631-4638.
8. Kogan SC, Ward JM, Anver MR, et al. Bethesda proposal for classification of nonlymphoid hematopoietic neoplasms in mice. *Blood.* 2002;100(1):238-245.
9. Toki T, Kanezaki R, Adachi S, et al. The key role of stem cell factor/KIT signaling in the proliferation of blast cells from Down syndrome-related leukemia. *Leukemia.* 2009;23(1):95-103.
10. Hegedus Z, Czibula A, Kiss-Toth E. Tribbles: a family of kinase-like proteins with potent signaling regulatory function. *Cell Signal.* 2007;19(2):238-250.
11. Yokoyama T, Nakamura T. Tribbles in disease: signaling pathways important for cellular function and neoplastic transformation. *Cancer Sci.* 2011;102(6):1115-1122.
12. Dedhia PH, Keeshan K, Uljon S, et al. Differential ability of Tribbles family members to promote degradation of C/EBPalpha and induce acute myelogenous leukemia. *Blood.* 2010;116(8):1321-1328.

From bloodjournal.hematologylibrary.org at Hirosaki University on March 15, 2012. For personal use only.

nature immunology

The kinase Btk negatively regulates the production of reactive oxygen species and stimulation-induced apoptosis in human neutrophils

Fumiko Honda[1], Hirotsugu Kano[2], Hirokazu Kanegane[3], Shigeaki Nonoyama[4], Eun-Sung Kim[5], Sang-Kyou Lee[5], Masatoshi Takagi[1], Shuki Mizutani[1] & Tomohiro Morio[1]

The function of the kinase Btk in neutrophil activation is largely unexplored. Here we found that Btk-deficient neutrophils had more production of reactive oxygen species (ROS) after engagement of Toll-like receptors (TLRs) or receptors for tumor-necrosis factor (TNF), which was associated with more apoptosis and was reversed by transduction of recombinant Btk. Btk-deficient *neutrophils in the resting state showed hyperphosphorylation and activation of phosphatidylinositol-3-OH kinase (PI(3)K) and* protein tyrosine kinases (PTKs) and were in a 'primed' state with plasma membrane–associated GTPase Rac2. In the absence of Btk, the adaptor Mal was associated with PI(3)K and PTKs at the plasma membrane, whereas in control resting neutrophils, Btk interacted with and confined Mal in the cytoplasm. Our data identify Btk as a critical gatekeeper of neutrophil responses.

Among 'professional' phagocytes with a sophisticated arsenal of microbicidal features, neutrophils are the dominant cells that mediate the earliest innate immune responses to microbes[1–3]. Neutrophils migrate to the site of infection, sense and engulf microorganisms, produce reactive oxygen species (ROS) and kill the invading microbes via ROS by acting together with antimicrobial proteins and peptides[1,2]. The enzyme responsible for the respiratory burst is NADPH oxidase, which catalyzes the production of superoxide from oxygen and NADPH. This enzyme is a multicomponent complex that consists of membrane-bound flavocytochrome b_{558} (gp91^{phox} and p22^{phox}), cytosolic components (p47^{phox}, p67^{phox} and p40^{phox}) and a GTPase (Rac1 or Rac2)[3–6]. Activation of NADPH oxidase is strictly regulated both temporally and spatially to ensure that the reaction takes place rapidly at the appropriate cellular localization. Activation of this system requires three signaling triggers, including protein kinases, lipid-metabolizing enzymes and nucleotide-exchange factors that activate the Rac GTPase[3–6].

Inadequate production of ROS is associated with various human pathological conditions. Deficiency of any component of the NADPH oxidase complex results in chronic granulomatous disease, in which bacterial and fungal infections are recurrent and life-threatening[4]. Abnormalities in the molecules involved in the signal-transduction pathway initiated by the recognition of pathogen-associated molecular patterns are accompanied by less production of ROS after exposure to specific stimuli and by susceptibility to bacterial infection. These abnormalities include deficiency in the kinase IRAK4, the adaptor MyD88 deficiency or the kinase NEMO (IKKγ)[7]. In contrast, many other human disorders are believed to be associated with or induced by excessive production of ROS that causes DNA damage, tissue damage, cellular apoptosis and neutropenia[8,9].

Here we focus on determining the role of the kinase Btk in production of ROS and cellular apoptosis in human neutrophils, as 11–30% of patients with X-linked agammaglobulinemia (XLA), a human disease of Btk deficiency, have neutropenia[10,11], and Btk is a critical signaling component of phagocytic cells[12–14]. The neutropenia of XLA is distinct from that of common variable immunodeficiency (CVID) *in that the neutropenia is induced by infection, is usually* ameliorated after supplementation with immunoglobulin and is not mediated by the autoimmune response[10,11,14]. Although a few reports have suggested that myeloid differentiation is impaired in mice with X-linked immunodeficiency[15,16], the reason for the infection-triggered neutropenia is unknown. The role of Btk in human neutrophils remains largely unexplored.

Btk is a member of the Tec-family kinases (TFKs) that are expressed in hematopoietic cells such as B cells, monocytes, macrophages and neutrophils[12]. It has a crucial role in cell survival, proliferation, differentiation and apoptosis, especially in cells of the B lineage. In humans with XLA, B cells fail to reach maturity and are presumably doomed to premature death by the *BTK* mutation that leads to the XLA phenotype[17]. Both mice with X-linked immunodeficiency that have natural mutations in *Btk* and mice in which *Btk* is targeted have B cell defects, but these are associated with much milder effects than those seen in XLA, which suggests species differences in the role of Btk[18,19].

[1]Department of Pediatrics and Developmental Biology, Tokyo Medical and Dental University Graduate School of Medical and Dental Sciences, Tokyo, Japan. [2]Department of Pediatrics, Teikyo University School of Medicine Hospital, Mizonokuchi, Kawasaki, Japan. [3]Department of Pediatrics, Toyama University School of Medicine, Toyama, Japan. [4]Department of Pediatrics, National Defense Medical College, Tokorozawa, Japan. [5]Department of Biotechnology, College of Life Science and Biotechnology, Yonsei University, Seoul, Republic of Korea. Correspondence should be addressed to T.M. (tmorio.ped@tmd.ac.jp).

Received 28 November 2011; accepted 12 January 2012; published online 26 February 2012; doi:10.1038/ni.2234

Btk is also an important signaling component of the innate immune system in phagocytic cells. Btk is involved in signaling via Toll-like receptors (TLRs) such as TLR2, TLR4, TLR7, TLR8 and TLR9, and is associated with the TLR adaptors MyD88, Mal (TIRAP) and IRAK1 (refs. 12–14,20–22). Defective innate immune responses have been observed in monocytes, dendritic cells, neutrophils and mast cells from Btk-deficient mice[12,14]. Neutrophils from mice with X-linked immunodeficiency have poor production of ROS and nitric oxide[15].

The contribution of Btk to the human innate immune system is less obvious. Stimulation via TLR2, TLR4, TLR7-TLR8 or TLR3 results in impaired production of tumor-necrosis factor (TNF) by dendritic cells from patients with XLA, whereas the TLR4-induced production of TNF and interleukin 6 (IL-6) by monocytes from patients with XLA remains intact[23–25]. Neutrophils from control subjects and patients with XLA show no substantial differences in their phosphorylation of the mitogen-activated protein kinases p38, Jnk and Erk induced by engagement of TLR4 or TLR7-TLR8 or production of ROS induced by the same stimuli[26].

Here we evaluate the role of Btk in the production of ROS and cellular apoptosis in human neutrophils through the use of Btk-deficient neutrophils, a protein-delivery system based on a cell-permeable peptide, and specific kinase inhibitors. Unexpectedly, and in con*trast to published observations of mice with X-linked immunodefi*ciency[15], the production of ROS was substantially augmented in the absence of Btk in neutrophils stimulated via TLRs, the TNF receptor or phorbol 12-myristate 13-acetate (PMA) but not in monocytes or in lymphoblastoid B cell lines transformed by Epstein-Barr virus. Excessive production of ROS was associated with neutrophil apoptosis, which was reversed by the transduction of wild-type Btk protein. Btk-deficient neutrophils showed activation of key signaling molecules involved in the activation of NADPH oxidase, and this was accompanied by targeting of Rac2 to the plasma membrane. Mal was confined to the cytoplasm in association with Btk but was translocated to plasma membrane and interacted with protein tyrosine kinases (PTKs) and phosphatidylinositol-3-OH kinase (PI(3)K) in the absence of Btk. Here we present our findings on the mechanism by which Btk regulates the priming of neutrophils and the amplitude of the neutrophil response.

RESULTS

Excessive production of ROS in Btk-deficient neutrophils

To investigate the production of ROS in the absence of Btk, we monitored ROS in neutrophils, monocytes and Epstein-Barr virus–transformed lymphoblastoid B cell lines obtained from patients with XLA, healthy controls and patients with CVID (disease control) by staining with dihydrorhodamine 123 (DHR123) and a luminol chemiluminescence assay. PMA-driven production of ROS in Btk-deficient neutrophils was three to four times greater than that in neutrophils from healthy controls or patients with CVID, and we observed augmented production of ROS with a suboptimal dose of PMA, whereas the baseline production of ROS was similar (**Fig. 1a–d**). Similarly, and in contrast to published reports[26], engagement of TLR2 (with its ligand tripalmitoyl cysteinyl seryl tetralysine lipopeptide (Pam_3CSK_4)), TLR4 (with its ligand lipopolysaccharide) or the TNF receptor (with TNF) followed by stimulation with formyl-Met-Leu-Phe (fMLP), an agonist of G protein–coupled receptors, elicited augmented ROS responses in neutrophils from patients with XLA (**Fig. 1e,f**). The production of ROS was minimal after stimulation with the TLR9 agonist CpG-A in neutrophils from patients with XLA and was not significantly different from that of neutrophils from healthy controls. The observed phenomena were reproduced in Btk-deficient eosinophils but not in monocytes or Epstein-Barr virus–transformed lymphoblastoid *B cell lines obtained from patients with XLA* (***Supplementary* Fig. 1**). These data indicated Btk-deficient neutrophils had excessive NADPH oxidase activity after various stimuli.

Augmented apoptosis in Btk-deficient neutrophils

Because high ROS concentrations are potentially harmful to cells, we investigated cell death induced by various stimuli in neutrophils from patients with XLA by staining with annexin V and the membrane-impermeable DNA-intercalating dye 7-AAD. Stimulation with PMA, TLR agonist plus fMLP, or TNF plus fMLP induced a significantly higher frequency of cells positive for annexin V among neutrophils from patients with XLA than among control neutrophils, whereas spontaneous cell death in the absence of stimulation was not significantly altered at 4 h in neutrophils from healthy controls versus those from patients with XLA (**Fig. 2a,b**). We observed cleavage of caspase-3, lower mitochondrial membrane potentials and degradation of proliferating

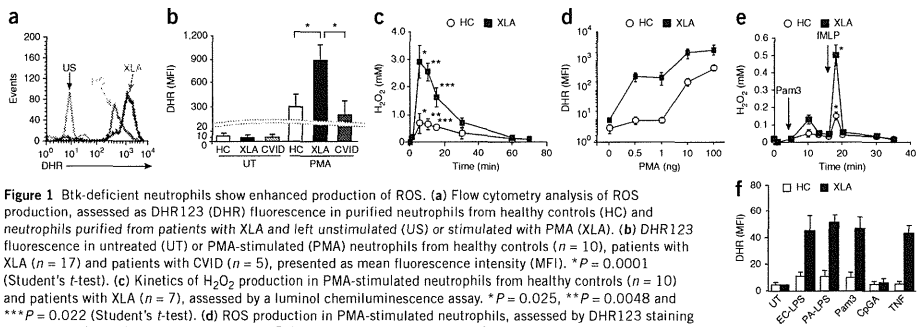

Figure 1 Btk-deficient neutrophils show enhanced production of ROS. (**a**) Flow cytometry analysis of ROS production, assessed as DHR123 (DHR) fluorescence in purified neutrophils from healthy controls (HC) and *neutrophils purified from patients with XLA and left unstimulated (US) or stimulated with PMA (XLA).* (**b**) *DHR123* fluorescence in untreated (UT) or PMA-stimulated (PMA) neutrophils from healthy controls ($n = 10$), patients with XLA ($n = 17$) and patients with CVID ($n = 5$), presented as mean fluorescence intensity (MFI). $^*P = 0.0001$ (Student's *t*-test). (**c**) Kinetics of H_2O_2 production in PMA-stimulated neutrophils from healthy controls ($n = 10$) and patients with XLA ($n = 7$), assessed by a luminol chemiluminescence assay. $^*P = 0.025$, $^{**}P = 0.0048$ and $^{***}P = 0.022$ (Student's *t*-test). (**d**) ROS production in PMA-stimulated neutrophils, assessed by DHR123 staining and presented as a dose-response curve ($n = 5$ donors per group). (**e**) Kinetics of H_2O_2 production in neutrophils stimulated with Pam_3CSK_4 (Pam3) and fMLP, assessed by a luminol chemiluminescence assay ($n = 7$ donors per group). $^*P = 0.005$ (Student's *t*-test). (**f**) DHR123 fluorescence in neutrophils incubated with lipopolysaccharide from *Escherichia coli* (EC-LPS) or *Pseudomonas aeruginosa* (PA-LPS), Pam_3CSK_4, CpG-A or TNF, followed by stimulation with fMLP ($n = 7$ donors per group). Data are representative of seventeen experiments (**a**) or are pooled from at least five (**b**,**c**,**e**,**f**) or four (**d**) independent experiments (mean and s.d. in **b**–**f**).

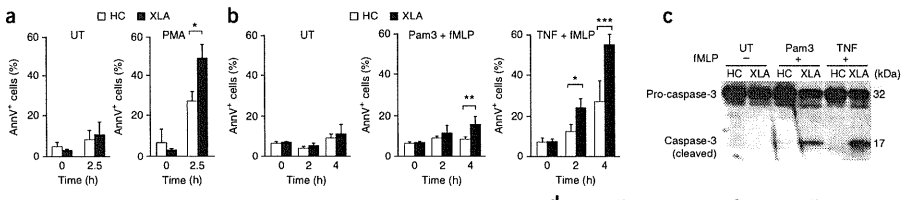

Figure 2 Btk-deficient neutrophils show augmented apoptosis due to excessive production of ROS. (**a**) Frequency of annexin V–positive (AnnV+) cells among neutrophils obtained from healthy controls and patients with XLA ($n = 11$ donors per group) and incubated for 0 or 2.5 h with dimethyl sulfoxide (UT) or PMA. $^{*}P = 0.001$ (Student's *t*-test). (**b**) Frequency of apoptotic cells among neutrophils obtained from healthy controls ($n = 10$) and patients with XLA ($n = 12$) and incubated for 0, 2 or 4 h in medium with dimethyl sulfoxide (UT), Pam_3CSK_4 plus fMLP or TNF plus fMLP, assessed by staining with annexin V and 7-AAD. $^{*}P = 0.036$, $^{**}P = 0.0083$ and $^{***}P = 0.0002$ (Student's *t*-test). (**c**) Caspase-3 cleavage in neutrophils from healthy controls ($n = 3$) and patients with XLA ($n = 3$), stimulated for 4 h as in **b** (above lanes). Pro-caspase-3 is the uncleaved form. (**d**,**e**) Frequency of apoptotic Btk-deficient neutrophils ($n = 5$ donors) stimulated for 2 h (**d**) or 2.5 h (**e**) with the antioxidant N-acetyl-cysteine (NAC). $^{*}P = 0.043$ and $^{**}P = 0.036$ (**d**) or $^{*}P = 0.026$ (**e**; Student's *t*-test). Data are representative of three experiments (**b**) or at least five independent experiments (**a**,**c**–**e**; mean and s.d. in **a**,**b**,**d**,**e**).

cell nuclear antigen; hence, cell death was caused by apoptosis (**Fig. 2c** and **Supplementary Fig. 2**). Apoptosis assessed by these methods was augmented considerably for neutrophils from patients with XLA. The observed apoptosis was most probably triggered by ROS, as coincubation of neutrophils with N-acetyl cysteine, an antioxidant, rescued the cells from apoptosis induced by TNF plus fMLP or by PMA (**Fig. 2d,e**). We detected much more ROS release and stimulation-induced apoptosis of neutrophils from all patients with XLA regardless of the site or mode of their mutation (**Supplementary Fig. 3**). In addition, we found no correlation between genotype and the extent of neutrophil production of ROS. These data suggested that neutrophils from patients with XLA are susceptible to apoptosis triggered by pathogens.

Normalization of the ROS response by transduction of Btk

We next determined whether the enhanced apoptosis noted above was due to a defect in Btk itself or abnormal myeloid differentiation in the absence of Btk. For this, we prepared three recombinant Btk proteins (full-length Btk; Btk with deletion of the pleckstrin homology (PH) domain; and Btk with deletion of the kinase domain) fused to the cell-permeable peptide Hph-1 (**Fig. 3a,b**). We purified the products and transduced the proteins into neutrophils lacking Btk. The efficacy of transduction was more than 95%; and Hph-1–Btk expression was stable for at least 12–24 h (ref. 27). We adjusted the expression of Btk to that in neutrophils from healthy controls by incubating 1×10^6 cells for 1 h with 1 μM recombinant fusion protein. Transduction of full-length Btk into neutrophils from patients with XLA restored the production of ROS and the frequency of apoptotic cells after PMA stimulation to that observed for neutrophils from healthy controls (**Fig. 3c,d**). Transduction of the recombinant fusion of Btk with deletion of the PH domain only modestly reversed neutrophil overactivation (**Fig. 3c**), which indicated that appropriate cellular localization and interactions with other molecules were required for Btk function. Transduction of the recombinant fusion of Btk with deletion of the kinase domain minimally corrected excessive production of ROS (**Fig. 3c**), which suggested that the kinase activity of Btk or molecules that interacted via the kinase domain were critical for the regulation of ROS. We also confirmed the importance of the kinase domain by an experiment that showed excessive production of ROS in normal neutrophils treated with 50 μM LFM-A13, an inhibitor of the kinase activity of Btk, but not in those treated with LFM-A11, a control compound (**Fig. 3e**). We also documented augmented apoptosis in control neutrophils treated with LFM-A13 (**Fig. 3f**). These data demonstrated that the enhanced production of ROS and apoptosis was directly related to a defect in Btk.

NADPH oxidase components in Btk-deficient neutrophils

The NADPH oxidase complex consists of the transmembrane component ($gp91^{phox}$ and $p22^{phox}$), a cytosolic component ($p47^{phox}$, $p67^{phox}$ and $p40^{phox}$) and Rac2 (refs. 3–6). The activity of NADPH oxidase is controlled by targeting of the cytosolic components to the plasma membrane or phosphorylation of the cytosolic components or both. To assess the mechanism of the excessive production of ROS in Btk-deficient neutrophils, we investigated the abundance, phosphorylation and subcellular localization of each component by immunoblot analysis.

The expression of each component of the NADPH oxidase complex was similar in neutrophils from patients with XLA and those from healthy controls (**Fig. 4a**). The amount of $p47^{phox}$, $p67^{phox}$ and $p40^{phox}$ in the cytoplasm and the membrane was not substantially different in neutrophils from patients with XLA and those from healthy controls (**Fig. 4b**). Similarly, the amount in the membrane-targeted fraction after stimulation with PMA was not very different in neutrophils from patients with XLA and those from healthy controls (**Fig. 4c**). Phosphorylation of Ser345 in $p47^{phox}$ and of Thr154 in $p40^{phox}$ are important for translocation of the cytosolic components to the membrane[4,5,28]. Those modifications were not altered in Btk-deficient neutrophils (**Fig. 4c**). In contrast, we detected Rac2 in the plasma membrane of Btk-deficient neutrophils before stimulation with PMA. We observed four- to fivefold higher membrane expression of Rac2 in neutrophils from patients with XLA than in those from healthy controls in the resting state (**Fig. 4b**).

Typically, 10–15% of $gp91^{phox}$ is located in the plasma membrane of unstimulated neutrophils, whereas the majority of the molecule resides in specific granules. Membrane expression increases after

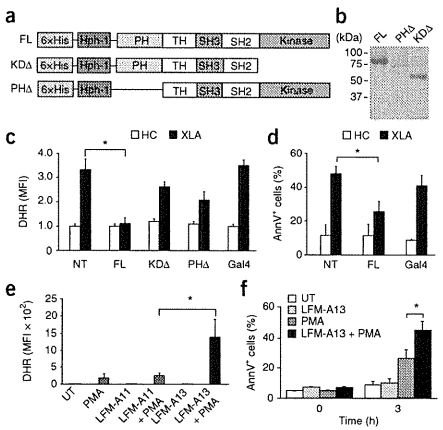

Figure 3 Excessive production of ROS and apoptosis in neutrophils from patients with XLA are abrogated by transduction of Hph-1–tagged full-length recombinant Btk but not by Hph-1–tagged Btk with deletion of the kinase or PH domain. (**a**) Hph-1–tagged Btk constructs: full-length Btk (FL); Btk with deletion of the kinase domain (KDΔ); Btk with deletion of the PH domain (PHΔ). 6×His, six-histidine tag; TH, Tec homology; SH3, Src homology 3; SH2, Src homology 2. (**b**) Size of purified Hph-1–tagged Btk proteins, confirmed by Coomassie brilliant blue staining. (**c**) ROS production in neutrophils from healthy controls ($n = 5$) and patients with XLA ($n = 5$), left untransduced (NT) or transduced with the constructs in **a** or Hph-1–tagged yeast transcriptional activator Gal4 (far right; control), presented as the MFI of DHR123 relative to that of untreated neutrophils from healthy controls, set as 1. (**d**) Frequency of apoptotic cells among neutrophils from healthy controls and patients with XLA, left untransduced or transduced with Hph-1–tagged full-length Btk or Gal4 (control). (**e**) DHR123 fluorescence in neutrophils from healthy controls ($n = 7$) left untreated or treated with PMA alone, or pretreated with LFM-A13 (Btk inhibitor) or LFM-A11 (control) alone or followed by stimulation with PMA (+ PMA). (**f**) Frequency of annexin V–positive cells among neutrophils from healthy controls ($n = 7$) left untreated or treated with PMA alone, or pretreated with LFM-A13 (50 μM, a concentration that does not inhibit other PTKs[47,48]) alone or followed by stimulation with PMA. $^{*}P = 0.0021$ (**c**), 0.019 (**d**), 0.021 (**e**) or 0.025 (**f**; Student's *t*-test). Data are representative of five experiments (**b**) or are pooled from six (**c**), three (**d**) or four (**e**,**f**) independent experiments (mean and s.d. in **c**–**f**).

signaling via TLRs or G protein–coupled receptors because of translocation to the plasma membrane[2]. Immunoblot analysis with antibody to gp91 (anti-gp91; **Fig. 4b**) and flow cytometry analysis of surface flavocytochrome b_{558} (**Fig. 4d**) showed higher gp91 expression in neutrophils from patients with XLA. Immunohistochemical analysis by confocal fluorescence microscopy showed localization of gp91 and Rac2 together in the membranes of resting Btk-deficient neutrophils but not in neutrophils from healthy controls (**Fig. 4e**). These results suggested that NADPH oxidase complex was partially assembled and ready to be activated in steady-state Btk-deficient neutrophils.

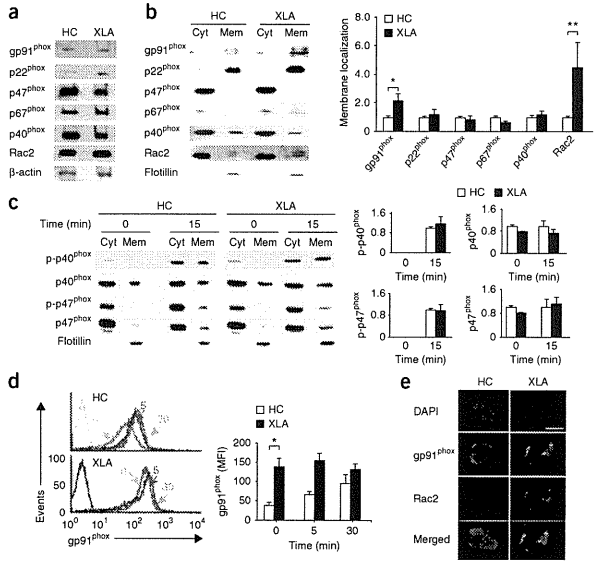

Figure 4 Btk-deficient neutrophils show targeting of Rac2 to the plasma membrane, colocalization of Rac2 with $gp91^{phox}$ and higher membrane expression of $gp91^{phox}$. (**a**) Immunoblot analysis of the components of the NADPH oxidase complex in neutrophils from a healthy control and a patient with XLA. β-actin serves as a loading control throughout. (**b**) Immunoblot analysis (left) of the components of the NADPH oxidase complex in the cytoplasm (Cyt) and plasma membrane (Mem) of neutrophils from healthy controls and patients with XLA ($n = 9$ per group). Right, quantification of the membrane expression at left, presented as band intensity relative to that of flotillin (loading marker for the membrane-raft fraction) in membranes of neutrophils from healthy controls, set as 1. $^{*}P = 0.045$ and $^{**}P = 0.027$ (Student's *t*-test). (**c**) Immunoblot analysis of total and phosphorylated (p-) $p40^{phox}$ and $p47^{phox}$ in the cytoplasm and membrane of PMA-stimulated neutrophils from healthy controls and patients with XLA. Right, quantification as in **b**. (**d**) Flow cytometry analysis of $gp91^{phox}$ on neutrophils from healthy controls and patients with XLA, left unstimulated (0) or stimulated for 5 or 30 min (above lines) with PMA, detected by staining with mAb 7D5 to gp91. Gray lines indicate staining with MsIgG (control). Right, quantification of the gp91 MFI in cells treated as at left. $^{*}P = 0.0039$ (Student's *t*-test). (**e**) Confocal microscopy of $gp91^{phox}$ (green) and Rac2 (red) in healthy controls and neutrophils from patients with XLA; nuclei are counterstained with the DNA-intercalating dye DAPI (blue). Original magnification, ×600; scale bar, 10 μm. Data are from one representative of nine independent experiments with seven healthy controls and nine patients with XLA (**a**), are representative of nine experiments (**b**), are from nine independent experiments (**c**), are pooled from seven independent experiments (**d**) or are representative of four independent experiments (**e**; mean and s.d. in **b**–**d**).